Physiological Roles of Robo Receptor during dendrite development of the multidendritic arborization neurons of the *Drosophila* peripheral nervous system

Dissertation

Hiermit, erkläre ich, dass ich die vorliegende Dissertation selbständig und ohne unerlaubte Hilfe angefertigt habe. Sämtliche Experimente wurden von mir selbst durchgeführt, auβer wenn explizit auf Dritte verwiesen wird. Ich habe weder anderweitig versucht, eine Dissertation oder Teile einer Dissertation einzureichen bzw. einer Prüfungskommission vorzulegen, noch eine Doktorprüfung durchzuführen.

München, den 18.10.2007 …………………………………
(Unterschrift)

1st Gutachter: Prof. Tobias Bonhoeffer
2nd Gutachter: Prof. John Parsch
Tag der mündlichen Prüfung: 12.12.2007

Die vorliegende Arbeit wurde zwischen November 2003 und August 2007 unter der Leitung von Dr.Gaia Tavosanis am Max- Planck Institut für Neurobiologie in Martinstried durchgeführt.

Abbreviations

2L	second left chromosome
Abl	Ableson Tyrosine Kinase
AEL	after egg laying
bd	bipolar neuron
BDNF	brain derived neurotrophic factor
cAMP	cyclic adenosine monophosphate
CC	conserved cytoplasmic sequence motifs
CLASP	CLIP associated protein
CLIP	cytoplasmic linker protein
CNS	central nervous system
Comm	*Drosophila* Commissureless
CREB	cAMP response element binding protein
CREST	calcium response transactivator
da	dendritic arborization
DCC	deleted in colorectal carcinoma
Df	Deficiency
DNA	deoxyribonucleic acid
Dock	*Drosophila* Dreadlocks
DRG	dorsal root ganglion cells
DSCAM	Down Syndrome Cell Adhesion Molecule
EcR	*Drosophila* Ecdyson Receptor

EGF	Epidermal Growth Factor
EGFP	enhanced Green Fluorescence Protein
elav	embryonic lethal abnormal vision
EMS	ethyl methane sulfonate
Ena	*Drosophila* Enabled
Eph	Ephrin receptor tyrosine kinase
ER	endoplasmatic reticulum
FAS	*Drosophila* Fasciclin
Fmi	*Drosophila* Flamingo
FN3	Fibronecting type 3
Fry	*Drosophila* Furry Kinase
GAL4	Galactosidase protein 4
GFP	Green Fluorescent Protein
GTPase	Guanosine Triphosphatase
h	hours
HSPG	Heparane Sulfate Proteoglycan
Ig	immunoglobulin domains
kb	kilo bases
LN	cholinergic local neurons
LRRs	leucine-reach repeats
MAP	Microtubule Associated Protein
MARCM	mosaic analyses with a repressible cell marker
MASs	muscle attachment sites

Mb	mega bases
md-da	multiple dendritic dorsal arborisation neurons
mRNA	messenger RNA
Nck	non-catalytic region of Tyrosine kinase
Neuro D	neuronal determination factor
Nos	*Drosophila* Nanos
Orbit/MAST	*Drosophila* Microtubule-associated protein
ORN	olfactory receptor neurons
Pak	p21-activated serine/threonine kinase
PB	primary branch
PN	projection neurons
PNS	peripheral nervous system
ppk	*Drosophila* Pickpocket
PRC	polycomb repressor complex
RGC	retinal ganglion cells
RNA	ribonucleic acid
Robo	Roundabout receptor protein
SB	secondary branch
Sema3A	Semaphorin 3A
SH	Src homology domain
Shh	Sonic Hedgehog
Sos	*Drosophila* Son of Sevenless
Src	Sarcoma Virus Oncogene

TB   tertiary branch

Trc   *Drosophila* Tricornered

UAS   upstream activating sequence

UPS   ubiquitin-proteasome system

UCSF   University of California San Francisco

VASP   vasodilator-stimulated phosphoprotein

Figure and Tables

Preface

The complex processes of axogenesis, or axon generation, dendritogenesis, or dendrite generation, and the following establishment of proper neuronal networks are molecularly regulated events each of which are of great interest and the object of major investigation in the field of neuroscience. Understanding the mechanisms that control these complex steps of neuronal development would contribute enormously to decoding how nervous system development is achieved. The most fascinating part of such understanding would help us to comprehend our unique ability to think, remember, dream, speak, and react to the environment.

Summary

Elaboration of a dendritic arbor and the extension of an axon define the neuronal shape and are the key morphological features defining neuronal maturation. How the process is molecularly regulated is only poorly understood.

In this study we used the dorsal multidendritic arborization (md-da) neurons of the *Drosophila* embryonic Peripheral Nervous System (PNS) to address the question about the Roundabout (Robo) receptor protein function during dendrite field development. We identified Robo as one of the proteins involved in regulating the balance between dendritic branch elongation and new branch formation during dendritic arbor specification of the morphologically most complex, filling-in Class IV neuron of *Drosophila* PNS.

To dissect the role of the Robo proteins during dendritogenesis, we performed detailed developmental analyses of dendrite field formation of md-da neurons and compared how dendrite morphogenesis differs in animals lacking Robo function or having too much of the protein in their sensory neurons. We observed that changing the function of Robo protein results in defects in the number and elongation of high order dendritic branches. With the help of cell-class specific genetic markers we also observed that Robo acts cell-class specifically and is required during dendrite field development of the morphologically most complex class of md-da neurons, Class IV. Based on MARCM (mosaic analyses with a repressible cell marker) rescue and expression pattern experiments we suggest that this function of Robo is cell-autonomous. By doing time-lapse analyses we assessed the mechanistic role of overexpressing Robo during dendrite field development. We could verify that this protein limits the elongation and new branch formation of fine dendritic processes of the *Dorsophila* Class IV neurons. We performed expression pattern analyses, ectopic expression experiments and MARCM experiments for *slit* and suggest that muscles and neurons themselves are possible sources for the ligand. There are few molecules known to mediate the activation of Robo via Slit in the growth cone of an axon. Among these are Dock, a SH2-SH3 adaptor protein and Ena, a member of the VASP family of proteins. Loss-of-function analyses for these two proteins

suggest that Ena is acting downstream of Robo during the regulation of dendrite field development of md-da neurons. Finally we propose a model in which Robo responsiveness to Slit is down regulated via Robo2 during axon patterning of dorsal md-da neurons.

1. Introduction

1.1 Molecular and cellular mechanisms underlying axongenesis.

Neurons are one of the most complex cell types in animal organisms because of their abilities to form complex networks, select specific types of information and process this information. The outcome of this computation is the behavioral response of an animal to its environment. Each neuronal cell type is determined by its functional specificity. This is characteristic for the type of connections a neuron has formed or by its morphological complexity and this makes neurons so unique.

Almost all neurons are composed of distinct compartments such as axons, synaptic terminals, dendrites and spines, with just a few exceptions: such as vertebrate dorsal root ganglion (DRG) sensory neurons that only possess axons, starburst amacrine cells or the recently identified cholinergic local neurons (LNs) in *Drosophila* which are composed only of dendrites (Masland, 2005; Shang et al., 2007). Furthermore, not all neurons possess spines. Dendrites are often highly branched and typically receive and process information. Axons on the other side relay this information to other neurons.

Once specified as an axon, this neuronal compartment is able to grow over long distances in order to find its target. Both *in vivo* and *in vitro* analyses have identified several important molecules, classified as axon guidance cues, to be involved in the process of axon guidance and/or targeting (Dickson, 2002; Tessier-Lavigne and Goodman, 1996). Among those are Slit, Semaphorins, Netrins and Ephrins. Slit, Semaphorins and Netrins act as secreted molecules, whereas Ephrins and a few Semaphorins are anchored on the cell surface. Each of these molecules, often presented in spatiotemporal, sometimes overlapping patterns can specifically interact with a receptor molecule expressed on the growth cone of an axon and thus induce a repulsive or attractive response that guide the growth cone to its target. Although the identification of these major guidance cues has increased our understanding of how the nervous system develops, the number of

molecules dictating the pathfinding events at the tip of an axon appears quite small in comparison to the immense complexity of nervous system wiring. In the search for other molecular components it was discovered that morphogenes such as Bone morphogenetic protein (BMP), Sonic Hedgehog (Shh), and Wnts and sugar molecules, such as heparane sulfate proteoglycans (HSPG), can navigate axons and act during synapse formation (Van Vactor et al., 2006; Zou and Lyuksyutova, 2007). How these molecules signal to the cytoskeleton to direct axon growth awaits further investigations. The major outcome of guidance receptor activation is the initiation of many intracellular signaling cascades which provide a growth cone with the ability to select the correct path towards its target. What exactly happens inside the growth cone to make it respond to these extracellular cues is an object of broad research interest. Mainly *in vitro* studies provide the findings that local protein turnover, transient bursts of calcium release, cyclic nucleotides, membrane macro domains of lipids and proteins and Rho family GTPases are some of the components mediating such specific responses (reviewed in Dickson, 2001; Song et al., 1998; reviewed in Wen and Zheng, 2006).

Upon reaching their targets, the morphology of growth cones changes dramatically with the formation of branches and synapses. The initiation, extension and navigation of axon collaterals can follow activity based competition mechanisms and requires the controlled and coordinated assembly and disassembly of the neuronal cytoskeleton (Hua et al., 2005; Kornack and Giger, 2005; Ruthazer et al., 2003). The molecular players known to be involved in this dynamic process of axon arborization have only been poorly investigated. Several recent studies demonstrated that extracellualr guidance molecules such as Slit, Semaphorin and Netrin can also influence the branching behavior of an axon (reviewed in Dent et al., 2004; Ma and Tessier-Lavigne, 2007). Our current understanding of how such primary mediators of axon guidance specifically control axonal branching is quite fragmentary. Excessive axonal branch formation during early stages of nervous system development is refined or pruned during later stages a process that has been shown in worms, flies and mammals (Bagri et al., 2003; Kage et al., 2005; Kantor and Kolodkin, 2003). Some of the molecular and cellular events that underlie axon remodeling have been identified. The Semaphorin family of molecules trigger such events in the hippocampus, while glia cells can selectively eliminate branch processes in

the *Drosophila* olfactory system and mushroom body (Bagri et al., 2003; Marin et al., 2005).

1.2 Molecular and cellular mechanisms controlling dendrite formation

Our understanding of the molecular mechanisms of axon guidance, branching, targeting and synaptogenesis, although only limited, are quite advanced in comparison to what we know about molecular and cellular mechanisms regulating dendrite development. The highly similar dendritic arbor that neurons of the same type develop supports the idea of a molecular and genetic control of dendrite morphogenesis. In the same neuron the axon differs from dendrites morphologically, functionally and molecularly; it is therefore not surprising that certain molecules are localized predominantly in dendrites but not in axons. In fact, this is of great advantage, because such molecular markers allow the separate visualization of dendrites or axons, enabling us to address specific questions aimed at understanding dendritogenesis versus axogenesis.

Only in the last 10 years have neuroscientists started answering questions about the events that regulate the establishment of a neuron's dendrite architecture and it was not surprising that the steps known to be involved in axogenesis turned out to be similarly used also during dendritogenesis; including ***initiation of outgrowth, elongation, patterning, branching, targeting, synapse formation, tiling and competition for space, refinement and maintenance*** (reviewed in Jan and Jan, 2003; Kim and Chiba, 2004; Miller and Kaplan, 2003; Parrish et al., 2007b) (Fig1).
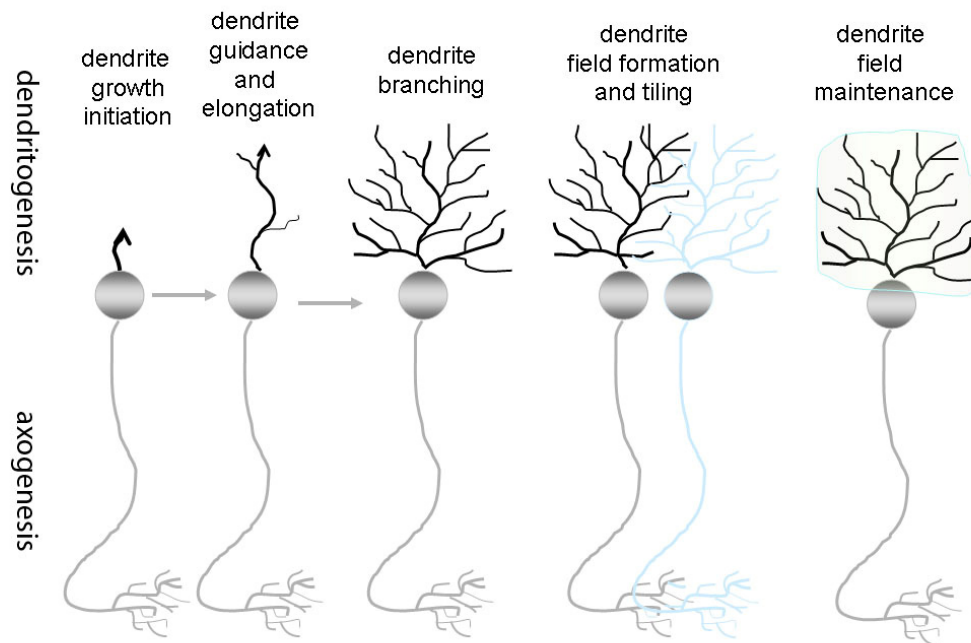
FIGURE 1. Schematic representation of the development of a dendrite tree.
The figure shows the steps of dendrite development, including the growth initiation of a
primary dendrite, which elongates in a defined direction. Next, new branches rising from
the primary dendrite are formed. These elongate and serve as a substrate for higher order
dendrite branches. Dendrite trees are able to tile. Once formed, the dendrite tree has to be
maintained.

In vivo, most neurons initiate dendrite ***outgrowth*** once the axon has developed or even
reached its target. The list of molecules known to be involved in regulating dendrite
outgrowth is relatively small. A forward genetic screen in *Drosophila* identified
Flamingo (Fmi), a seven-pass transmembrane Cadherin, as a molecular factor required to
suppress precocious dendritic outgrowth of dorsal multidendritic neurons in *Drosophila*
(Gao et al., 1999; Gao et al., 2000). The same molecule however, is required *in vitro* for
maintenance of a well established dendrite tree of pyramidal and purkinje neurons (Shima
et al., 2004).

Different types of neurons, growing in different organisms or environments (such as
cultures or slices) can differ in their developmental behavior. In a culture dish, each type
of neuron can display a different capacity of dendrite and/or axonal growth compared to

in vivo situations. On one hand, such experiments have been demonstrative for the intrinsic capacity of a neuron to grow; on the other, there is a complex interplay between intrinsic and extrinsic cues that are crucial for the neuron to become mature and functional.

Few molecules, all known previously for their role in axon patterning, are active and can **direct the growth** and **elongation** of dendrites as well. Semaphorins, Slit, Ephrins or Netrin, can work also as regulators of dendrite growth, guidance and branching (Furrer et al., 2003; Komiyama et al., 2007; Polleux et al., 2000; Whitford et al., 2002). For example, contrary to its repellent function for axons, Semaphorin-3A appears to serve as an attractant for the apical dendrites of pyramidal neurons in cortical slices (Polleux et al., 2000). In addition, Slit and its receptor Robo, Netrin- and its *Drosohila* receptor Frazzled/DCC and the Semaphorin- Plexin ligand-receptor pair can dictate the directionality of dendrite growth (Kim and Chiba, 2004; Komiyama et al., 2007). Slit and Netrins can direct the growth of motor neuron dendrites at the ventral midline of the CNS of *Drosophila*, while Semaphorin-1a and its receptor Plexin control the dendrite growth and patterning of olfactory projection neurons (PN). Contrary to their primary *in vivo* function as dendrite guidance molecules, *in vitro* the Slit/Robo signaling system promotes the growth and branch formation of dendrites in cultured cortical neurons (Whitford et al., 2002).

It is well established that dendrite branching, similar to axon branching, provides a single neuron with the ability to establish synaptic contacts with multiple targets and is therefore crucial for the formation of neuronal networks. Forward and reverse genetic screens in *Drosophila* have provided a list of molecules that can exert specific intrinsic control on **dendrite branch formation** and growth. Some of these, including the mRNA binding proteins Nanos (Nos) and Pumillio, and the transcription factors Abrupt and Cut, can act cell- class specifically, and appear to be neuronal type specific regulators of dendrite morphology (Grueber et al., 2003a; Li et al., 2004; Sugimura et al., 2004; Ye et al., 2004). Identifying intrinsic cues that regulate mammalian dendrite development has been more difficult; there are only a few transcription factors known to be major targets of calcium- dependant regulation of dendrite morphogenesis, such as CREST, CREB and

Neuro D (Redmond and Ghosh, 2005Aizawa et al., 2004; Gaudilliere et al., 2004; Wayman et al., 2006).

The initiation, extension and navigation of dendritic collaterals require the controlled and coordinated assembly and disassembly of the neuronal cytoskeleton. Inside the cell regulators of the two major cytoskeletal components, actin and microtubules can induce changes in their dynamics ultimately leading to impairment or promotion of dendrite branch formation. For example Cypin, a protein with guanine deaminase activity can regulate dendrite number in hippocampal neurons *in vitro* by binding directly to Tubulin and promoting microtubule assembly (Akum et al., 2004; Chen et al., 2005a). Among others, the Rho family of GTPases (Rho, Rac and Cdc42) has emerged as an important determinant of dendrite structure. Working as integrators of extracellular cues, these molecules can induce actin or microtubule dynamics in the dendritic cytoskeleton in a similar fashion as in axons (Li et al., 2000; Luo, 2000; Luo et al., 1996; Newey et al., 2005; Van Aelst and Cline, 2004).

Technical advances in imaging living neurons in real time have revealed that the morphological complexity of a dendrite tree of a developing neuron is dependent on a balanced process between extension and/or retraction, stabilization and elongation of filopodia-like processes. Some of these develop into mature dendrite branches, while others completely disappear (Wu and Cline, 2003; Wu et al., 1999). Stabilized branches extend and become the substrate for further branch addition; hence a dendrite arbor gradually becomes more complex during development (Gao et al., 1999; Wu and Cline, 2003).

A wealth of evidence suggests that the ***final size*** and ***shape*** of a ***dendrite arbor*** is more likely determined by signals from the environment. These signals can be either secreted molecular cues from the surrounding tissue or interactions from neighboring cells of the same kind or contacts with presynaptic partners (reviewed in Jan and Jan, 2001; McAllister, 2000).

Dendrites of the same neuronal type can recognize each other; this recognition mechanism prevents dendrite branches of the same type from growing over each other. Such complete, but non redundant coverage of a receptive field is known as ***tiling*** and is observed in different types of sensory neurons in *Drosophila, Manduca* and in some

vertebrates (Amthor and Oyster, 1995; Grueber et al., 2001; Grueber et al., 2002; Grueber et al., 2003b; Lin et al., 2004) . In the vertebrate retina, tiling is the principle of organization used by direction- selective retinal ganglion dendrites of the same type (Amthor and Oyster, 1995; Lin et al., 2004). The molecular mechanisms that control these principles of dendrite field development are only now beginning to be defined. Furry (Fry) and Tricornered (Trc) are two evolutionarily conserved protein kinases essential for dendrite tiling of sensory neurons of *Drosophila* (Emoto et al., 2004). Furthermore, Gallegos and Bargamnn reported that the Sax-1 and Sax-2 homologues of Trc and Fry have similar function in *C. elegans*, although the definition of tiling of neurons which form only a single dendrite can be used only in the context of non-overlap (Gallegos and Bargmann, 2004).

Analyses of the Down Syndrome Cell Adhesion Molecule (DSCAM) in sensory md-da neurons in *Drosophila* revealed an additional mechanism used to limit overlap of dendrite branches of the same neurons, namely ***self-avoidance***. This mechanism ensures the proper spreading of dendrite branches and a more uniform coverage of the receptive field area innervated by the dendrites of the same neurons. Dorsal sensory neurons lacking DSCAM, fail to repel each other and form branches that tend strongly to fasciculate together (Hughes et al., 2007; Matthews et al., 2007; Soba et al., 2007)

Once formed, the architecture of a dendrite tree needs to be ***maintained*** in order to form stable connections with axonal or dendritic partners. The molecules and mechanisms that control this process are not well understood. A few genes, all known to act during dendrite maintenance and tiling of multidendritic sensory neurons in *Drosophila* have been recently identified. The tumor suppressor Warts/Lats can act together with the tumor suppressor Hippo to regulate dendrite maintenance and tiling of the morphologically most complex class of *Drosophila* sensory neurons, Class IV. Members of the Polycomb repressor complex (PRCs) can act in the same pathway, and specifically control dendrite maintenance of dorsal sensory neurons (Emoto et al., 2006; Parrish et al., 2007a). Although it has not yet been shown that these molecules might play a similar role in dendrite tree maintenance of vertebrate neurons, the highly conserved molecular structure of these proteins gives reason for this speculation. Dendrite stabilization and maintenance are also molecularly regulated processes in mammals. For example few

studies nicely demonstrate a role for BDNF (brain derived neurotrophic factor), Integrins and classical Cadherins in mediating a stable dendritic shape (Gorski et al., 2003; Marrs et al., 2006).

A key future endeavor will be to identify and characterize the molecular players that promote a mature neuron to respond to environmental changes and thus undergo *morphological remodeling* processes. Little is known about the large-scale remodeling of mature dendrites, which in most cases has been observed to be concomitant with axonal remodeling (Lee et al., 2000; Marin et al., 2005; Truman and Reiss, 1995; Watts et al., 2003). During insect metamorphosis the larval nervous system is extensively modified, presenting the opportunity to dissect the basis of neuronal remodeling events. Few studies have shown that the md-da neurons of the PNS of *Drosophila*, while undergoing metamorphosis, poses both cell- intrinsic and cell-extrinsic abilities to selectively remodel their dendrites. These molecular mechanisms involve matrix metalloproteases, the Ubiquitin-proteasome system (UPS) and Ecdysone receptor (EcR) signaling (Kuo et al., 2006; Williams et al., 2006; Williams and Truman, 2005). Contrary to the case in insects, dendrite remodeling processes in mammals have been reported as a phenomenon accompanied by activity-dependent mechanisms and mostly in neurons of the visual and olfactory systems (Cline, 2001; Lohmann and Wong, 2005). The molecular mechanisms underlying neuronal activity induced dendritic arbor rearrangements are only poorly understood and imply NMDA receptor activation and its two major signaling targets; Calcuim/calmodulin-dependant kinase and Mitogen-activated kinase (Chen et al., 2005b).

Finally, the cellular machinery enabling neuronal dendritic and axonal formation and growth is one of the least understood and analyzed systems. During the construction of such a complex dendrite tree, the addition of plasma membrane is required. Only recently it has been demonstrated that components of the secretory pathway including ER and Golgi apparatus contribute significantly to the differentiation of dendrites and in establishing their complex arbor (Horton et al., 2005; Ye et al., 2006).

1.3 Roundabout receptors and their ligand Slit
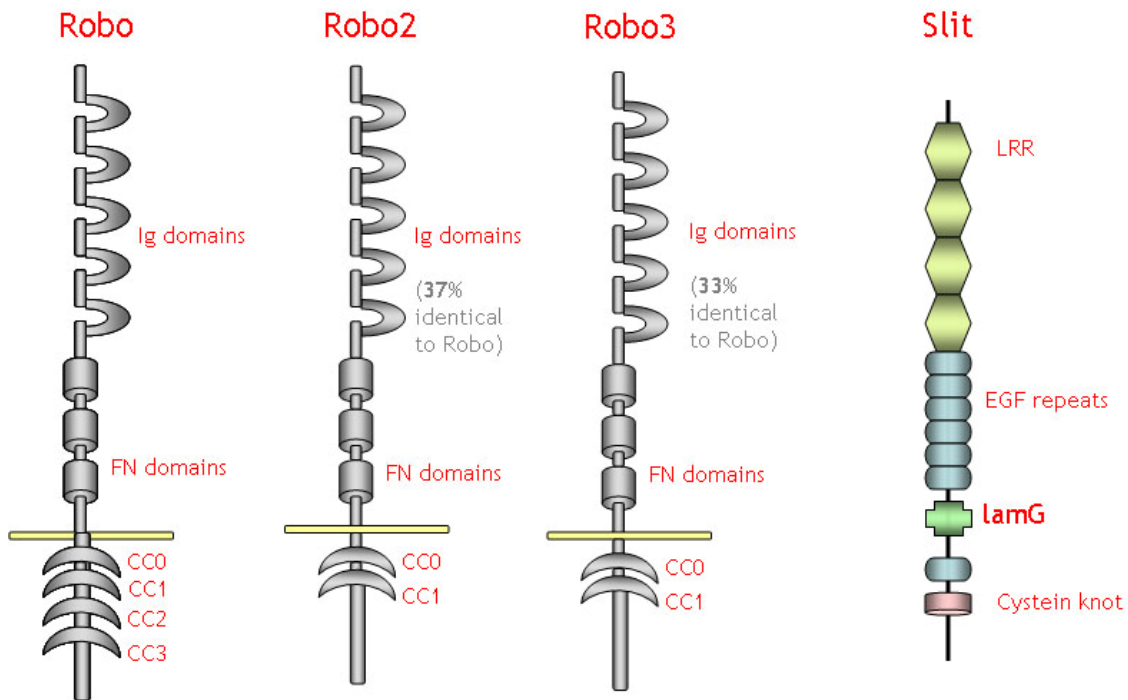
FIGURE 2. *Drosophila* **Robo receptors and Slit proteins and their domain organization**.
Robo proteins are highly conserved among different species. These are characterized by the presence of five Immunoglobulin (Ig) domains, three Fibronectin (FN) domains, a transmembrane domain and four conserved cytoplasmic motifes (CC) in Robo (but only two in Robo2 and Robo3) The extracellular domains of Robo2 and Robo3 are ~37% and ~33% identical to Robo and 49% identical to each other (described in Rajagopalan et al., 2000b; Simpson et al., 2000b). The N-terminal region of Slit contains four Leucine Rich repeats (LRR), followed by six Epidermal growth factor (EGF) repeats. The C-terminal region of Slit contains a Laminin-G domain, one EGF repeat and a cystein knot.

Roundabout (**Robo**) was first identified in a genetic screen for mutants showing commissural axon pathfinding defects at the ventral midline of *Drosophila* (Seeger et al., 1993). In *robo* mutant fly embryos, axons including both ipsilateral and commissural axon cross and recross the ventral midline of the central nervous system (CNS) of *Drosophila* (Kidd et al., 1998; Seeger et al., 1993). Further analyses revealed that the protein is highly enriched at growth cones of CNS axons (Kidd et al., 1998). At the same time, two other *robo* genes have been identified and cloned – *robo2* and *robo3* (Fig.2) (Kidd et al., 1998; Rajagopalan et al., 2000b; Simpson et al., 2000a). The proteins of all three genes have been biochemically and genetically shown to bind to the same ligand Slit (Fig.2) (Brose et al., 1999; Kidd et al., 1999). Up to date three Robo proteins are known to exist in *Drosophila* (Fig 2) one in *C.elegans (*known as SAX-3*)*, two in zebra fish, two in humans and four in mice (Robo1, Robo2, Robo3 (Rig-1) and Robo4) (Challa et al., 2001; Huminiecki et al., 2002; Kidd et al., 1998; Long et al., 2004). Robo4, also known as magic Robo, has not yet been assigned a proven function during nervous system development but is required during angiogenesis and vasculature development (reviewed in Carmeliet and Tessier-Lavigne, 2005).

As with many other protein families, Robo molecules have been classified as members of the same family due to amino acid sequence homology within their extra cellular domains (Kidd et al., 1998). Most Robo proteins contain an extracellular region composed of five Immunoglobulin domains (Ig) and three fibronectin type III (FN3) repeats, a single transmembrane segment and a cytoplasmic domain, which is poorly conserved among Robos (Fig2). Some elegant studies with chimeric receptors provide solid evidence for the importance of the extracellular region of Robo(s) in ligand recognition and interaction. However, the biological response to such interaction is encoded by each receptor's cytoplasmic domain (Bashaw and Goodman, 1999). Robo's intracellular region, in contrast to Robo2 and Robo3, contains four short conserved cytoplasmic sequence motives (CC), which are interaction sites for various signaling proteins (Fig3). Among these are Dreadlocks (Dock) /Nck, a SH2-SH3 adaptor protein that links receptor activation to cytoskeleton rearrangements and can specifically bind to the CC2 and CC3 motifes (Fan et al., 2003; Yang and Bashaw, 2006). Another well studied mediator of Slit/Robo signaling is a member of the actin polymerizing proteins

Ena/VASP (Bashaw et al., 2000). In light of the well known interaction between Ena and Abl tyrosine kinase, the observation that Abl protein can interact with Robo and thus contribute to its signaling, was highly anticipated. Although both Ena and Abl can directly bind the cytoplasmic domain of Robo, the first mediates Robo's repulsive signal, while the second antagonizes Robo signaling (Bashaw et al., 2000) (Fig3). Genetic analyses of the *Drosophila* nervous system development and *Xenopus* growth cone motility provide some hints that the microtubule plus end trafficking protein Orbit/MAST/CLASP mediates Robo signaling downstream of Abl (Lee et al., 2004). In the same study the authors suggest that Abl, acting downstream of Robo can simultaneously regulate the dynamics of the two major cytoskeleton systems, namely actin and microtubules during growth cone response; via Orbit/MAST/CLASP mediates microtubule assembly, and, via the actin binding protein Capulet actin assembly/disassembly. In addition, binding of Slit to Robo can signal via pathways to the small GTP-ases Rac, Cdc42 and Rho promoting actin filament dynamics. The signaling components linking these molecular events are not well understood. More recently Son of sevenless (Sos), a Rac Guanine exchange factor (GEF) was shown to be implicated in the activation of Rac downstream of Slit/Robo signaling. The formation of a multiprotein complex composed of Slit-Robo-Dock-Sos and Rac is thought to be one pathway that mediates a repulsive response at the growth cone of an axon (Yang and Bashaw, 2006).

In addition to their most well understood role during axon development and guidance in *Drosophila* and mammals (Erskine et al., 2000), several studies have shown that the Robo/Slit signaling system can also guide migrating muscles cells, orchestrate the assembly of the *Drosophila* heart tube, regulate neuronal cell migration and contribute to tracheal system development of the fly (Englund et al., 2002; Kramer et al., 2001; Kraut and Zinn, 2004; Piper et al., 2000; Qian et al., 2005). Surprisingly, it was found that during some of these developmental processes activation of Robo via Slit can also elicit a positive influence, such as an attractive response, on cell migration and/or guidance. Hence, given the highly pleiotropic and bifunctional roles of Robo it is tempting to speculate that intracellular events downstream of receptor activation are more complex, involving other molecular players that still need to be identified.

Slit, similarly to Robo, was also identified in a genetic screen, of factors that control embryonic patterning defects in *Drosophila* (Nusslein-Volhard C, 1984). The protein obtained its "historical" function as a "classical" axon guidance cue, once it was isolated in a genetic screen for molecules involved in commissural axon path finding (Hummel et al., 1999; Seeger et al., 1993). In *slit* null mutant embryos all axons collapse together at the midline of *Drosophila* CNS (Kidd et al., 1999; Li et al., 1999; Rothberg et al., 1990). The *slit* loss-of-function phenotype together with the functional analyses for all Robo proteins revealed that Slit, expressed by midline glial cells acts as both a short-range and long-range repellent signal through Robo(s) to prevent ipsilateral axons from crossing the midline and commissural axons from recrossing. Axons expressing different combinations of Robo proteins show distinct sensitivity to Slit and accordingly project away from it by following specific lateral pathways along the CNS midline (Rajagopalan et al., 2000a; Rajagopalan et al., 2000b; Simpson et al., 2000a; Simpson et al., 2000b). This function of Robo(s) and their ligand Slit is conserved among species, since similar phenotypes have been observed in nematodes, zebrafish or knock-out mice for Slits proteins. To date, there are three Slit proteins identified in mice (Slit-1,Slit-2 and Slit-3)(Long et al., 2004) and only one in *Drosophila*, two in zebrafish and one in worms (Hao et al., 2001; Hutson et al., 2003).

The molecular structure for all Slit proteins is well characterized and known to be composed of a series of four leucine-rich repeats (LRRs), seven to nine epidermal growth factor (EGF)–like domains, a laminin G-domain and a C- terminal cysteine rich domain (Fig 2) (Kidd et al., 1999). Most Slit proteins are cleaved within the EGF-like region, although it is not yet clear what the biological impact of this cleavage is. (Brose et al., 1999; Wang et al., 1999)(Fig2). *In vitro* experiments suggest that the C-terminal fragment of Slit mediates repulsion at the growth cone, while the N-terminal fragment has an opposite, rather positive effect acting as a branch promoting factor for axons (Wang et al., 1999).

Biochemical analyses have provided the structural basis for Slit recognition by Robo. Slit's second LRR domain appears to be the binding site recognized by the extracellular Ig domains 1 and 2 in all three receptors, Robo, Robo2 and Robo3 (Fig3) (Howitt et al., 2004; Liu et al., 2004).
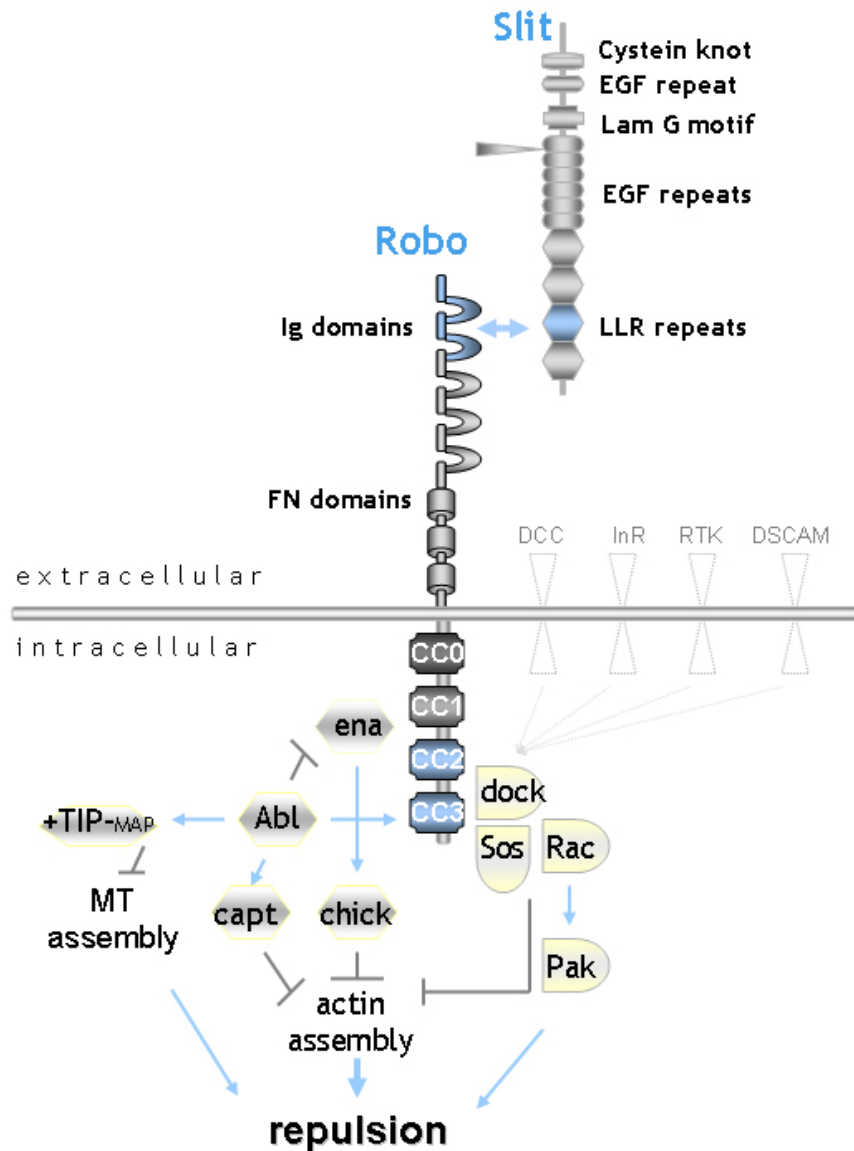
FIGURE 3. Slit/Robo signaling cascade at the growth cone of an axon.
Binding of Slit to Robo results in recruitment of Dock, a SH2-SH3 adaptor which can further activate SOS, a Rac GEF, followed by activation of Rac. Formation of this protein complex promotes cytoskeletal rearrangements leading to growth cone repulsion. Genetic and biochemical experiments provide some evidence that Dock, Rac and Pak function together to couple Robo receptor activation to the regulation of actin cytoskeleton. Another pathway that mediates repulsion independently of Dock is via Ena. Binding of Ena to Robo is thought to block actin assembly through Profilin (Chick). Phosphorylation of the CC3 motif of Robo via Abl has an antagonistic effect on Ena binding to Robo. Simultaneously, when bound to the CC3 motif of Robo, Abl can influence the dynamics of the two major cytoskeleton components; actin and microtubules. Capulet and Orbit/MAST/CLASPS molecules have been identified to be some of the players involved in these processes.

29

1.4. *Drosophila melanogaster* and its PNS as a model system to study denditogenesis.

What makes **Drosophila melanogaster** such a successful model organism is the power of genetic screens to identify molecules involved in a biological process of interest (reviewed in Adams and Sekelsky, 2002; St Johnston, 2002).

The entire genome of the fly has been sequenced (Myers et al., 2000) and already for the fifth time resequenced, providing us with quite reliable and detailed information about the genes and their organization on the four chromosomes that comprise the *Drosophila* genome. The Release 5.1 annotation of the heterochromatin region of the *Drosophila* genome has been published recently, filling many of the gaps of unsequenced regions of the genome and adding an additional ~250 protein coding genes to the ~15,000 identified to date (Smith et al., 2007).

Another great advantage the fly offers as a model organism is low maintenance cost and simple genetics. It takes only around 10 days for one generation to mature, allowing the full developmental process to be followed in a very short period of time. Furthermore, there are many genetic tools and fly lines available, allowing the manipulation of almost any gene of interest.

the PNS of Drosophila

a model system to study dendrite development
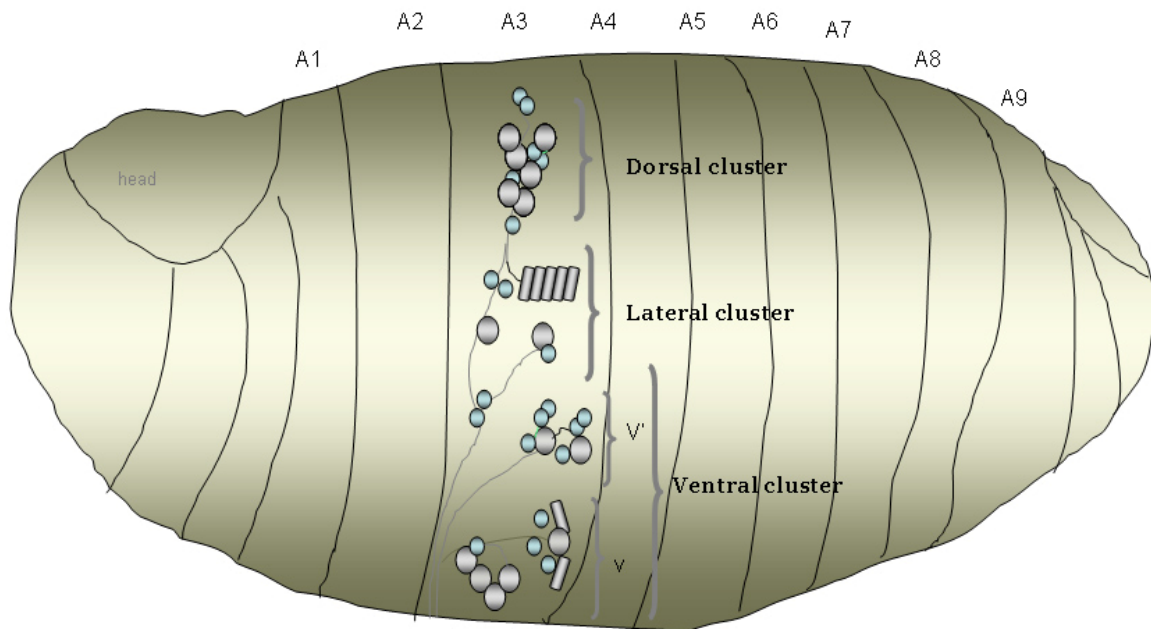
FIGURE 4. The PNS of *Drosophila*; a model system used to analyze dendrite field development.
Each abdominal segment, depicted here as A1 to A9 contains three clusters of PNS neurons, organized in a highly stereotyped manner. Due to the position of these clusters we distinguish dorsal, lateral and ventral clusters of sensory neurons. In addition the ventral cluster is separated into ventral prime and ventral. The dendrite arborization neurons are depicted as big gray circles. Smaller blue circles represent other types of sensory neurons, such as chordotonal, bipolar or tracheal.

Using these advantages, the laboratory of Yuh Nung Jan at UCSF-USA generated a Gal4-UAS-GFP enhancer trap fly line assigned as a ***80G2*** in which it was possible for the first time to visualize dendrite projections of the highly arborized multidendritic neurons of the *Drosophila **Peripheral Nervous System (PNS)*** in detail. (Gao et al 1999). In this line, a Gal4 construct inserted in a tissue specific manner drives the expression of the GFP (green fluorescence protein) protein and allows the genetic visualization of dendrite projections of all multidendritic arborization neurons, the bipolar neurons, the tracheal

innervating neurons and the chordotonal neurons (Gao et al 1999). These neurons, together with the remaining sensory neurons which are not visualized in the 80G2 line, form clusters within each abdominal segment of the *Drosophila* embryo. Thus, we distinguish a ventral, lateral and dorsal cluster of neurons within the PNS with a highly stereotyped organization (Bodmer et al., 1989) (Fig4).

The advantages the 80G2 line offers are several; labeled with GFP genetically, the cell bodies, the axons and the whole dendrite tree are nicely and stably visualized throughout the whole development of *Drosophila*. Located directly under the transparent epidermis of the embryo, these neuronal processes can be directly observed in living intact animals. The dendrites of PNS neurons project their fields in a two-dimensional space, pressed between the muscles and the epidermis of embryo or larvae, allowing for easy observation of each single branch.

In vivo time-lapse imaging and developmental analysis of the dendrite trees of md-da neurons revealed that the dendrite field morphology at embryonic stage 18-20h AEL (after egg lying) is highly stereotyped among animals, suggesting that this development is under a genetic control. Further analysis at a single cell level revealed that the dorsal cluster of md-da neurons is composed of six dendritic arborization neurons, which due to morphological differences, have been subdivided into four different classes, ranging from Class I with the simplest morphology to the Class IV with the most complex (Fig5) (Grueber et al., 2002; Grueber and Jan, 2004). Each of these neurons projects its dendritic tree in a preferentially dorsal direction and its axon along a ventral pathway (Fig5).
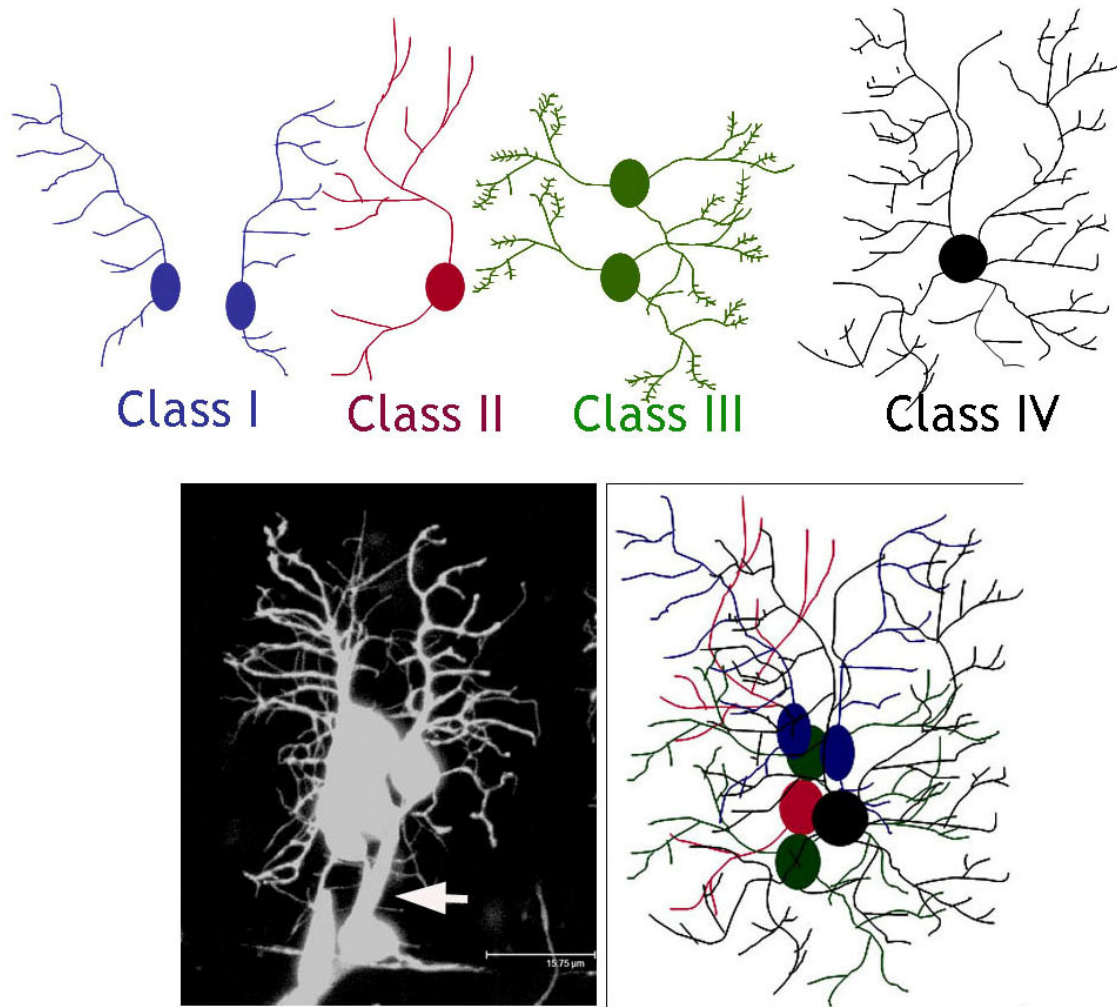
FIGURE 5. **Multidendritic arborization neurons of the *Drosophila* PNS; schematic view of the four different Classes;**
Based on morphological characteristics the dendritic arborisation neurons have been subdivided into four different classes; Class I (depicted in blue), the morphologically simplest class of neurons develop only a few primary branches, laterally oriented secondary branches and few tertiary branches. Class II neurons (red) develop a simple dendrite tree, similar to Class I. Class III neurons (green) develop several primary, secondary and tertiary order branches, which are decorated with short filopodia-like protrusions called spikes. There are only three Class IV neurons per abdominal segment. These are morphologically the most complex type of neurons, whose dendrite tree covers the whole abdominal dorsal/lateral or ventral segment. Depicted are only the cell bodies with their dendrite projections. All four classes of neurons are organized in a cluster as represented in a living intact embryo (image on the left, scale bar 16µm) or schematically (image on the right).White arrow points to the axons.

This highly stereotyped pattern of dendrite field organization, and the mentioned above advantages that *Drosophila melanogaster* offers as a model organism led to the design of a genetic screen on the second chromosome, aiming to identify recessive lethal mutations that affect dendrite routing, patterning and outgrowth (Gao et al 1999).

1.5 The Role of Robo during dendrite filed development

Three studies have addressed the role of Robo(s) and their ligand Slit during dendrite differentiation; so far the only *in vivo* work, as previously mentioned, has demonstrated a guidance role for Robo, but not Robo2 or Robo3 receptors during motor neuron dendrite growth at the CNS of *Drosophila* (Furrer et al., 2003). Given the model system used in this study it was difficult to asses whether further aspects of dendrite development such as growth and/or branching are also under the control of Robo protein. Such a role for the protein has indeed been demonstrated in a study from Ghosh and M. Tessier-Lavigne labs showing that Slit mediated receptor activation can induce more growth and branching for dendrites of rat cultured cortical neurons (Whitford et al., 2002). However, given the technical limitations and the complexity of a rat brain, this study could not further demonstrate that such function for Robo is present also *in vivo*. Studies on the giant fiber motor system of *Drosophila* suggest that this molecular system might indeed act to regulate the growth of dendrites, and furthermore be involved in synapse formation. Certainly, a weak point in their work is the lack of evidence demonstrating an endogenous role of Robo during these processes (Godenschwege et al., 2002).

Taken all these evidence together, it is not yet clear what the role of the Robo receptor and its ligand Slit is during dendrite morphogenesis *in vivo*.

The aim of my PhD work;

Given the advantages of the *Drosophila* PNS as a model system, and particularly the dorsal multiple dendritic arborisation neurons, I tried to elucidate what the physiological role of the Robo receptors and their ligand Slit is during dendrite field development.

To dissect the function of the Robo proteins during dendritogenesis:

1. I performed detailed developmental analyses of dendrite field formation of md-da neurons and compared how dendrite morphogenesis differs in animals completely lacking Robo function or overexpressing the protein in their md-da neurons.

2. With the help of cell-class specific genetic markers, I observed that Robo acts cell-class specifically and is required during dendrite field development of the morphologically most complex classes of md-da neurons, Class IV.

To assess whether this functions is cell-autonomous

3. I performed expression pattern analyses, rescue analyses and generated single cell mutant clones with the MARCM (mosaic analyses with a repressible cell marker) technique.

To assess how Robo might mechanistically regulate dendrite branch formation

4. I performed time-lapse analyses of dendrite field development Class IV neurons overexpressing Robo protein.

To assess how the ligand Slit specifically activates Robo during dendritogenesis;

5. I performed expression pattern analyses, ectopic expression experiments and addressed possible cell-autonomous function for that protein by doing MARCM for Slit.

Biochemical and genetic data have shown that Dock, an SH2-SH3 adaptor protein and Ena, a member of the VASP family of proteins, can act downstream of Robo at the growth cone of an axon.

6. By doing loss-of-function analyses for *ena* and *dock,* I tried to elucidate whether these molecules are acting downstream of Robo during dendrite field development of md-da neurons.

Finally, the presence of an axon guidance phenotype in *robo2* but not *robo* and *slit* single mutants or *robo, robo2* double mutants raised the question about the role of Robo2 during axon guidance of md-da neurons; to address this question

7. I performed phenotype analyses of the axonal projections of md-da neurons in different genetic combinations and compared their phenotypes to those of control animals.

The initial idea for the project was based on the identification and characterization of a single mutant allele named "*girandola*" which was isolated in ethyl methane sulfonate (EMS) mutagenesis screen performed in Y.N. Jan's lab at UCSF and classified as a line with dendrite overgrowth and routing phenotype. Mutation identification revealed that *girandola* is a new *robo2* allele. This led me to the thorough analyses of the role of Robo receptors and their common ligand Slit in dendrite differentiation.

2. Results

2.1. Identification and characterization of the *girandola* mutant

2.1.1 Mapping the *girandola* mutation

girandola is a single mutant allele isolated from the chemical (EMS) mutagenesis screen performed in Y.N.Jan's lab at UCSF (Tavosanis G., Cox D., Grueber W. unpublished data). The goal of the screen was to isolate recessive lethal mutations, localized on the second chromosome of *Drosophila* affecting dendrite branching, routing and outgrowth. The EMS mutagenesis was performed on 80G2 flies in which Gal4 drives the expression of GFP in all 6 md-da neurons, together with a bipolar, and a tracheal neuron. This was an F_3 screen (see crossing scheme) in which EMS induced recessive lethal mutations, causing gross dendrite defects, could be directly monitored. This was possible because of the nicely and stably genetically labeled dendrites of md-da neurons which elaborate their dendrites just underneath the transparent epidermis of a *Drosophila* otherwise homozygous mutant embryo.

Crossing strategy used to isolate recessive lethal mutants on the second chromosome of 80G2 line;

F_0 ♂ 80G2 (+ EMS)   x   ♀ yw; Pin/CKG

↓

F_1 ♂ 80G2,* /CKG   x   ♀ yw;Pin/CKG   (*…stays for mutation)

↓

F_2 ♂♀ 80G2,* /CKG   - **mutant stock**   screen for lethality

↓

F_3 ♂♀80G2,*…………screen homozygous mutant embryos for
                        dendrite defects
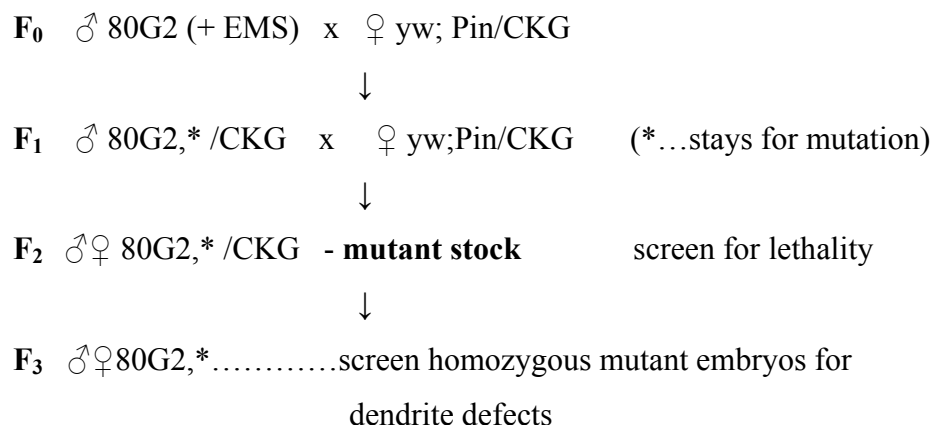
The mutation in the *girandola* gene causes dendrite routing and overgrowth defects of md-da neurons. The penetrance of the phenotype is 100%, however the phenotype varied from animal to animal (Fig 6).
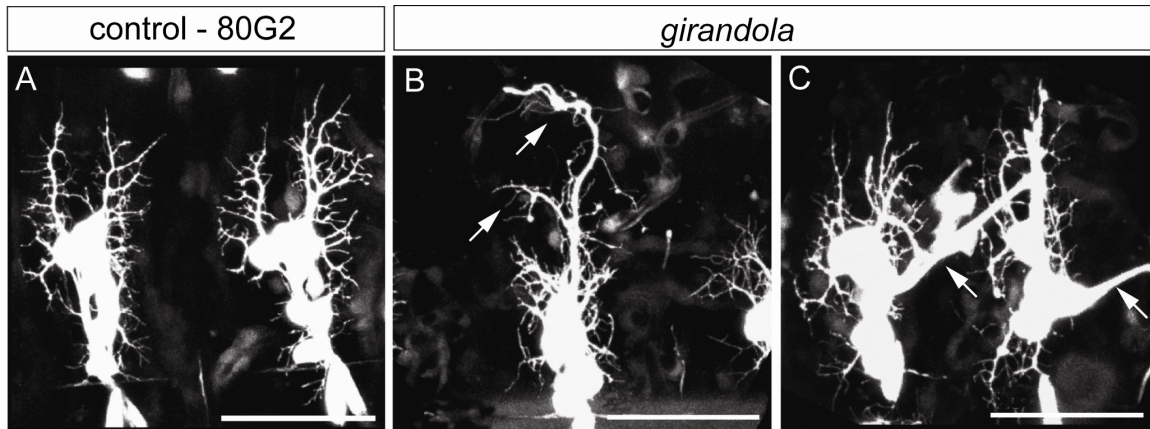
FIGURE 6. Misprojection of neurite processes in *girandola* mutant embryos. Confocal images of dorsal cluster of md-da neurons in 80G2 (control) **A)** and *girandola* mutant embryos at embryonic stage ~18h AEL **B) and C)** Arrows show the abnormally projecting neuronal processes. Scale bars; **A)** 35µm **B)** and **C)** 25 µm. Dorsal is up, anterior is right.

In wild type animals at 18h-19h AEL, the dendrite field of md-da neurons show highly stereotyped very characteristic features (Fig 6A). There are two dorsally projecting bundles of dendrite processes oriented parallel to each other. From these two main bundles of dendrites, laterally oriented, secondary and higher order branches grow anteriorly and posteriorly, towards the adjacent segment boundaries of an abdominal segment (Fig 6A). This quite stereotyped principle of dendrite field organization is lost in g*irandola* mutants. Several neuronal processes (dendrites or axons) exhibited abnormal routing and growth towards the dorsal midline or the adjacent abdominal segment boundary. Often these processes are fasciculated and overshoot the dendrite field (Fig 6B and 6C, arrows). This pattern of dendrite arborization defects, appeared not in all but only in few dorsal abdominal segments of *Drosophila* embryo, corresponding to ~ 28% expressivity of the phenotype (n=27/96 segments of 14 embryos). In the most severe cases, these overgrowing processes formed a loop, a phenotype suggestive for the name *girandola* (*girandola* means "windmill" and was named by Dr. G. Tavosanis). These defects in neurite projections were initially classified as a dendrite specific phenotype and

suggested that the gene affected in *girandola* mutant is required during dendrite field development of dorsal abdominal md neurons.

First, we started with mapping the *girandola* mutation;

The localization of a recessive lethal mutation on a chromosome involves tree major steps; rough mapping, fine mapping and cloning the gene and identification of the mutation (Fig.7)
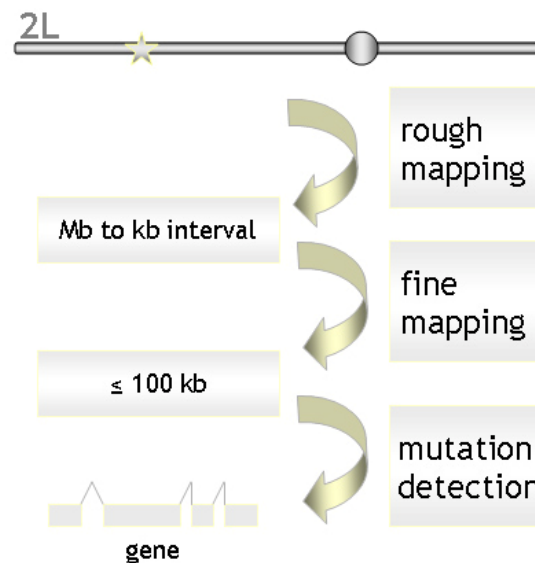
FIGURE 7. **Schematic outline of the principle of gene mapping**.

The grey bar represents a chromosome (mainly the second left one (2L)) that contains a mutation to be identified (depicted as a star). First, a rough mapping step allows determination of a region that can span up to Mega base (Mb). A fine mapping step leads to further narrowing down a mutant interval to less then 100 kb. The final step is the positional cloning of the gene and mutation identification.

The Deficiency (Df) mapping assay can be used for a rough mapping test. A public center, the *Bloomington stock center*, provides scientists working with *Drosophila*, with a whole collection of fly lines, containing a deleted chromosomal region. Thus collections of Deficiency lines uncovering the second, the third or the first chromosome almost completely; (percentage of coverage; 93% for second right (2R) chromosomal arm and 94,8% for second left (2L) chromosomal arm; http://flystocks.bio.indiana.edu/Browse/df-dp/dfkit-info.htm) can be used to screen a whole chromosome of interest at once.

Each Df line contains a relatively large chromosomal deletion (more than 100kb, often Mb) defined as cytological positions on the *Drosophila* chromosome.

To perform this assay *girandola* mutant males were crossed with virgins of each Deficiency lines for the second chromosome. By doing this, around 40 crosses are obtained (due to the number of lines that a Df kit for the second chromosome contains); as a first step, the progeny of each of that cross was screened for lethality. Three of the Deficiency lines, Df(2L)ast4, Df(2L)ast2 and Df(2L)S3 failed to complement the *girandola* mutant. This and the complementation result of Df(2L)BSC16 with *girandola* allowed localizing a recessive lethal hit on the second chromosome, determined by the cytological numbers 21C8 (given by the right breakpoint of Df(2L)BSC16) and 21E1, (given by the left breakpoint of Df(2L)ast5). The next step was to define whether the mutant interval containing the lethal mutation is responsible for the dendrite phenotype in *girandola* embryos. Animals carrying the *girandola* allele in trans to either Df(2L)ast5(n=11/11 embryos) or Df(2L)ast2(n=12/15embryos) showed the same dendrite field projection defects as observed in *girandola* homozygous mutant embryos. Surprisingly, embryos transheterozygous for the *girandola* allele and Df(2L)ast6 (n=0/25) and Df(2L)ast4 (n=0/13 embryos), revealed normal dendrite architecture comparable to those of control animals (in this case embryos transheterozygous for 80G2 chromosome and the appropriate Df line).The complementation and phenotype analysis allowed the definition of a new interval of the gene causing the *girandola* phenotype, namely between the cytological numbers 21E2-22A1 (determined by the two breakpoints given by Df(2L) ast5) (Fig.8). This is a relatively large region of ~370kb containing ~57 genes.
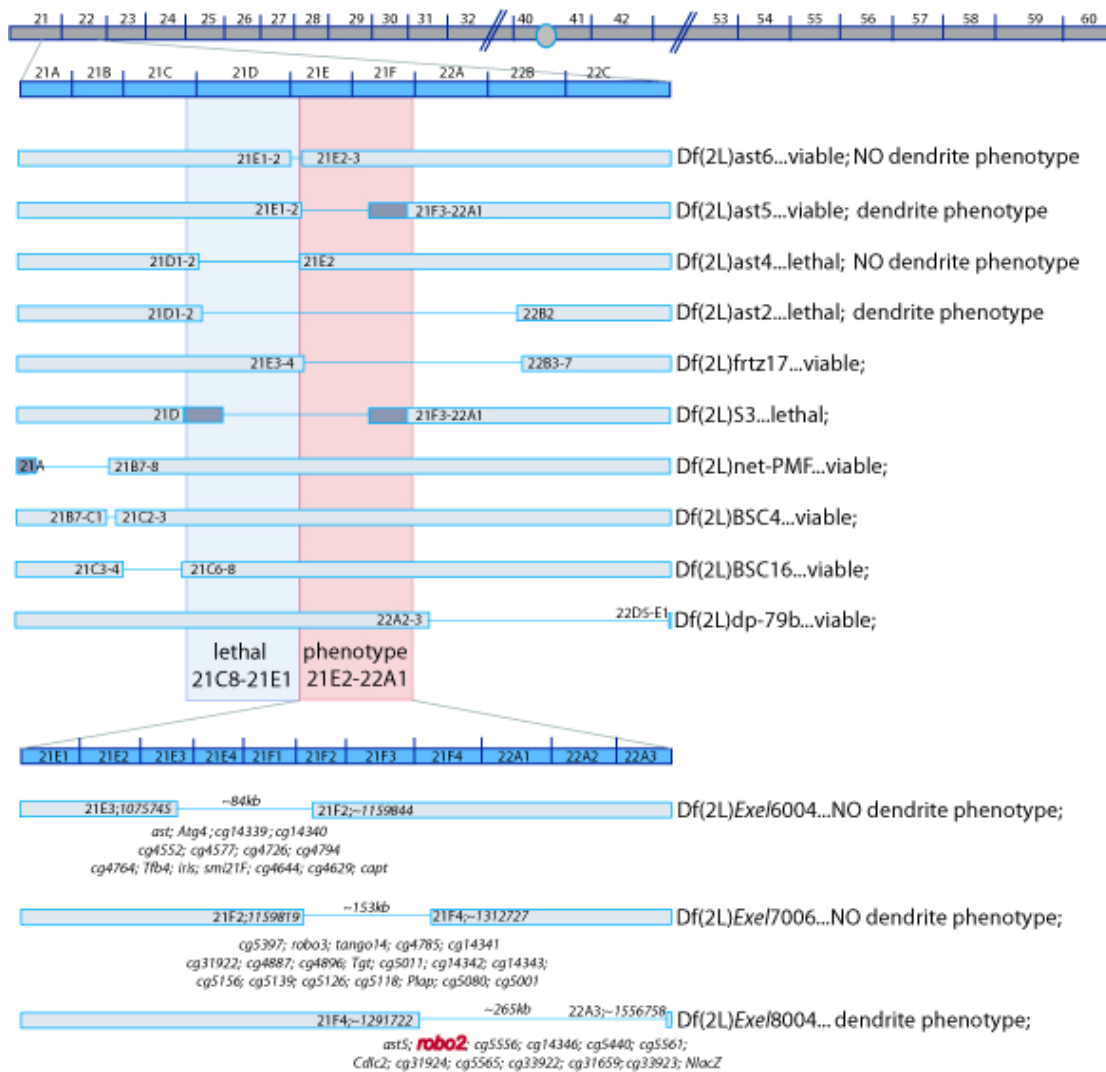
FIGURE 8. Schematic view and summary of the informative results of the Df mapping test.

The second chromosome is indicated as a dark gray bar. Depicted are the cytological numbers, the circle represents the centromere. The blue bar is a magnification of the 21st and 22nd cytological region of the second left arm of the chromosome where *girandola* mutant interval and a region of a recessive lethal mutation were determined. A magnification of the ~370kb "*girandola*" mutant interval (21E2-22A1) is depicted also as a blue bar.

3 Excelixis Df lines having deletions within that region allowed the further narrowing down of the *girandola* mutant interval to a region determined by the left breaking point of Df(2L)Exel8004 and the right breaking point of Df(2L)ast5. This ~120kb interval contains only 13 genes, the largest is *robo2* (*lea*).

Once a mutation has been localized on the chromosome, the next step is a fine mapping, which aims to further narrow down the region of interest to a low number of genes. The final step is the map based positional cloning of a gene and mutation detection (Fig7).

For the fine mapping step we used newly generated Deficiency lines obtained via a P-mediated excision. In these lines the deleted fragment of the chromosome is very small (a few hundred kb) and exactly determined to the level of a single nucleotide (Parks et al., 2004). Three such "Excelixis" Df lines spanning the girandola mutant interval were chosen. Phenotype analyses of embryos carrying any one of the three Df chromosomes in trans to the *girandola* allele, allowed further narrowing down the *girandola* region to ~120kb (Fig.8). This region contains only thirteen genes and the best candidate among those was *robo2 (*known also as *lea*), for the following reasons:

First, the function of *robo2* during nervous system development in both CNS and PNS of *Drosophila* has been previously demonstrated (Rajagopalan et al., 2000a; Rajagopalan et al., 2000b; Simpson et al., 2000a; Simpson et al., 2000b; Zlatic et al., 2003).

Second, it is the largest gene in the region. EMS binds preferentially Guanine or Cytosine, and genes are CG rich, suggesting that larger genes are more accessible for mutagenesis.

Third at the time point of mapping, a study by the Whitington lab described a role for *robo2* during axon guidance of PNS neurons of *Drosophila* The axonal phenotype of dorsal sensory neurons described in their work strongly resembled the one of *girandlola* mutants (Parsons et al., 2003).

Proving the finding that *girandola* may indeed be a new *robo2* allele.

The first hint came from the phenotype analyses of embryos transheterozygous for *girandola* and a *robo2^8* (null) allele. These showed the same defects of misprojected neurite as the one in *girandola* homozygous mutants (data not shown).

Secondly, DNA from *girandola* homozygous embryos was isolated and the complete open reading frame of the gene was sequenced. We identified a nonsense mutation in the 13th exon of the gene, coding partially for the cytoplasmic region of the protein. Such a

mutation leads to an amino acid alteration in the protein sequence from AAG (Lys_{1284}) to

TAG, creating a translation-termination (Fig9).
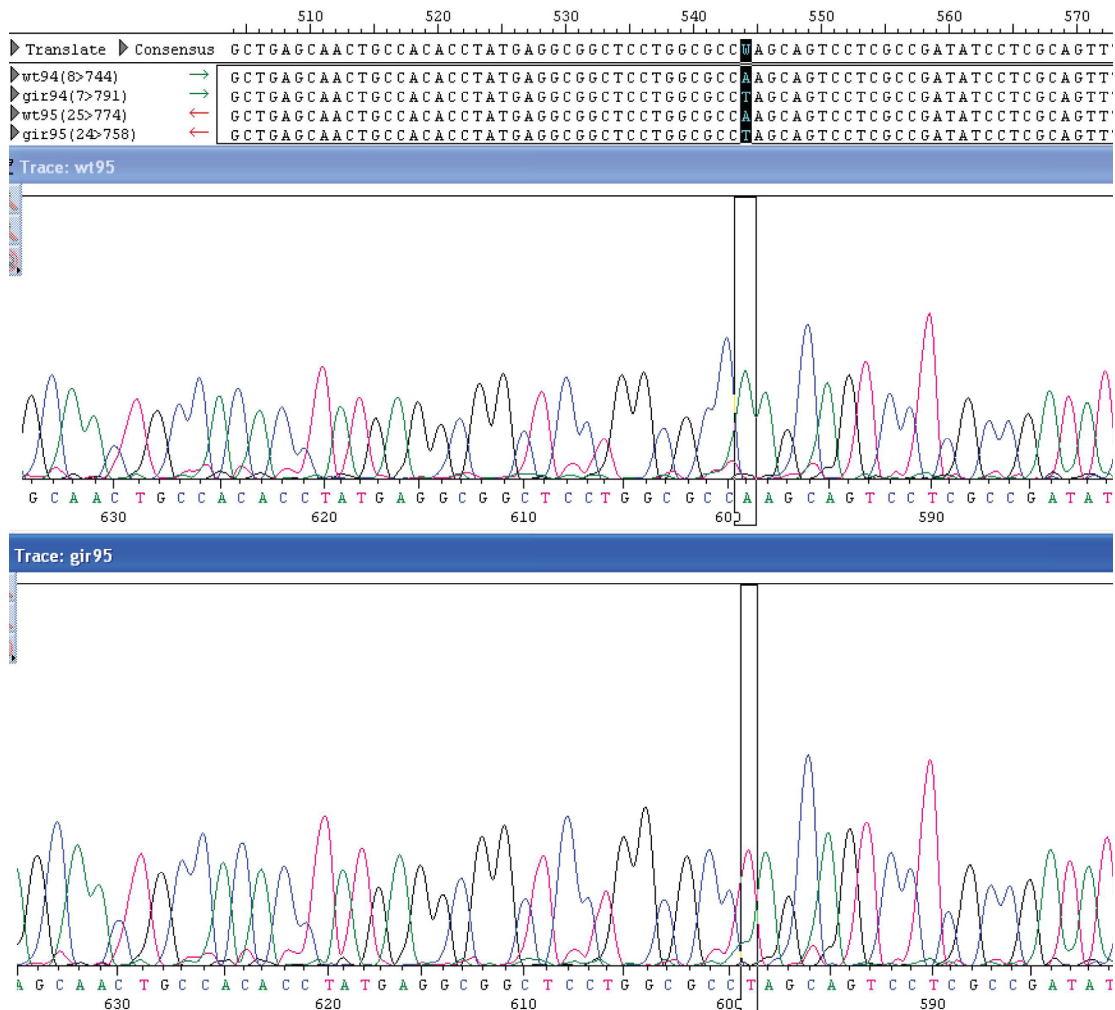
FIGURE 9. **Sequencing of *robo2^girandola* and mutation identification.** The nucleotide sequence region showing the nucleotide exchange causing a missense mutation in *robo2^girandola*. At an **A** position (green peak) in 80G2(control) animals, corresponds a **T** (red peak) in *girandola*. This nucleotide exchange results in an alteration from Lysine to a Stop signal.

Lack of Robo2 function results in defects of the third axon fascicles (second + third fused

together), midline crossing defects and/or occasional breaks or fasciculation errors in the

first and second fascicle (Rajagopalan et al., 2000a; Rajagopalan et al., 2000b; Simpson

et al., 2000a; Simpson et al., 2000b). The phenotype can be visualized when axons of the

CNS are stained with antibody recognizing the cell-adhesion molecule Fasciclin II (Lin et al., 1994). Therefore, we performed anti-FASII staining in wild type, $robo2^9$ (hypomorph) and *girandola* mutant filet embryos and compared how axons at the CNS midline of *Drosophila* project in all these tree different genotypes (Fig 10). The very similar axon guidance defects in both *girandola* and $robo2^9$ homozygous mutant embryos further support our finding that in the *girandola* mutants the affected gene is a new *robo2* allele. Quantification of the phenotype and its expressivity revealed that indeed the number of segments showing midline crossing defect or fusion of the second and third fascicles was comparably similar in both *girandola* and *robo2* mutants (table 1).

	girandola	*%*	$robo2^9$	*%*
(2+3) fused fascicle	38/165 segments	23%	39/140 segments	28%
Midline crossing defects	18/165 segments	11%	21/140 segments	15%

TABLE 1 *Midline crossing defects in girandola and robo2⁹ mutants*

Finally, we looked at how the axon of dorsal sensory neurons project. To label these neuronal processes, we used an antibody raised against the MAP-1b protein (the *Drosophila* futsch). This antibody allows nice visualization of the axons of all sensory neurons of the PNS and motor neuron axons of the CNS of *Drosophila*. (Hummel et al., 2000). Both *girandola* mutants and $robo2^9$ mutants showed similar PNS axon guidance defects, with comparably similar expressivity of their phenotypes; 33% for *girandola* (n=32/98 segments) and 38% (n=35/91segments) in $robo2^9$ (Fig 10D, 10E and 10F arrows).

In summary, sequence and phenotype analyses strongly indicate that *girandola* is a new *robo2* allele. Based on genetic and molecular criteria, we think that this is a new hypomorph allele.
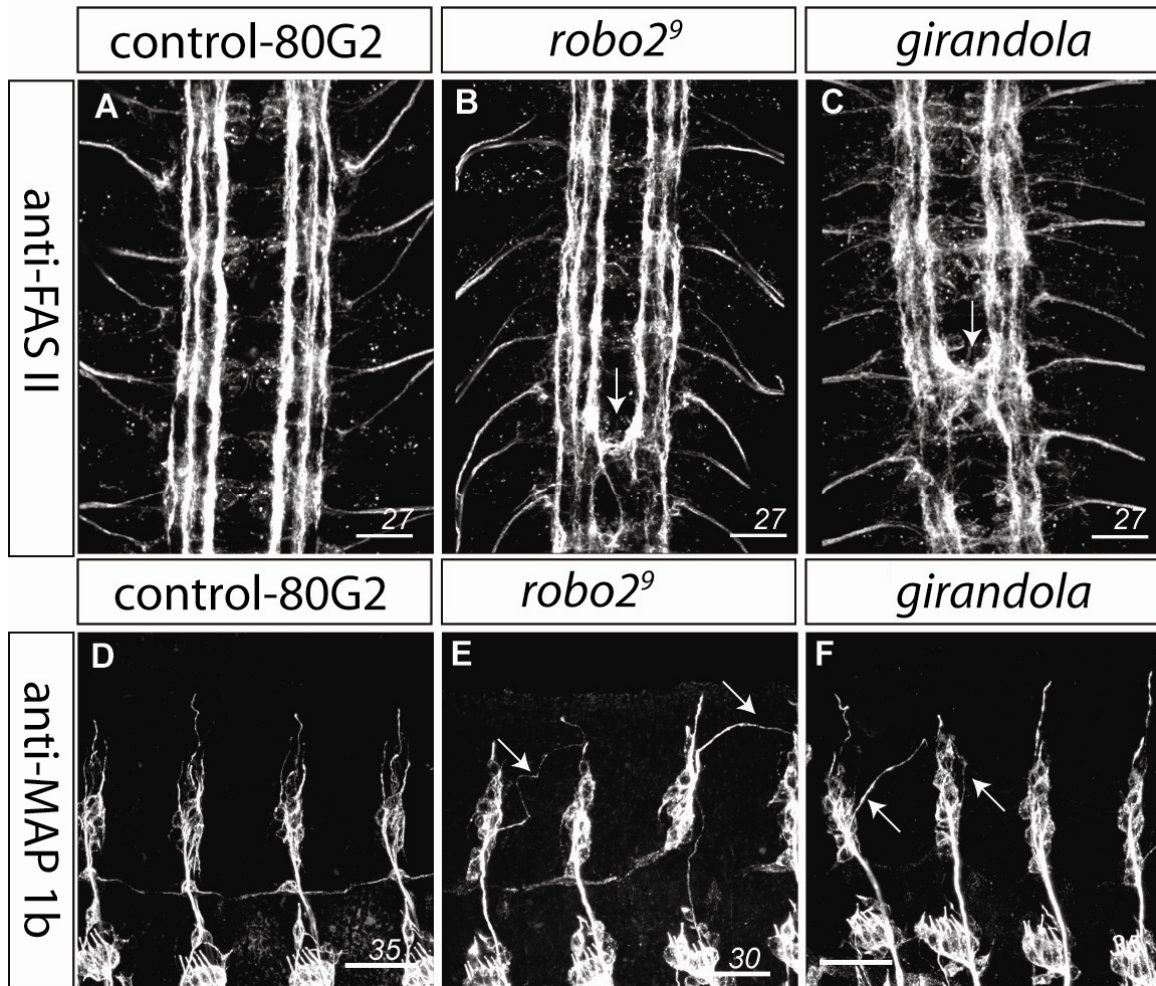
FIGURE 10 CNS and PNS axonal misprojections in *girandola* and *robo2*[9] (hypomorph) embryos are similar.
A), **B**) and **C**) confocal images of filet embryos in which the tree axonal fascicles projecting along the CNS midline of *Drosophila* were visualized via anti Fasiclin II staining. Similar axon guidance defects were observed in both *girandola* and *robo2*[9] mutants (arrows in **B** and **C**). Scale bars; 27µm
D), **E**) and **F**) confocal images of the dorsal cluster of neurons and their axonal projections visualized via immunolabeling against futsch (MAP1b). Similar axon guidance defects are produced in both *girandola* and *robo2*[9] mutant embryos (arrows in **E** and **F**). Scale bar; 35 µm

2.1.2 Characterization of the *robo2^girandola* mutant

While analyzing the axon guidance PNS phenotype of both *robo2^9* and *girandola* it became clear that whole fascicle of dorsal sensory axons were often growing dorsally, within the dendrite field. Thus, the axonal phenotype cast the primary role of *robo2* during dendrite field formation into strong doubt. Therefore, we performed a set of experiments aimed at understanding whether *robo2^girandola* has, if any, a role during dendrite field formation of md-da neurons.

Taking advantage of the different time points of axogenesis and dendrtitogenesis of md-da neurons (Gao et al., 1999), we next analyzed ~14h AEL old embryos and asked how dendrite outgrowth is initiated in dorsal cluster of neurons also showing axon patterning defects. In all of the analyzed embryos, neurons with misguided axons did show normal dendrite outgrowth or projection of their primary dendrite branches (Fig.11A and 11A1 arrows point to misguided axons coming from a neighboring cluster of neurons, arrowhead points to a normally projecting newly formed primary dendrite branch).

Looking at later time points, it became evident that by 18h-20h AEL, in *robo2^girandola* mutants 30% of the dorsal cluster of md-da neurons showed axon guidance defects only, and the remaining 70% of dorsal cluster md-da neurons showed both, axonal plus dendrite phenotype (Fig.11C, 11D, arrows indicate misguided axons). We could not observe dorsal md-da cluster of neurons showing only a dendrite phenotype.

Taken together, the observations described here suggest that the observed dendrite defects in *robo2^girandola* mutants are due to misguided axons, suggesting that removing *robo2* function severely affects axonal projections primarily, but not dendritogenesis.
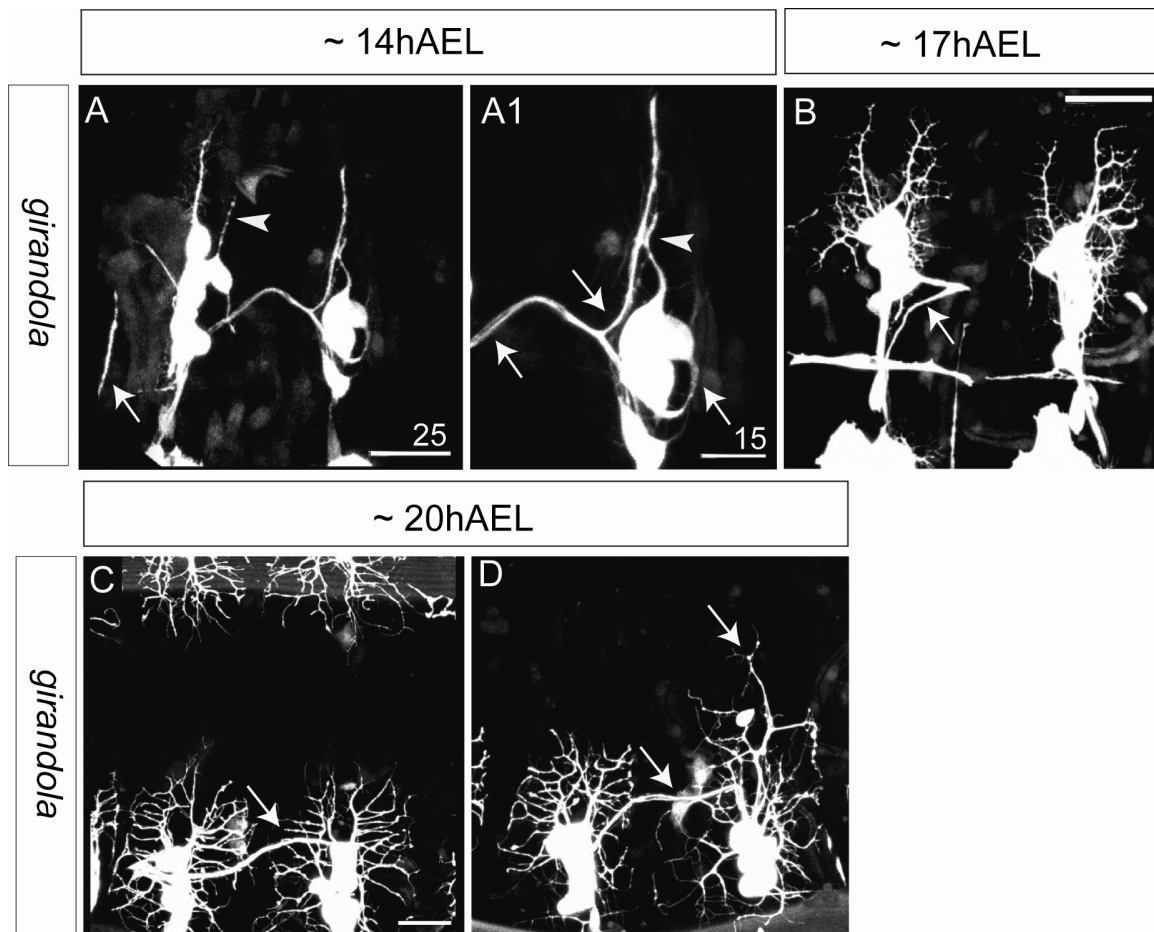
FIGURE 11. Axons affect dendrite field projection in *girandola* mutants
A) and **A1**) ~14h AEL old embryos, misprojecting axons from a dorsal cluster of neurons are innervating the future dendrite field of the neighboring dorsal cluster (arrows). The initiation of dendrite outgrowth in these affected clusters of neurons looks normal (arrowhead). **B**) An example of a ~17hAEL old embryos in which a dorsal cluster of neurons show an axon guidance defects but not dendrite field developmental defects. **C**) and **D**) two different examples of older embryos (~20h AEL) reminiscent of those shown in **A**) and **B**) and putting forward the idea that the dendrite field development in *girandola* mutants are caused by the misguided axon. Scale bars 25μm

2.3. Developmental analysis of dendrite arborization neurons of control animals during late embryonic/larval stages.

We next looked at how dendrite field development of md-da neurons proceeds during late embryonic/larval stages. We performed detailed developmental analyses on dendrite formation of md-da neurons starting from 20h AEL until the entire receptive area of the *Drosophila* epidermis was fully covered with dendrites; this happens by the end of second instar larvae stage (data not shown; and see Fig 20) To investigate this, we used the 80G2 line which allows a clear and detailed visualization of the dendrites of all 6 md-da neurons (Gao et al., 1999).

In vivo time lapse imaging of embryos/larvae would require anesthetizing the animals. To avoid this and the possible artifacts such experimental conditions might cause (Grueber et al., 2002; Medina et al., 2006), we examined the dendrite development of md-da neurons by imaging 18-20 different animals per given time point (Fig.12).

20hAEL	21hAEL	22hAEL	23hAEL	24hAEL
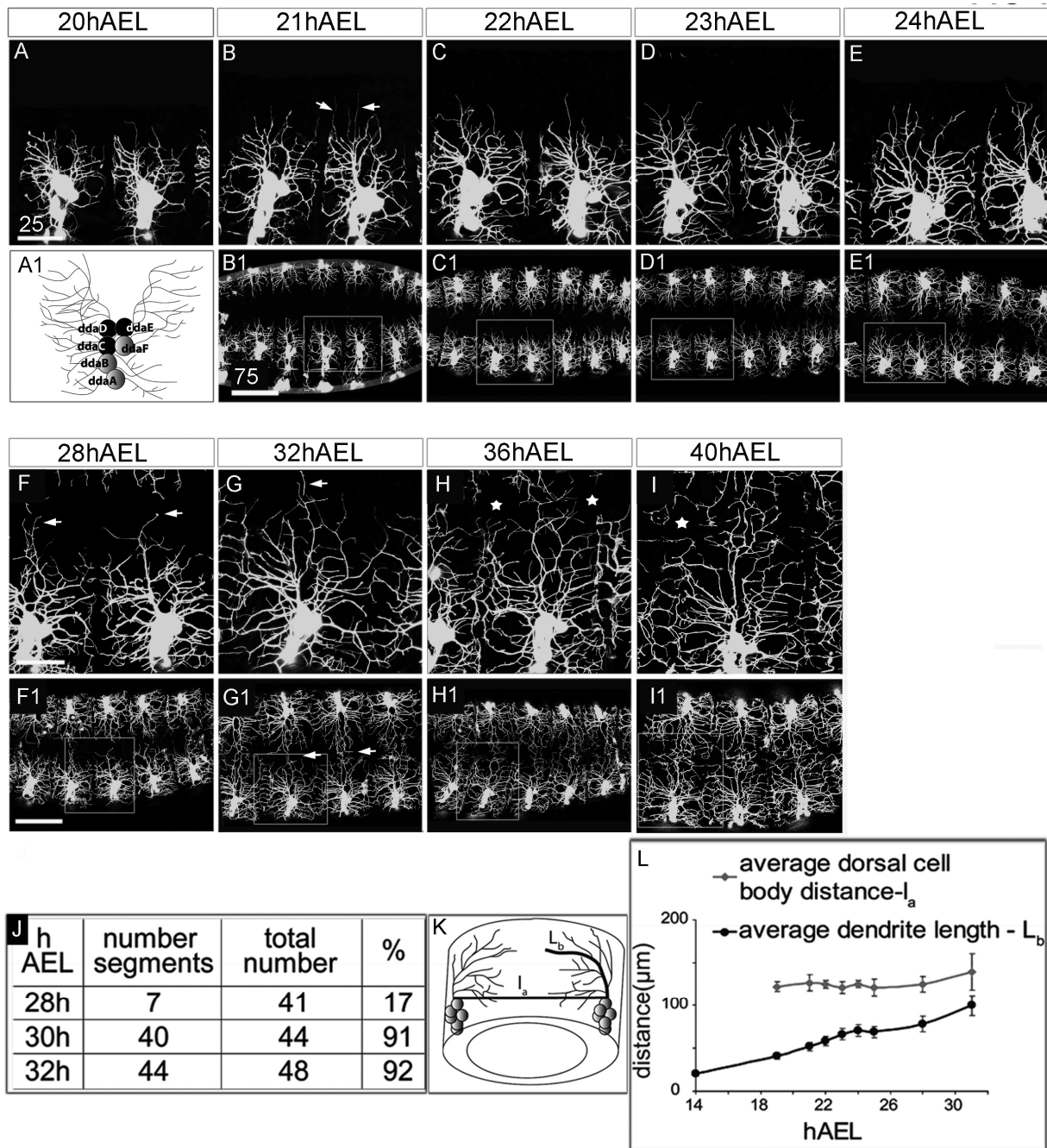
FIGURE 12. Dendrite field development of dorsal abdominal clusters of neurons in 80G2 animals. A1) a schematic view of all 6 md-da neurons. **B-I)** Confocal images representing an abdominal segment of a late embryo/larva (B1-I1 squares) at each of the time point analyzed. Starting from 20h AEL **A)** and analyzing 8 different time points it appears that the process of dendrite field development is stereotyped during late embryonic/larval stages. Innervation of the dorsal midline is a step-wise process, starting first at ~32h AEL (G). At 36h or even 40h AEL, dendrite-free areas can still be found dorsally (stars in H and I)**.**

J) Percentage of abdominal segments for which dendrites meet at the dorsal midline supporting the observation that dorsal midline innervation happens continually during 1st instar larval stage. **K)** Schematic view representing the principle of the quantification depicted in the graph in **L**) Measuring the average longest dendrite projecting dorsally for each of the time points analyzed revealed that this process happens linearly with the time. L_b average dorsal cell body distance. L_a average dendrite length Scale bar A-I is 25µm. B1-I1 is 75 µm. Dorsal is up, anterior is right.

Summary of observations of dendrite field development:

Between 18h-20h AEL the dendrite field of da neurons was eventually stabilized and its size seemed to be determined by the morphologically simplest class of neurons, Class I (ddaE and ddaD) (Fig.12A1). At 21h AEL, the dendrite field of an abdominal dorsal cluster of da neurons did not differ visibly significantly from that at 20h AEL. There were only few fine processes/branches extending in the dorsal direction (Fig.12B arrows).

Over the following eight hours, the dendrite field size increased slowly in size but did not show any significant changes in the overall branching complexity (Fig12C-12F). Moreover, the dorsal midline remained dendrite-free until 28h AEL (Fig.12G1). By 28h AEL in few larvae dorsal single dendrite processes reached and crossed the dorsal midline (Fig.12F and 12G arrows). This was observed in 17.1% (7/41 segments) of the abdominal segments of analyzed larvae for this time point. Over the next few hours the percentage of abdominal segments showing a covered dendrite dorsal midline increased significantly to ~92% (44/48 segments) (Fig.12J). Importantly, dendrite tips of contra lateral neurons showed dendritic exclusion, suggesting that at the dorsal midline, mechanisms including self-self recognition and hetero-neuronal tiling are initiated and functional at this point of development. We observed that each dendrite field had a centrally positioned "leading edge". One or two dendrite branches were always faster than the others and extended toward the dorsal midline to meet their contralateral. This pattern of development seemed to occur in almost all animals. Between 31h and 40h AEL, *Drosophila* larvae displayed a pattern of dendrite field organization at the dorsal midline comparable to a zebra crossing (Fig.12G1, H1 arrows).

To estimate, how dendrite growth proceeds throughout larval development we measured the length of the longest dendrite extending in a dorsal direction from10 different animals (Fig.12K and 12L) As a reference for lateral body growth, the average distance between the most dorsally positioned contra-lateral neuronal cell bodies of an abdominal segment was measured (Fig.12K, L_a=distance between dorsally positioned cell bodies within a segment; L_b= longest dorsally projecting dendrite process). Although the quantification described here has some potential caveats and gives a rough estimate of the growth of dendrites only in dorsal direction, it suggests that the average dorsal elongation rate of the dendrites (~4.68µm/h) is almost 3.2-fold higher than the average lateral body growth rate of the animal (1.45 µm/h) (Fig.12L).

In summary, the developmental profile of dorsal da neurons suggests that during embryogenesis and larval stage, the temporal increase of dendrite length is stereotyped, suggesting that dendrite branch elongation and innervation of receptive field area are under a molecular control.

2.3 Dendrite field developmental analyses of *robo*, *robo2* and *slit* single mutants and *robo, robo2* double mutants.

To determine whether the Robo2-Robo-Slit system regulates dendrite morphogenesis of md-da neurons during embryogenesis and later (during larval stages), we performed detailed developmental analysis of the dendrite field formation in $slit^2$, $robo^{GA285}$, and $robo2^8$ single null mutants and $robo^{GA285}$,$robo2^8$ double null mutants (Fig.13).

To visualize the dendrite in these mutants we recombined the Gal4 109(2)80 reporter line with each of the above mentioned mutants. Importantly, two independent studies on the PNS of *Drosophila* have previously shown that dorsal da neurons express both, Robo and Robo2 proteins, but not Robo3 (Parsons et al., 2003; Zlatic et al., 2003).

We began the phenotype analyses at a time point when axogenesis is completed and dendritogenesis is initiated between 13h and 14h AEL. One reason for this is that we wanted to make sure whether the loss-of-function of any of these proteins has a primary effect on dendrite development due to axon misprojections as described for *robo2*[8] mutants. Neither *robo*[GA285], *slit*[2] nor *robo*[GA285], *robo2*[8] double mutants exert axon guidance defects of dorsal da neurons (Fig.13A-A3, B-B3, C-C3, D-D3, E-E3 and Fig.22). Another reason for these early embryonic analyses was because we wanted to know whether dendrite outgrowth initiation takes place differently in any of the above mentioned mutants as compared to the control. The analyses revealed that embryos mutant for *robo, slit, robo2* or both *robo* and *robo2* genes did not initiate dendrite outgrowth precociously, suggesting that control of dendrite outgrowth is not under the Robo receptors (Fig.13 and Fig.22).

We then looked how the dendrite field develops in mutant embryos, beginning from 18h AEL onwards. Between 18h and 20h AEL the dendrite fields of dorsal cluster da neurons are eventually stabilized. Dendrite fields in *robo*[GA285], *robo2*[8] and *slit*[2] null single mutants and *robo*[GA285], *robo2*[8] double mutants resembled that of control animals and did not show any obvious abnormalities (Fig.13A-A2, B-B2, C-C2, D-D2, and E-E2) as also previously reported by Gao *et al* (Gao et al., 1999)..
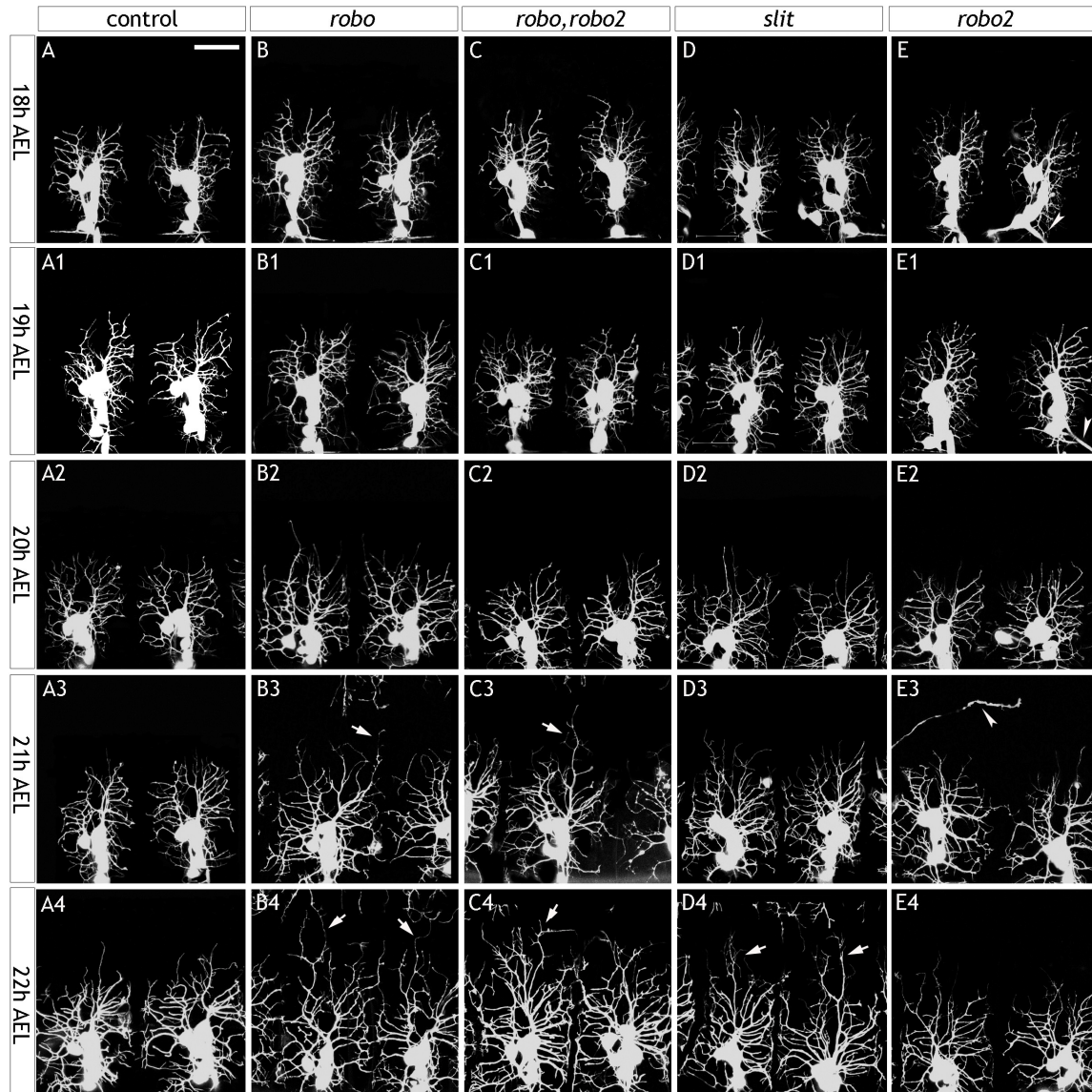
FIGURE 13. **Dendrite fields of *robo*, *slit* and *robo2* single mutants and *robo, robo2* double mutants show abnormal dendrite projection at late embryonic stages.**
A-A4) confocal images of control (80G2) dorsal abdominal segment. **B-B4**) dendrite field development in *robo* mutants. Up to 21h AEL md-da dendrites project normally, the first defects in dendrite branch length appearing at 21h AEL and onwards. (arrows in B3 and B4). **C-C4 and D-D4**) similar defects of dendrite branch elongation defects can be observed in *slit* single and *robo,robo2* double mutants (arrows in C3, C4 and D4)
E-E4) *robo2* mutants develop normal dendrite fields at all of the analyzed time points. In these mutants, axons of some abdominal segments are misprojected (arrowheads in E, E1, and E3).

By 21h AEL, *35*% of the abdominal segments in *slit*^{2} mutants (n=144), 50.9% in *robo*^{GA285} mutants (n=106) and 46.3% *robo*^{GA285}, *robo2*^{8} (n=123) developed few dendrite branches which were much longer compared to controls (Fig.13B3 and 13C3 arrows and Table2). In wild- type animals, dendrite growth proceeds equally for all abdominal dorsal cluster and in only 8.9% (n=17/190) of the abdominal segments, few branches exceeded the level of normal extension.

At 22h AEL this overextension of certain dendrite processes became more pronounced and the expressivity in all three type of mutants (*robo*^{GA285} and *slit*^{2} single and *robo*^{GA285}, *robo2*^{8} double mutants) increased to ~60% (Table2)

	affected segments	total segment number	%	affected segments	total segment number	%
	21hAEL	21hAEL	21hAEL	22hAEL	22hAEL	22hAEL
control	17	190	8.9	13	191	6.8
slit /+	4	77	5.2	10	114	8.8
robo,robo2 /+	9	92	9.8	11	98	11.2
robo2	16	146	10.95	11	116	9.5
slit	51	144	35.4	94	161	58.4
robo	54	106	50.9	77	134	57.8
robo,robo2	57	123	46.3	92	135	68.2

Table 2. **Dendrite branch elongation defects in *slit*, *robo* and *robo2* single mutants and *robo, robo2* double mutants**
Quantitative representation of the phenotype for all genotypes analyzed at 2 different time points 21h and 22h AEL

In all three mutant types including *slit*^{2}, *robo*^{GA285} single mutants and *robo*^{GA285}, *robo2*^{8} double mutants, dendrites invading the neighboring fields appear to respect their contra-laterals and did not show an overlap, suggesting that Robo-Slit interaction is not involved in hetero-neuronal tiling.

Despite the loss-of-function mutation in *robo* or *slit* genes, these animals die between 23h -24h AEL. Because of this, later time point analyses of dendrite field development in these mutants were not possible.

The developmental profile of dendrites in *robo2*^{8} mutants 21h AEL and 22hAEL did not show any phenotype defects and was comparable to those of the control animals,

suggesting that this protein, unlike Robo, is not required during dendrite field formation of md-da neurons (Fig.13E-13E4).

In addition to the dendrite overgrowth phenotype, we also observed for all mutants, subtle cell migration and clustering defects (data not shown).

To asses any dose requirement for the *robo* or *slit* gene product in dendrites we analyzed animals heterozygous for *slit^2* or *robo^{GA285},robo2^8* mutants. We could not detect any obvious defects and the dendrite field in these animals was normal as compared to controls, suggesting that one copy of *robo* or *slit* gene can provide a functionally normal developmental condition for the dendrites of da neurons.

To confirm that the observed phenotype in *robo^{GA285}* mutants is specific, we expressed wild-type *robo* in the md-da neurons of *robo* mutant embryos using a *UAS-robo* transgene (Rajagoplan, 2000 Cell) and the *109(2)80* Gal4 driver (Gao 1999). With one copy of the *UAS-robo* transgene we could partially rescue the expressivity of the *robo* mutant overgrowth phenotype from 57.8% (n=77 affected segments out of 134 in total) to 17.7 % (n=22 affected segments out of 124 in total) (Table 3 and Diagram).

	affected segments	total number	%
control(80G2)	13	191	6.8
robo	77	134	57.8
robo;UAS-robo	22	124	17.7
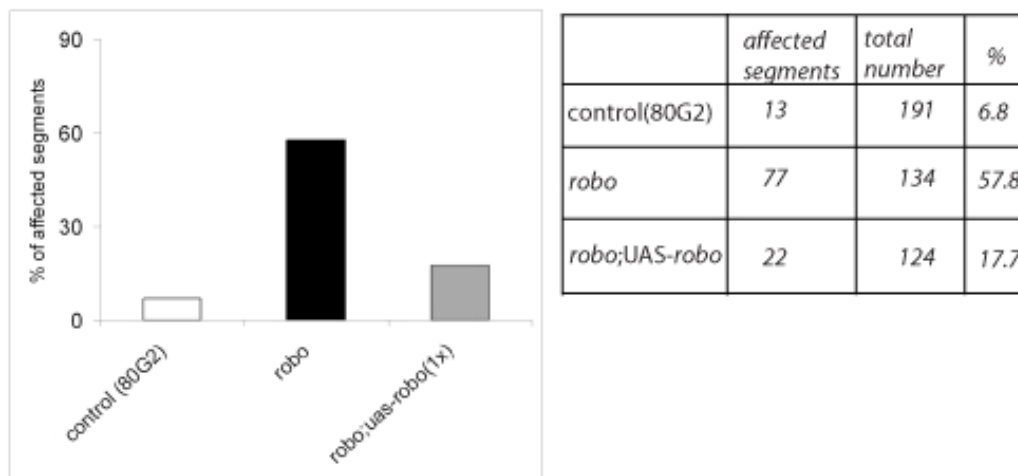
Table 3. Graphic representation of the rescue experiment.
At 22h AEL introducing one copy of UAS-*robo* transgene results in the reduction of abdominal segments showing dendrite projection defects

This partial cell-autonomous rescue, together with the highly similar phenotype obtained in *robo* and *slit* mutant embryos, suggests that the observed phenotype is due to the

mutation in the *robo* gene. Furthermore, it provides the first indication that the Robo protein acts cell-autonomously during dendrite field development of md-da neurons.

The lack of dendrite overgrowth phenotype in *robo2* mutants and the highly similar phenotypes in *slit²*and *robo^{GA285}* single mutants and *robo^{GA285}, robo2^8* double mutants indicates that Robo is the only receptor for Slit used by the dendrites of md-da neurons.

In summary, the described late embryonic dendrite branch elongation phenotype, suggests that Slit acts via the Robo receptor preferentially during late embryonic/early larval stages to control elongation of dendrite branches of md-da neurons.

2.4. Robo and Robo2 are differentially expressed in the PNS of *Drosophila* during late embryogenesis.

Given the late embryonic phenotype in *slit²* and *robo^{GA285}* mutants we aimed to determine the expression pattern of Slit and its receptors at 21h AEL and later.

The Robo family of proteins has been extensively analyzed in *Drosophila* and several studies have shown detailed expression pattern analysis for all three receptors, Robo, Robo2 and Robo3 in the periphery of the embryo (Kidd et al., 1998; Kramer et al., 2001; Kraut and Zinn, 2004; Parsons et al., 2003; Qian et al., 2005; Rajagopalan et al., 2000b; Zlatic et al., 2003). However, little is known about the expression of Slit and Robo during larval stages.

We used antibodies directed against the Slit, Robo and Robo2 proteins to assess the distribution of these proteins during late embryonic and larval stages (Rajagopalan et al., 2000b). In embryos stained at 21h AEL, we could detect high levels of Robo in the PNS of *Drosophila*, notably in the dorsal cluster of sensory neurons (Fig.14B and B1 circled region in 14B1). Robo is enriched at muscle attachment sites (MASs) and in the

myocardial cells of the dorsal midline (Fig.14B1 arrows point to MASs). We observed striking overlap between the expression patterns of Robo and Slit in the myocardial cells of the dorsal midline (data not shown). This was consistent with recent work on *Drosophila* cardiac morphogenesis (Qian et al., 2005). The enrichment of Slit in a row of cells at the dorsal midline mirrors the pattern of expression at the ventral midline. This staining is completely absent in *slit* null mutants showing that the anti-Slit antiserum is specific (Fig.14A and 14A1, red arrow points to dorsal myocardial cells; and 14A3). Slit, similarly to Robo, is expressed in MASs and faint staining of the protein can be detected in the muscles. Prior to 3rd instar larval stages, this expression pattern becomes more prominent (Fig.14A, 14A2 arrows point to MASs; and 14A4 arrowhead shows high localization of Slit in muscle tissue). At late third instar larvae stage Slit and Robo were coexpressed by neurons as well. We could detect a positive signal for both proteins in the soma and the axons of da neurons and some primary dendritic branches (Fig.14A4 and 14A5, darts point to Slit positive primary dendrite branches, 14B2 and 14B3 darts point to Robo positive dendrite branches).

We could not detect any Robo3 expression in any type of tissue in the periphery or neurons at this or earlier (16h-18h AEL) embryonic stages. This was also consistent with previous results (Englund et al., 2002; Zlatic et al., 2003)

Unlike Robo, Robo2 is expressed in dorsal da cluster of neurons only by stage 13-14th (9h-10h AEL). However, by stage 17th (16h-23h AEL), its expression is restricted to the chordotonal neurons, trachea and a layer of pericardial cells at the dorsal midline (Fig.14C and 14C1 red arrow shows pericardial, Robo2 positive cells, green arrows point to Robo2 positive tracheal tube). Interestingly, at early stages of embryogenesis, Robo2 is highly enriched in layers of dorsal epithelial cells. These cells form a corridor of Robo2-free zones, within which are spaced the dorsal da neuronal cell bodies, at this stage also Robo2 positive (Fig.14C2 and 14C3 merge). Such a dynamic expression pattern of Robo2 is consistent with the requirement for the protein during axon path finding of md-da neurons.

In summary, the expression pattern analysis revealed a rather similar but not complementary expression patterns for Slit and Robo in the periphery of *Drosophila* throughout development. The presence of Robo in md-da neurons throughout embryonic

and larval stages supports the observation that Robo may act cell-autonomously during dendrite tree development (see also Results 2.9). Due to the broad expression pattern of Slit present in muscles, MASs and neurons, we were unable to conclude how it may mediate the specific activation of its receptor Robo, during dendrite field development. We anticipate a model in which Slit secreted from either muscles or/and neurons can act as a short-range cue during the process of dendrite branch elongation.

FIGURE 14. Expression pattern analyses of Slit, Robo and Robo2 performed on embryos and larvae.
A, A1, A2) Confocal images of embryos (~16h and ~21hAEL) and 1st instar larvae stained for Slit. The expression pattern of Slit is quite specific for the ventral midline (dashed line along the midline in A and A1). During embryogenesis Slit is also expressed in dorsal myocardial cells (red arrow). and in the MASs (white arrows).
A3) The signal is absent on *slit* (null) mutant embryos. **A4, A5)** Slit expression can be detected on the soma, axons and dendrites (dart) of dorsal clusters of neurons (green is a GFP positive signal due to genetically labeled md-da neurons).
B, B1) Robo protein can be detected on the MASs (arrows) and dorsal cluster of PNS neurons (circled). The protein is highly enriched in the chordotonal neurons (curved arrows). **B2, B3)** Similarly to Slit, Robo protein is expressed in the soma, axons and dendrites of md-da neurons also during larval stages. **C, C1**) antibody staining against Robo2 revealed localization of the protein in pericardial cells (red arrow) and in tracheal cells (green arrowheads) **C2, C3**) during early stages of embryogenesis, Robo2 expression is restricted to layers of epidermal cells that surround the PNS neurons (stained in red with anti-futsch AB). At this stage Robo2 is expressed also by PNS neurons (circled with white line). The expression of Robo2 in chordotonal cells is maintained throughout embryogenesis (curved arrows in C1 and C2).
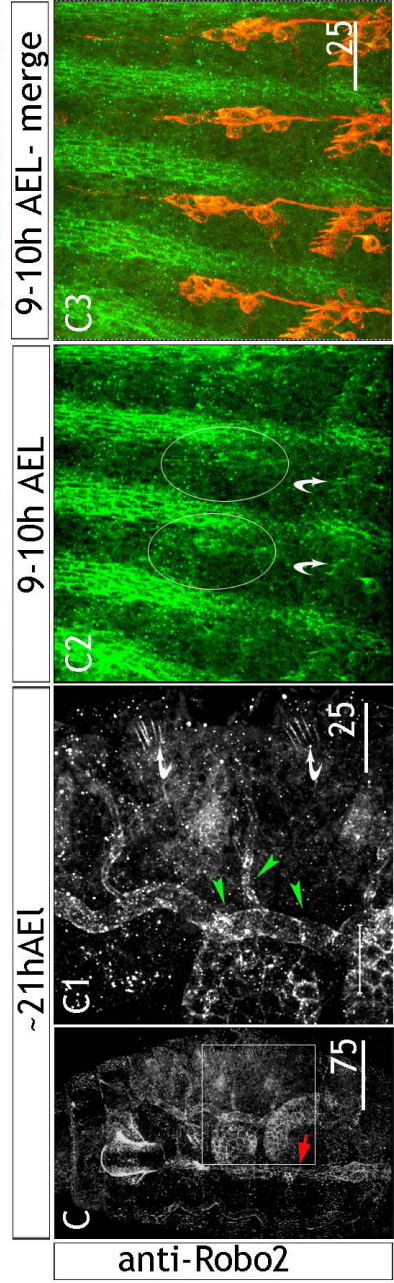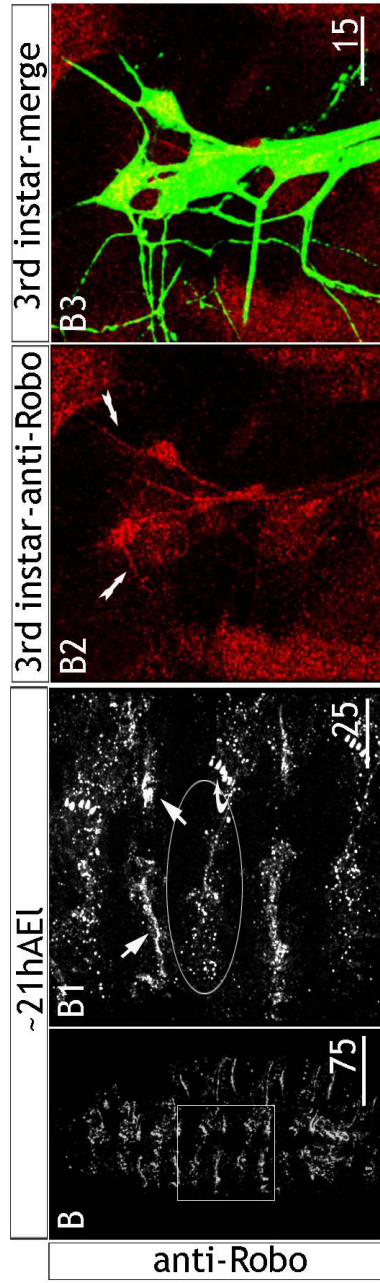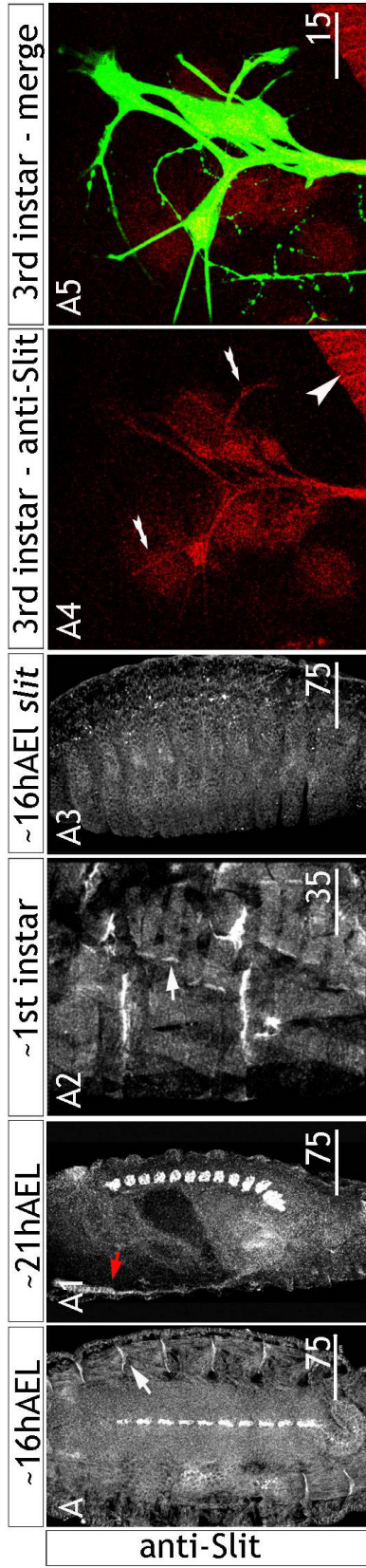
2.5 Overexpression of Robo affects dendrite branch distribution.

We wanted to investigate how md-da neurons forced to express additional levels of Robo protein would develop their dendrite fields. To test this, we overexpressed Robo in all md-da neurons using a *UAS-robo* transgene (Rajagopalan et al., 2000b) and *80G2*, including the *109(2)80* Gal4 driver (Gao et al., 1999). Pan-neuronal overexpression of Robo in sensory md-da neurons had visible effects on dendrite high order branch distribution and length. In many cases we observed extensive short filopodia-like processes, formed at the tips of a basal dendrite branch, but only few lateral branches formed along its shafts. This effect appeared more typically at 21h and 22h AEL (Fig.15B1 and 15B2).

The lack of any detectable phenotype before 21h AEL upon Robo over expression, just as for *robo* loss-of-function, indicates a role for Robo during late embryonic/early larval stages of dendritogenesis, but not at earlier stages of development.

The conclusion one can draw from this experiment is that Robo protein has maybe limiting effect on high order dendrite branch elongation. Given its specific function during late embryogenesis/early larval stages suggests that protein function is dispensable during the establishment of the basic architecture of a dendrite tree, containing mainly of low (primary, secondary, tertiary) order basal branches. In addition, elevated protein levels of Robo can affect dendrite branch distribution. Further analyses are required to elucidate the mechanism regulating this (see time lapse analyses, Section 2.8).
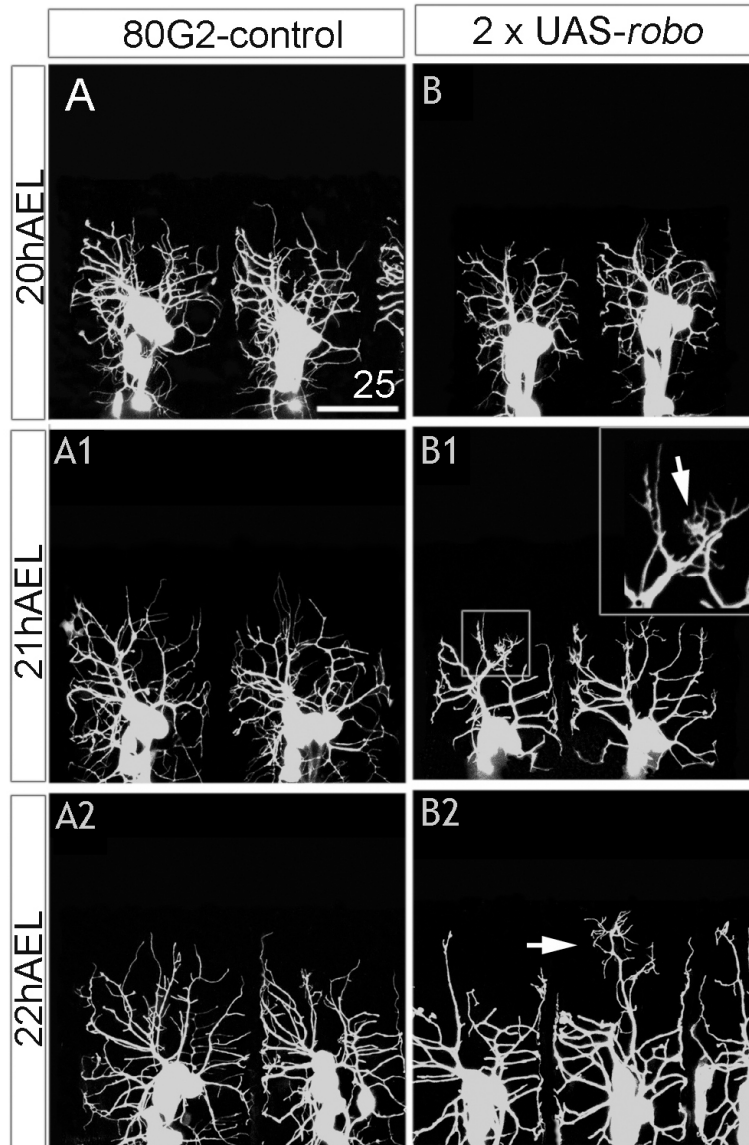
FIGURE 15. Robo overexpression results in ectopic branch formation at the tip of a dendrite.
A, A1, A2) 80G2 control animals at 20h, 21h and 22hAEL.
B, B1, B2) 80G2 animals in which 2 additional copies of UAS-*robo* transgene have been introduced. The effect of the overexpression of Robo in md-da neurons first appears at late embryogenesis, ~21h AEL. In these embryos, dendrite fields show morphological alterations, appear less branched, and form ectopic branches at the tip (arrows in B1 and B2).

2.6. Robo acts cell-class specifically to mediate the dendrite field formation of Class IV but not Class I neurons

The loss-of-function analyses on *robo*^{GA285} mutants in which all md-da dendrites are labeled together, limits the possibility to assess the dendrite phenotype at the level of a single neuronal cell type. Thus, we asked whether Robo protein function is required in all four different classes of neurons.

Recent *in vivo* time lapse analysis, using cell-specific Gal4 reporter lines, have shown that the different classes of neurons (particularly Class I and Class IV for which there are existing genetic markers), within a dorsal cluster, use different strategies for dendritic branching, growth and development (Grueber et al., 2003b; Sugimura et al., 2003).

Class I neurons, the morphologically simplest, achieve their overall complexity by the end of embryogenesis (18h-20h AEL). Unlike Class I, Class IV neurons (ddaC), which form the most expansive and highly branched arbor, accomplish their final morphological complexity by the beginning of third instar larvae (~70h AEL) and use mechanisms such as competition, self-self recognition and tiling (Sugimura et al., 2003).

Thus, given the different strategies and temporal control of dendrite development in the distinct classes of md-da neurons we asked how mutations in *robo* or *slit* affect the dendrite field formation of any in these neurons. In order to analyze this question, we used two different reporter lines, each of which allows the selective visualization of Class I or Class IV neurons.

A transgenic line, in which enhanced GFP (eGFP) was fused with the promoter of the *pickpocket* (ppk-eGFP) gene allows the specific labeling of Class IV neurons in the whole PNS of *Drosophila* (Grueber et al., 2003b). We assembled the ppk-eGFP chromosome with *robo*^{GA285} or *slit*^{2} to generate mutants in which only Class IV neurons were GFP labeled.

We performed the phenotype analyses on 22h AEL old *robo*^{GA285} or *slit*^{2} mutant embryos and ppk-eGFP controls and compared how their Class IV dendrite trees develop. Analyzing 22h AEL old embryos but not younger ones was preferred also for technical reasons: eGFP expressions in the ppk-eGFP line starts at early stage 17th and by 20h

AEL GFP levels are not high enough to reliably visualize all branches and fine dendritic processes.

When compared to control ddaC, $robo^{GA285}$ and $slit^2$ mutant ddaC showed dendritic architecture, visibly distinguishable from that of the controls. Neurons of mutant embryos displayed defects in both branching number and branch length (Fig.16A, 16B and 16C arrows).

Quantitative analysis revealed that the total number of branches in $robo^{GA285}$ and $slit^2$ mutants was highly reduced compared to the control (57.0 ± 15.6 $robo^{GA285;}ppk$-$eGFP$ and 56.3 ± 6.5 in $slit^{2;}ppk$-$eGFP$ and 84.8 ± 11.4 control, p<0.001 between control and $robo$ and p<0.001 between control and $slit$; n=10 neurons for all 3 genotypes, Fig.16a1). Surprisingly, in both mutants the average total dendrite length of ddaC neurons was not modified (689.46μm ± 159.97 in $robo^{GA285}$; ppk-$eGFP$, 668.04 μm ± 85.1 in $slit^2$; ppk-$eGFP$ and 688.67μm ± 63.4 in ppk-$eGFP$; p=0.5 Fig.16a2). Given the lack of significant difference in total dendrite length, but significantly reduced total dendrite branch number, it would be expected that the ratio between the total dendrite length and total branch number was significantly higher in $robo$ and $slit$ mutants compared to those in controls (12.39μm/branch ± 1.64 in $robo^{GA285}$; ppk-$eGFP$; 11.88 μm/branch ± 1.00 in $slit^2$;ppk-$eGFP$ and 8.19μm/branch ± 0.7 in ppk-$eGFP$; p<0.001 between control and $robo$ and p>0.001 between control and $slit$ Fig.16a3). Such quantitative representation suggests that the numbers of branches is reduced but branches are longer in both $robo$ and $slit$ mutants.

The overall architecture of the dendrite fields in both mutants and control ddaC neurons looked visibly similar. This was mostly determined by number and length of lower order branches (such as primary and secondary) and high order branch distribution.

Further, we asked how the morphology of Class I neurons (ddaE and ddaD) would differ in control and $robo^{GA285}$ mutants. To visualize ddaE and ddaD neurons, we used a GAL4-GFP reporter line (Grueber et al., 2003b). After 20h AEL, a strong GFP expression under the control of a GAL4[221]-Class I-specific driver allowed detailed visualization of the morphology of these neurons. The dendrite morphology of Class I neurons in $robo^{GA285}$ mutants was the same as in the controls (data not shown). These analyses suggest that the

function of Robo is not required during dendrite field formation of the morphologically simplest Class I neurons

In summary, the quantitative analysis on dendrite morphology of ddaC neurons during late embryonic stage of development (22h AEL) is consistent with the phenotype observed in *robo*^{GA285} and *slit*^{2}mutant embryos in which a pan-da neuronal Gal4 driven marker allows the visualization of the entire arbor of all 6 md-da neurons. In addition, these single-cell analyses revealed a requirement for Robo in Class IV neurons which indicates a function the Slit/ Robo signaling system in dendrite high order branch elongation control.

2.7. Robo overexpression results in less branched dendritic shafts of Class IV neurons.

Loss of *robo* function determines a reduction in the number of branches and an increase in average dendrite branch elongation of the morphologically most complex class of neurons, ddaC: how would overexpression of Robo affect the dendrite field architecture of this neuron?

Similarly to the previous experiment, we tested the effect of *robo* overexpression on Class IV dendrite morphology. To this aim we expressed *UAS-robo* in all md-da neurons using the *109(2)80* driver line (Gao et al., 1999), but in combination with the *ppk-eGFP* reporter (Grueber et al., 2003b) which allows visualization of only Class IV neurons.

No significant effect can be detected upon overexpression of *robo,* using two copies of the transgene; in the total dendrite length of ddaC at 22h AEL (721.62μm ± 175.53 for G4$^{109(2)80}$;UAS-*robo,ppk-eGFP*, n=9 animals and 688.67μm ± 64.41 for ppk-eGFP; p=0.6, Fig.16a2). However, overexpression of *robo* results in a significantly fewer total

number of dendrite branches when compared to control animals (84.8 ± 11.1 in control and 63.8 ± 9.89 in G4[109(2)80];UAS-*robo,ppk-eGFP*; n=9 neurons; p<0.01; Fig.16D and 16a1). Furthermore, as suggested by the previous set of experiments (Fig.15), ddaC dendrites bear many filopodia-like processes at their tips at 22h AEL but show rather low dendrite branch decoration along their shafts (Fig.16D arrowheads). Similarly, as in *robo* mutant Class IV neurons, the ratio between total dendrite length and total number of branches results in significantly increased average branch length (8.19μm/branch ± 0.7 in control and 11.35μm/branch ± 2.37 in G4[109(2)80];UAS-*robo,ppk-eGFP*; p<0.01; Fig.16a3) Interestingly, looking at later time points of development (second instar larvae, ~ 48h AEL), when the target area is fully covered with dendrites and ddaC neurons have gained significantly in complexity, Class IV neurons overexpressing *robo* showed significantly reduced number of branches (76 ± 20.3 in G4[108(2)80];UAS-*robo*,ppk-eGFP n=5 neurons, and 223.2 ± 25.6 in controls, n=5 neurons; Fig.16G and 16b1) and developed dendrite tree with a visibly simplified dendrite arbor (Fig.16G). Due to the decreased branch number, their total dendrite branch length was also significantly decreased (3355.9 ± 675.1 in controls and 1253.9 ± 223.98 in G4[108(2)80];UAS-*robo*,ppk-eGFP , p<0.001) (Fig.16b2). At this stage the average dendrite branch length, meaning the ratio between total dendrite length and number of branches, was comparable to controls (15.03 μm/branch ±1.75 in control and 16.95μm/branch ±2.71 in G4[108(2)80];UAS-*robo*,ppk-eGFP Fig.16b3). Furthermore, neurons overexpressing *robo* failed to fully cover the appropriate target area and in all analyzed larvae we observed dendrite-free zones (Fig.55G arrowheads). Interestingly, some of the branches appeared to loop back on themselves, this is never observed in the wild-type (Fig.16G, dart). Additionally, overexpression of Robo results in the formation of membrane ruffles and lamellipodia-like structures which appear to be formed at branching points or at the tip of a branch (Fig.16G1, arrows**).**

Taken together, these observations support a model in which elevated levels of Robo might be working as a limiting factor for high order branch elongation. Furthermore the defects in dendrite branch elongation and their distribution at earlier time points due to Robo overexpression are followed by defects only in branch number at later time points resulting in a highly simplified dendrite tree.
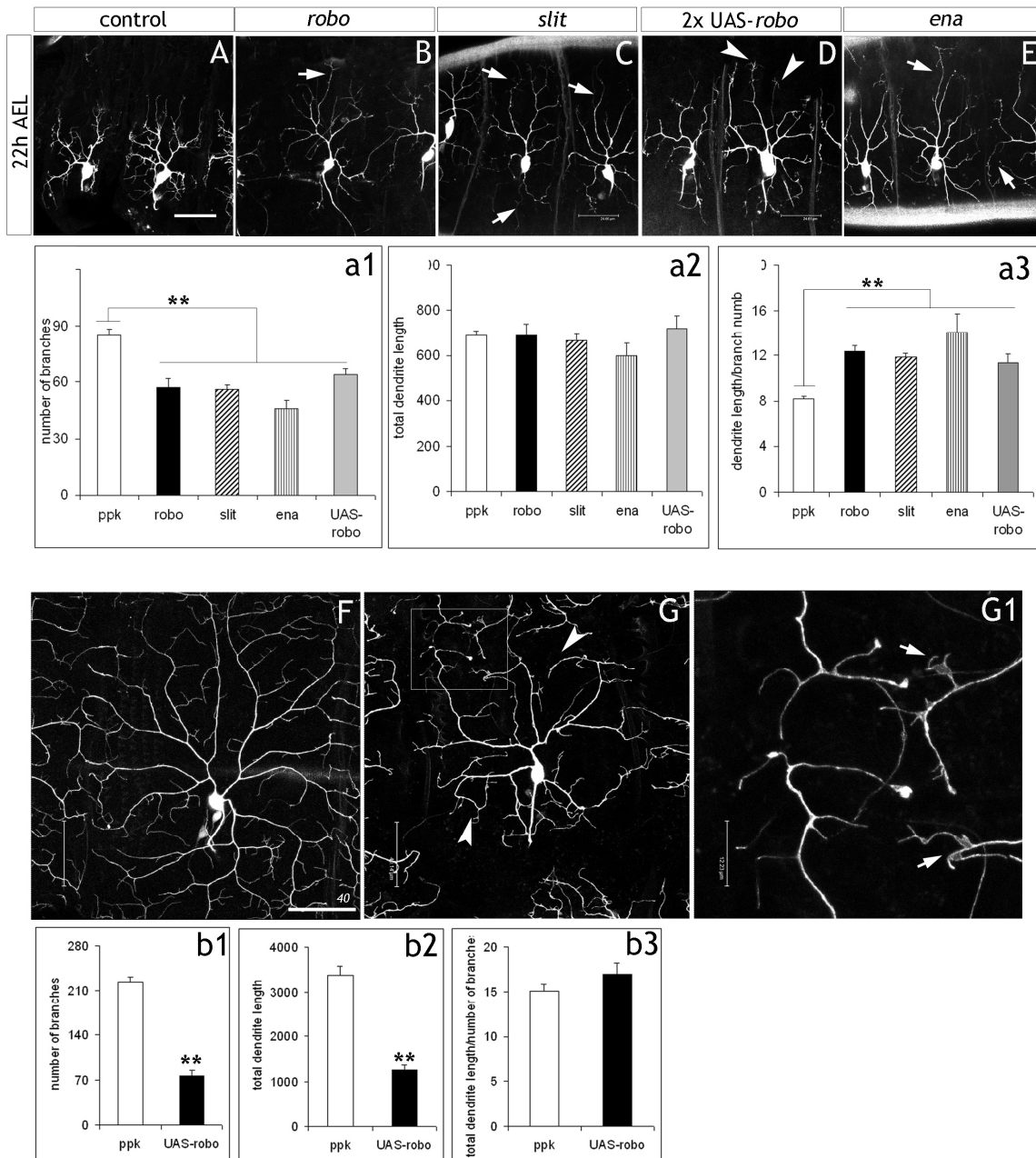
FIGURE16. Dendrite field developmental analyses of Class IV neurons in *robo, slit, ena* mutants and UAS-*robo* animals. A) Control animals **B, C, E)** Loss-of-function analyses of *robo, slit,* and *ena* (see later, Results 2.12) Class IV neurons result in less branched dendrite tree (arrows) **D)** effect of Robo overexpression on Class IV neurons results in a less branched dendrite tree and ectopic formation of branches at the tip a basal branch (arrowheads) Scale bar for all images 25μm. **a1)** quantification of the dendrite morphology in each of the different genotypes revealed for all (*robo, slit* and *ena*) a decreased total number of branches. Similarly, overexpression of Robo results in a significantly lower total number of branches. **a2)** The total dendrite length was similar as in control. **a3)** the ratio between the dendrite length and number of branches suggests that the average branch length in all genotypes analyzed is increased.

F) Confocal image of a control ppk-eGFP neuron at ~48h AEL. Scale bar 40μm in F) and G) and 12 μm in G1)

G and G1) Overexpression of Robo at later time points ~48h AEL results in highly simplified dendrite morphology, branch number is significantly decreased and so is the total dendrite length. Some primary branches show a loopback (arrowheads)

G1) the effect of high levels of Robo results in formation of lamellipoda-like structures (arrows).

b1, b2, b3) Quantitative analyses of dendrite field morphology of Class IV neurons at 48h AEL revealed that the total number of branches is significantly reduced compared to controls and so is the dendrite length. At this stage of development the average branch length is not altered.

2.8. Time lapse imaging of Class IV neurons overexpressing Robo

Overexpression of Robo does not lead to an increased dendrite branch formation but, similar to *robo* loss-of-function, reduces the dendrite arbor complexity of Class IV neurons. Thus Robo alone is not sufficient to promote new branch formation. However, the loss- and gain-of-function phenotype analyses suggest a role for the protein in restricting dendrite branch elongation and as a result of this, probably in mediating new branch formation To explore further the mechanistic requirement for Robo during this process, we performed time-lapse recordings by collecting images at 10 min intervals for up to 60 minutes. We compared branch dynamics in second instar larvae of Class IV neurons of controls and those overexpressing Robo. We chose this developmental stage for technical reasons mainly; pressed between a specially designed microscopic sieve (*thanks to Madhuri Shivalkar, a PhD student in our lab*) and a cover slide and mounted in halocarbon oil, second instar larvae could be imaged without anesthetizing the animals. We observed formation of new branches for both control and *robo*-overexpressing neurons; however the branch formation rate was much higher in controls than in the *robo*-overexpressing Class IV dendrites (Fig.17 and Fig.18**).**

FIGURE 17. Time lapse imaging of a fragment of Class IV neuron in both control and Robo overexpressing second instar larvae.
Stable branches are traced in black**,** newly formed are in red, partially retracting in blue and branches that become longer are depicted in green. Blue arrows point to branches that have retracted completely. The red arrow points to the formation of a ruffle-like structure as a consequence of retracted branches.

ppk-eGFP

Gal4[109(2)80]; UAS-*robo*,ppk
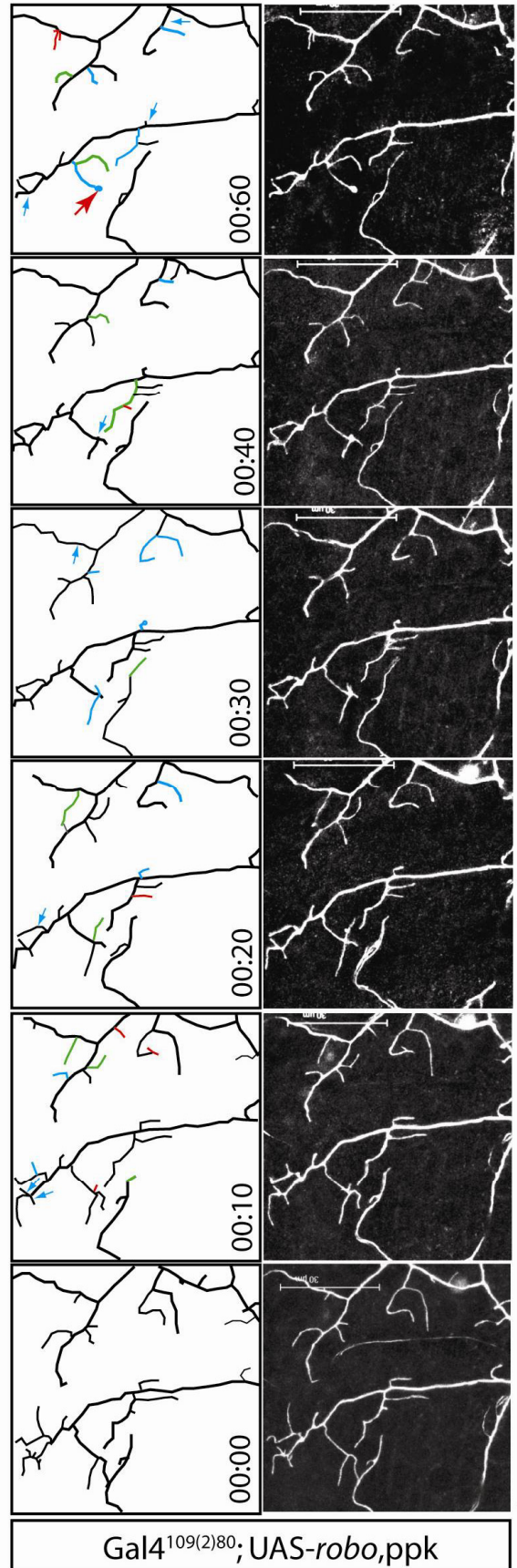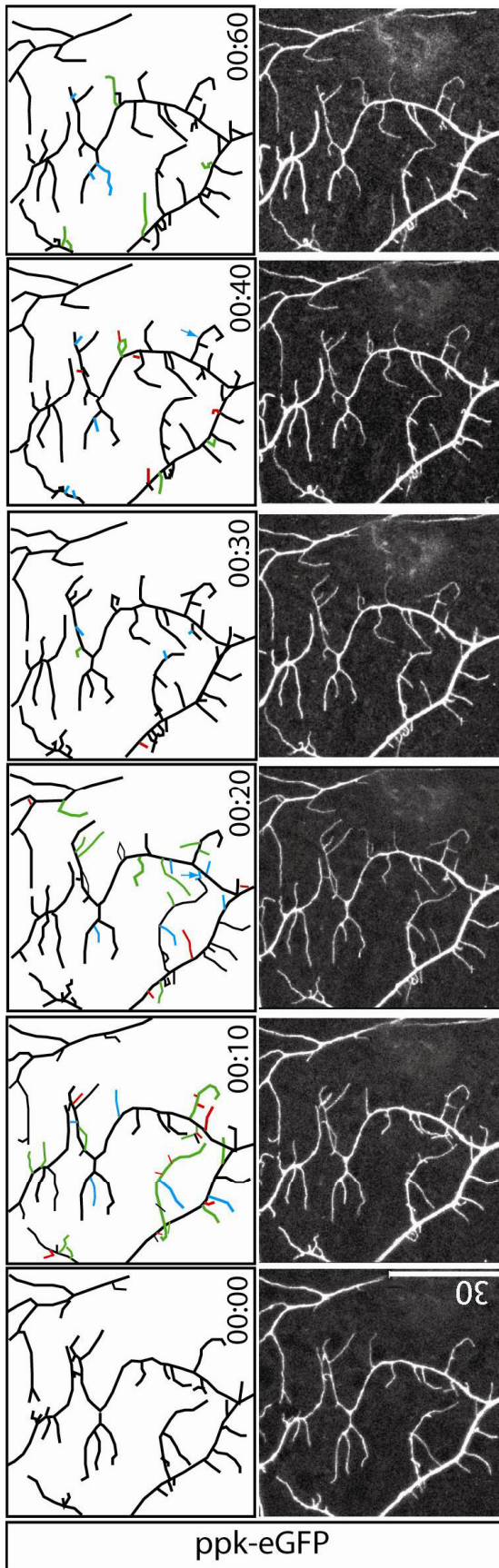
FIGURE 18. Tracing of the start and end point of time-lapse imaging in control (ppk-eGFP**) and UAS-*robo* examples**.
Different colors depict different type of branches; red - newly formed, blue - partially retracted, orange – transient, green –elongated. Blue arrows point to branches that have been fully retracted. Red arrow depicts the formation of a lamelipodia like/bulb like structure upon branch retraction. Quantification of the branch number per 10μm basal dendrite branch and minute (y axis) suggests that the number of newly formed branches is significantly lower in UAS-*robo* neurons than in controls. Branches that have elongated over time are also significantly less.
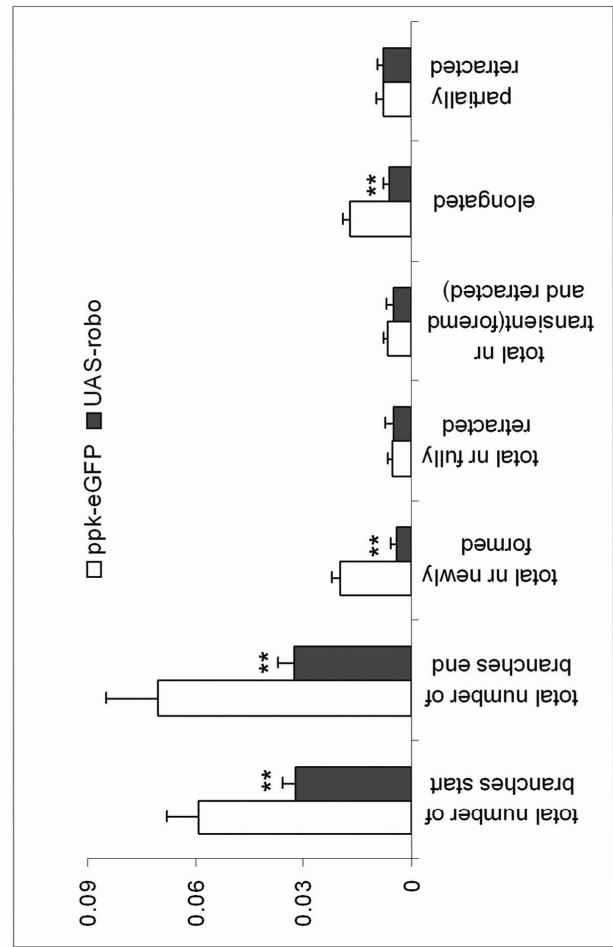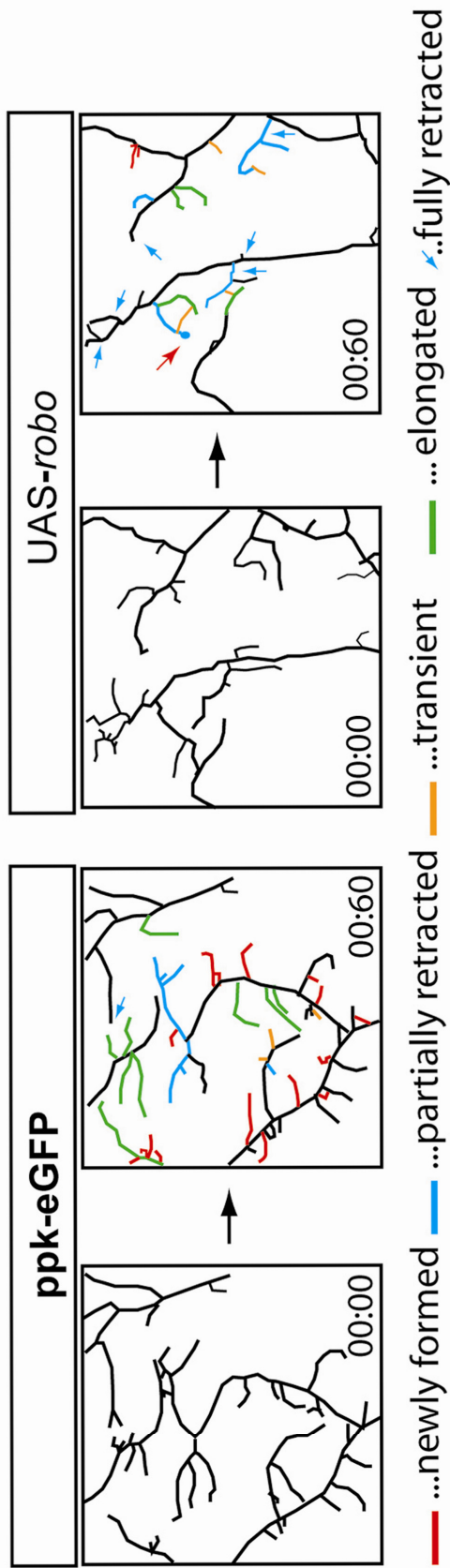
This observation was supported by counting the number of newly formed branches at the end of recordings and normalizing these to a basal dendrite branch length of 10μm and per minute (Fig.18). In all the analyzed control examples, the dendrite branch morphology became more elaborate at the end of the time-lapse recordings (n=6/6). In contrast, the new branch formation rate in Class IV neurons overexpressing *robo* was significantly decreased, additionally, existing dendrite branches showed tendency to retract in comparison to controls. These events led to a more simplified dendrite segment at the end of the imaging (n=4/6) (Fig.18). We observed the formation of membrane lamellipodia-like structure or bulb-like structures at a tip of a branch as a result of full retraction of an existing branch(es) (n=4/6) (Fig.17 and Fig.18 red arrow). In another example, from an already existing membrane ruffle, a short branch formed but then retracted over a period of ~20 min. We observed also some cases (n=2/6) where a lamellipodia like structure formed as a consequence of branch tip dilation. Importantly, in both control and Class IV neurons overexpressing *robo* number of transient branches (newly formed and retracted) was comparably similar, suggesting that branch dynamic stability is not affected upon *robo* overexpression. The number of fully or partially retracting branches was also similar for both genotypes (Fig.18 graph).

Taken together, the similar dynamics of branch retraction but the significantly lower number of newly formed branches in Class IV neurons overexpressing *robo* suggest that elevated Robo levels reverts the process of dendrite elaboration to dendrite arbor simplification, due to increased repulsion events. In support of this is the observation that in Class IV neurons overexpressing *robo* there is a significantly lower number of branches undergoing elongation; however this process was not completely obstructed and while some branches did retract, at the same time others elongated (n=3/6 and Fig 17).

.

2.9. Robo regulation of dendrite fields of Class IV neurons is cell-autonomous

Certainly, an important question is whether the proposed function of Robo during dendrite field formation is cell–autonomous. To address this question, we performed MARCM (mosaic analysis with a repressible cell marker) (Lee and Luo, 2001). This method allows the specific removal of Robo from a single neuron and the analyses of its loss-of-function effect in an otherwise heterozygous background. In this assay, abnormal dendrite development reflects cell-autonomous function of the protein of interest.

We recombined $robo^{GA285}$ and $robo2^8$ into the MARCM configuration required for the second left and second right chromosomes. Due to the low level of GFP expression at earlier time points, with this approach we could visualize the clone neurons with a high level of resolution only at the stage of third instar larvae (70h-72h AEL) when the development of the neuron is completed and has acquired its final dendrite morphology.

We mainly focused on the analysis of Class I and Class IV neurons for which the functional analysis on $robo^{GA285}$ mutant embryos revealed a cell-specific role for Robo in dendrite morphogenesis. Moreover, the embryonic phenotype of ddaC neurons in $robo^{GA285}$ loss-of-function mutants suggests a requirement for Robo in preventing overextension of fine dendrite branches and helping to mediate high order branch formation of Class IV but not Class I neurons.

We obtained clones of each of the two dorsal Class I neurons ddaE and ddaD, and $robo^{GA285}$ or $robo2^8$ mutant clones showed normal dendrite morphologies (n=10; Fig.19D, 19E and 19F). Quantification of the average total dendrite length and number of branches revealed no significant differences from control clones (Fig.19J and 19K).These results are consistent with the loss-of function analysis of Class I dorsal da neurons in $robo^{GA285}$ mutant embryos.

We found that in $robo^{GA285}$ clones, ddaC developed a dendrite tree with highly decreased number of fine branches (n =5; Fig. 19A and 19B). The almost two-fold reduction of high order dendrite number (113.6 ± 25.8 in $robo^{GA285}$ and 255.3 ± 75.5 in controls p<0.005) resulted in a two-fold reduction of the overall total length of high order branches (3179.14μm ± 396.1 in $robo^{GA285}$ and 8622μm ± 2170 in controls p<0.001) (Fig.19G and

19H). Surprisingly, the overall size of the dendrite field in $robo^{GA285}$ mutant ddaC was visibly reduced (Fig.19L). This apparently contradictory finding might be due to the significantly reduced number of high order branches, which made the dendrite field appear smaller (Fig.19G).

Compared to controls, dendrites in Class I and Class IV *robo2* mutant clones showed normal dendrite morphologies (Fig 19C, Fig19F). Quantification of the average total length and number of branches revealed no significant differences from control clones (Fig.19G, 19H, 19I, 19J and 19K; n=4 for Class IV and n=10 for Class I.). These results are consistent with the lack of dendrite phenotype in late embryonic $robo2^8$ mutants as well as the lack of detectable Robo2 immunoreactivity in these neurons at this stage.

We found that in $robo2^8$ ddaC clones axons showed guidance defects with variable severity of the phenotype. Confocal imaging revealed that the misguided axons were lying in a different plane from that of the dendrites (Fig.19C arrow). We could not be certain of a cell-autonomous requirement for Robo2 in the axons of class I neurons.

In agreement with the partial rescue experiment, and expression pattern analyses, the MARCM results suggest that the Robo protein acts cell- autonomously during dendrite field development of Class IV neurons. Taken together, the data suggest that Class IV neurons, the only neuron able to fill in the receptive field area with dendrites, seems to require Robo as a receptor that mediates the regulation of high order dendrite branch elongation and new branch formation to efficiently cover a whole abdominal segment. As observed in *robo* gain-of- function experiments, this suggests that defects in high order dendrite branch length at earlier stages leads to the generation of highly simplified dendrite architecture of the field at the final stage of development.
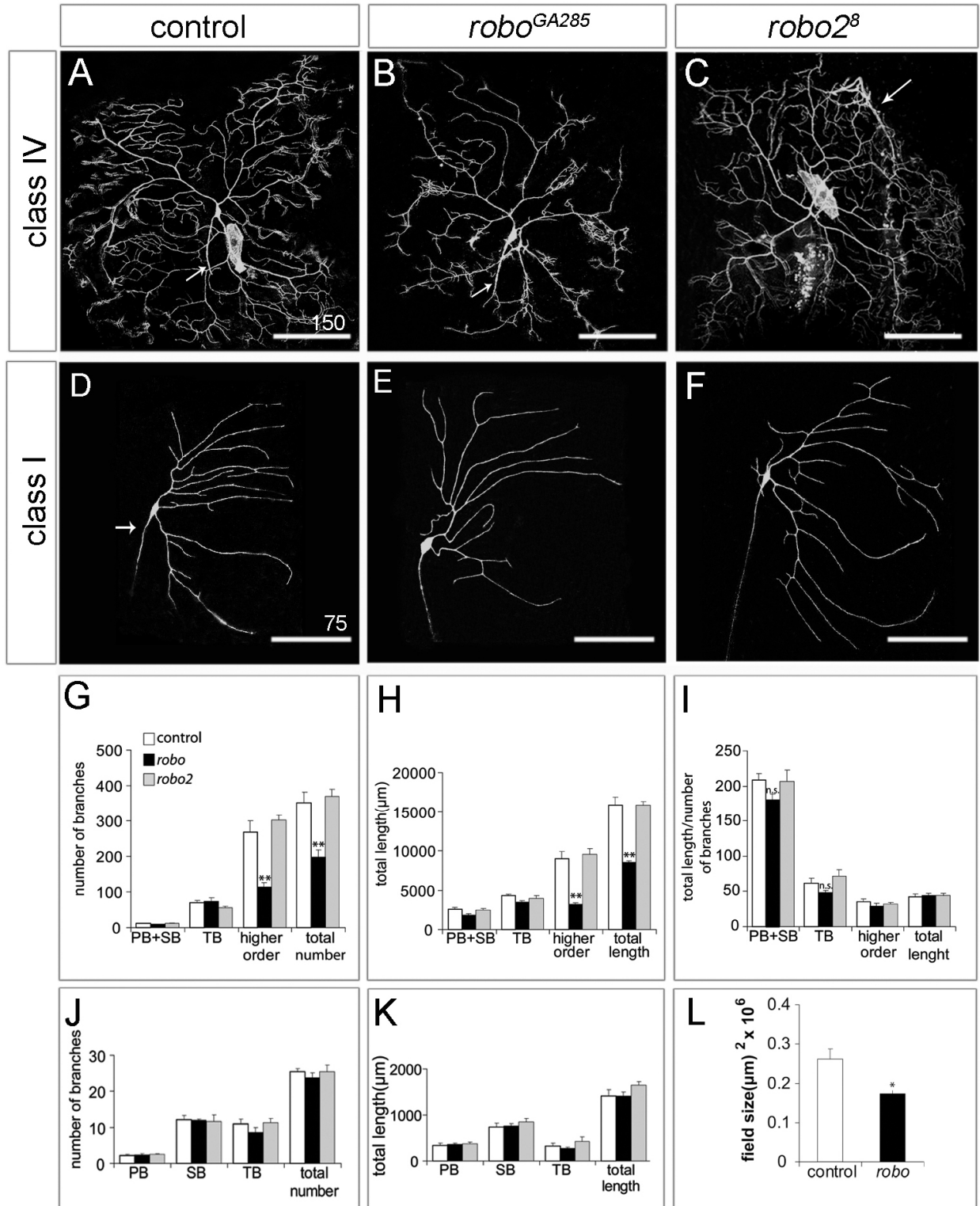
FIGURE 19. Robo acts cell-autonomously in Class IV neurons.

A, B, C) Control, *robo* and *robo2* mutant Class IV clones

robo mutant Class IV neurons develop less high order branches and show highly simplified dendrite arbor. *robo2* mutant Class IV neuron develops a normal dendrite tree but their axons are misprojected (arrow in C).

G, H and I) Quantitative analyses of dendrite tree morphology of Class IV neurons revealed a significant reduction of high order branches in *robo* mutant Class IV neurons and significantly reduced dendrite branch length (H). The ratio between dendrite branch length and dendrite numbers revealed similar values (I).

D, E and F) *robo* and *robo2* Class I clones appear with normal dendrite architecture, similar to the Class I controls.

J and K) Quantitative analyses showed that neither Robo nor Robo2 is required during dendrite field development of Class I neurons.

L) Measurements of dendrite field area of *robo* and control Class IV clones.

Scale bars in A, B and C 150μm and D, E and F 75 μm

2.10. Differentiation of Class IV neurons

We wanted to address how Class IV neurons obtain their complexity and what might the developmental requirement of Robo be in dendrite field development of Class IV neurons.

To determine in more detail how Class IV neurons sculpt their denritic arbors we performed static-time point analyses by collecting images at 10 different time points. This imaging protocol allowed us to assess further whether the pattern of development of Class IV neurons at different stages is also a stereotyped process.

We started our analyses by looking at ~19h AEL old embryos, the earliest time at which dendrite processes of Class IV neurons were visible in the *ppk-eGFP* line. The last time point of our imaging was ~80h AEL corresponding to 3rd instar larvae stage and the final stage of ddaC dendrite field development (Fig.20).

During the late embryonic stages, by 19h-20h AEL, ddaC sends out one or two primary branches which are oriented dorsally and enriched in filopodia-like processes (Fig.20A). Between 20h and 21h AEL few processes initiate their extension and send branches also ventrally (Fig.20B and 20C, arrowheads). Between 22h and 24h AEL the neuron visibly increased in branching complexity (Fig.20D and 20E), and by later time points also in dendrite field size (Fig.20F and 20G). By 40h AEL we could still observe small dendrite-free zones (Fig.20G, star). The full coverage with dendrites of a dorsal abdominal segment was achieved by 48h AEL (Fig.20H), consistently with what we observed when all md-da neurons were visualized (Fig.12). Thus appears that during larval stages, the dendrite field size of the dorsal cluster of md-da neurons is determined at least in part by the dendrite field size of Class IV neurons. In second instar larvae, by 48h AEL, Class IV neurons dendrites are almost fully developed (Fig.20H). Between 48h and 66h AEL the number of high order branches and the field size increase, accompanied by an increase in the total dendrite length (Fig.20K, 20H and 20I). The plot of number of average total dendrite branch shows a gradual linear increase over the period of time between 22h AEL and ~60h AEL. Such an increase in branch number reflects an increase in total branch

length (Fig.20K and 20L). To gain a more quantitative understanding of Class IV dendrite growth pattern, we analyzed the number of branches falling within a certain length category for each developmental stage (Fig.20M). Interestingly, the number of the shortest branches, possibly the newly formed and/or retracting ones, reached its peak by the second instar larva, at ~48h AEL. Furthermore, the normalization of the number of branches of each length category to the average total number of branches for each developmental time point, shows that all the distribution curves fused (Fig.20N), suggesting that between 22h and 48h AEL the fraction of branches that falls into a certain length category is kept constant. Furthermore, for each time point of development we analyzed, the dendrite architecture of Class IV neurons was highly comparable among different animals (n=10 animals/time point), suggesting that the morphological dendrite development of ddaC neurons employs highly stereotyped mechanisms.

Taken together, the detailed quantitative and qualitative analyses of Class IV neurons presented here, combined with the studies of Sugimura and colleagues, (Sugimura et al., 2003), suggest that the neuron gains on dendritic complexity by using highly stereotyped mechanisms including the iterative addition of new branches which then elongate and stabilize to become a substrate for others.

FIGURE 20. Analyses of dendrite field developmental of Class IV neuron.
A to **J**) Confocal images of the different time points analyzed. At late embryonic stages ~20h-21h AEL dendrite branch growth predominantly follows a dorsal direction (arrowheads). Later on (~22h, 24h AEL) the morphological complexity increases as well as the dendrite field size
G). By 40h AEL the receptive field area is not yet fully covered with dendrites (star), this is accomplished by 48h **(H)**.
K) and **L)** show quantification of the total dendrite length and total dendrite branch number for the different time points.
M) number of branches (depicted on the y axis) falling within a dendrite branch lengths (depicted as x axis).
N) branch curve distribution normalized to the total branch number.
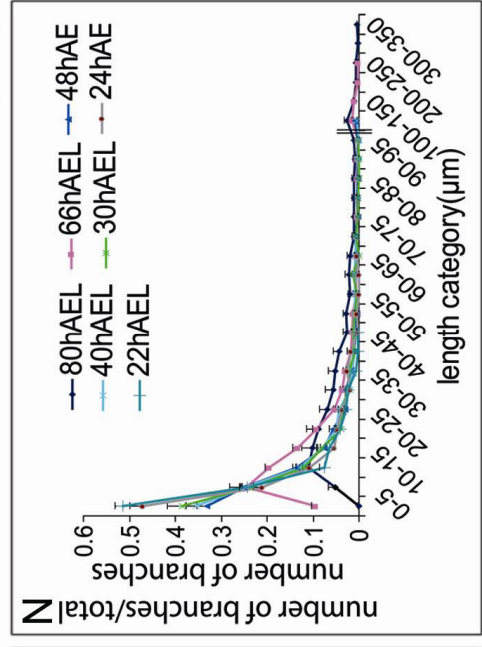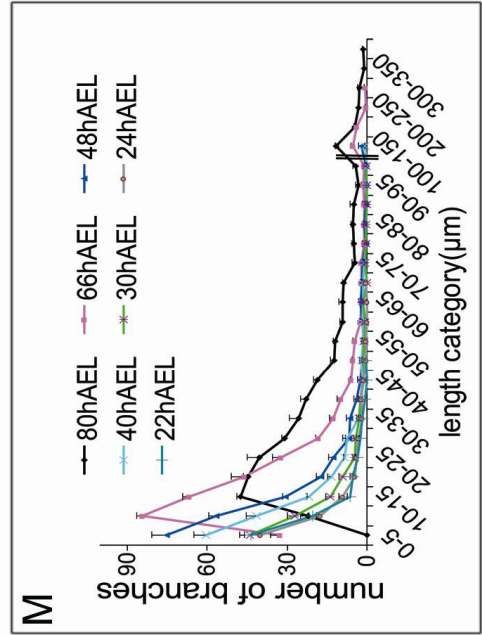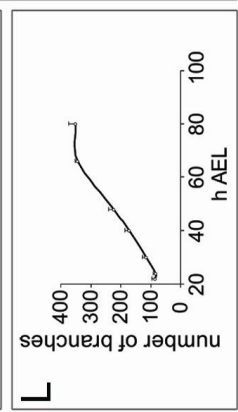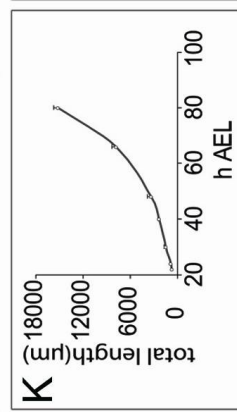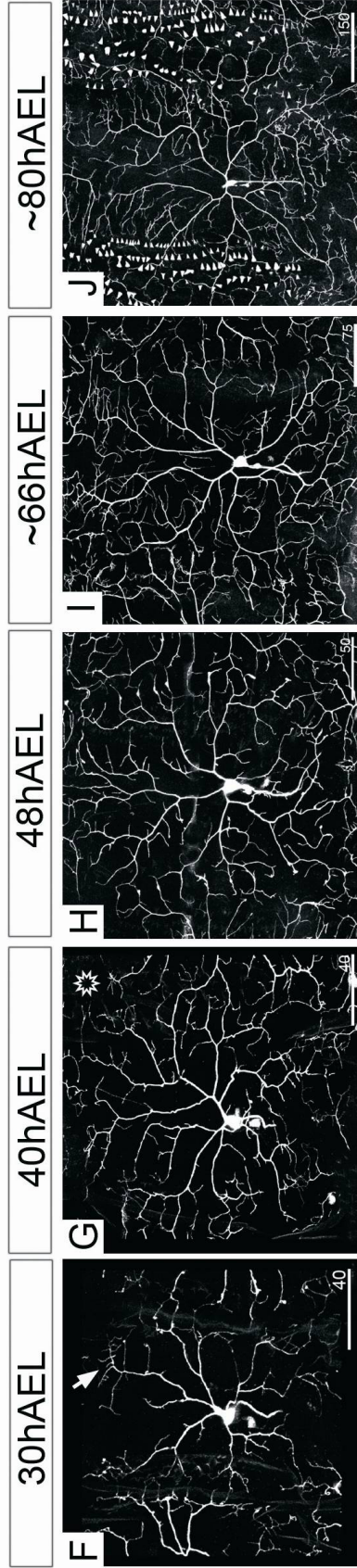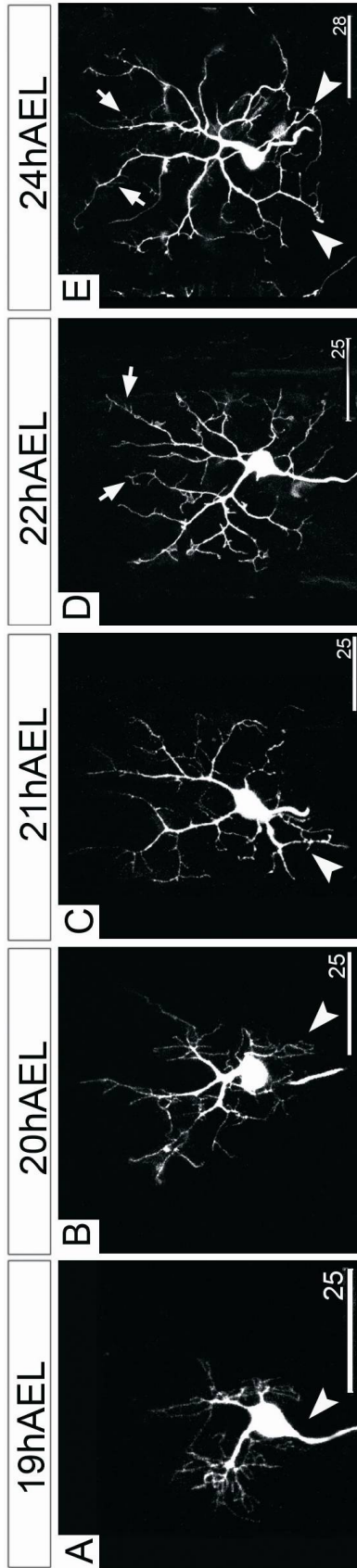
2.11. How is mediated the specific activation of Robo via Slit during dendrite field development of Class IV neurons?

We also wanted to look at how Slit and Robo specifically interact with each other to regulate the complex developmental processes of dendrite arborization of Class IV neurons.

slit mutant Class IV neurons, show dendrite morphological defects that quantitatively and qualitatively resemble those observed in *robo* mutant Class IV neurons. Furthermore, analogous phenotypes of the two different genotypes were observed in two different genetic backgrounds. Importantly, in none of the analyzed animals, including *robo* loss- and gain- of function and *slit* loss-of-function mutants the dendrite phenotype show direction-specific defects. In addition both proteins show a quite similar pattern of expression during larval stages in neurons and MASs. Only muscles seem to express Slit but not Robo. Taken together, this data suggest that Robo receptor is activated via its ligand Slit to mediate dendrite field development of Class IV neurons. These observations are followed by the question about the source of Slit.

To address this question experimentally we performed a set of experiments, however none of these allowed us to gain a better knowledge about the ligand source and distribution.

First, we performed ectopic over expression experiments.

We generated a fly line in which a UAS-*slit* (Kidd et al., 1999) construct (a gift f G.Bashaw) is recombined together with the ppk-eGFP construct, allowing the separate visualization of Class IV neurons when Slit is ectopically overexpressed. We then used several Gal4 driver lines to force stronger expression of Slit in either the muscles (Gal4[24B])(Greig and Akam, 1993), or epidermis (Gal4[69B]) (Brand and Perrimon, 1993) or md-da neurons (Gal4 [109 (2)80]). For all of the performed experiments we observed no alterations of the dendrite architecture of md-da neurons. Due to some experimental limitation, (e.g. only one copy of the Gal4 driver and one of the UAS-*slit* construct are present), perhaps the level of Slit expression was not high enough to induce any visible

effect on the dendritic architecture of Class IV neurons. Alternative speculations providing some explanations for the lack of effect on dendrite field development upon Slit overexpression are discussed in the "**Discussion**" chapter.

Expression pattern analyses of Slit revealed a positive signal for the protein in the md-da neurons. This suggests a possible short-range signal of Slit, acting either cell- or non-cell-autonomously in neurons. Additionally, there is also the possibility that the highly specific anti-Slit-antibody used in the experiment may also detect Robo-bound Slit protein on the neurons.

To test a possible cell-autonomous requirement for Slit in the md-da neurons we performed MARCM experiments. We recombined a null allele $slit^2$ on a FRT^{42D} chromosome in order to generate fly stock; FRT^{42D}, $slit^2$/CyO.

We obtained Class I, Class III and Class IV mutant *slit* clones, all showing normal dendrite morphology comparable to that of control clones. To gain a better view we quantified the morphology of Class IV neurons (n=4 neurons). These quantifications confirmed the lack of a phenotype in *slit* mutant clones, arguing against a cell-autonomous function of the protein in the neurons (Fig.21D and 21E).

Alternatively, Slit, expressed in the neurons, may acts non-cell-autonomously, secreted from one class of neuron, to influence the dendrite growth of the neighboring ones.

To explore such a possibility the best approach would be a reverse MARCM in which the neuron of interest is a wild type while the non-labeled, surrounding tissue is a *slit* homozygous mutant. Unfortunately, a "reverse" MARCM experiment in *slit* mutant animals is not possible because of the lethal embryonic phenotype of the mutation.

Thus, we took an alternative approach and asked how overexpression of Robo in a single type of md-da neuron would influence dendrite field development. We performed a conventional MARCM experiment using an *elav*-Gal4 driver, and UAS-*robo* transgene assembled with the FRT^{42D} chromosome. Class IV overexpressing *robo* clones showed, as similarly observed in the previous experiment, dendrite tree with highly simplified dendrite architecture. Differently from what was observed in the previous gain-of-function experiment, two of the clones (n=2/4) showed a preferential growth of the

dendrite arbor in only one direction (Fig.21C). Such results may be indicative, of the presence of a Slit signal from neighboring neurons.

Taken together, it is not yet conclusive how a specific activation of Robo via Slit can regulate the process of dendrite field development. Expression pattern analyses together with the data obtained from MARCM *robo*-overexpression experiment suggest that the neurons themselves may be one of the potential sources for the ligand Slit in mediating the activation of Robo.
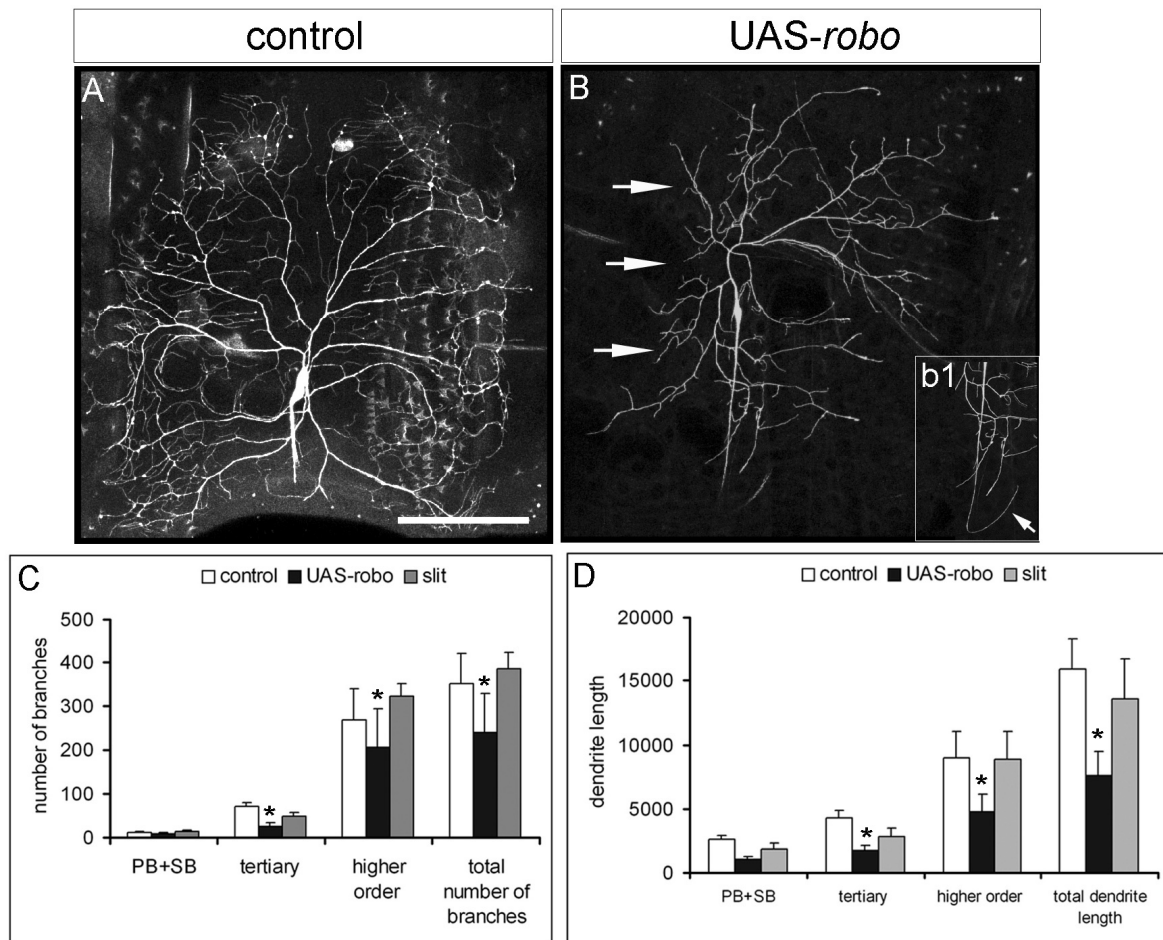
FIGURE 21. Mosaic overexpression of Robo results in simplified dendrite field morphology
A) control Class IV clone
B) UAS-*robo* clone which developed a severely simplified morphology with a side directed orientation of the dendrite field (arrows). Overexpression of Robo also causes axon guidance defects as shown in **b1**) of **B**).
C and **D**) Quantification of the dendrite morphology of UAS-*robo* and *slit* clones
Scale bar in A) and B) 150µm

2.12. The role of Ena and Dock during dendrite field development.

The next question was to determine the signaling events downstream of Slit that mediate Robo activation during dendrite field formation.

Interestingly, in *ena* mutant embryos, the dendrite field of md-da neurons look relatively simplified in their structure (Gao et al., 1999). Further mosaic analyses for the same mutant allele of *ena* revealed that the protein acts cell-autonomously to promote fine dendritic process formation of Class IV neurons. Without the proper function for Ena, ddaC dendrite tree appeared highly simplified in its arbor, a phenotype resembling those of *robo* mutant ddaC clones (Li et al., 2005).

To further address a possible role of Ena acting downstream of Robo during dendrite field formation of Class IV neurons, we undertook a phenotype analysis and compared the difference of dendrite field projection in *ena^{46}*;ppk-eGFP, *robo*;ppk-eGFP and (control) ppk-eGFP animals in 22h AEL old embryos. We found *ena^{46};*ppk-eGFP mutant Class IV dendritic arborization defects resembled those of *robo* ddaC mutant neurons (Fig.16E). Quantifications of the morphology of *ena* mutant Class IV neurons revealed a significantly reduced total number of branches (45.8 ± 14.14 *ena*;ppk-eGFP compared to 84.8 ± 11.41 for controls; p<0.001, n=10 neurons Fig.16a1). However, similarly to *robo* and *slit* mutants, the total dendrite length was the same as in the control (599.84μm ± 168.85 for *ena*;ppk-eGFP and 688.67μm ± 63.41 for control, Fig.16a2). As a consequence, the ratio between the total dendrite length and number of branches is significantly increased in *ena* mutants (14.08 μm/branch ± 5.26 and 8.19 μm/branch ± 0.74 in control p<0.003, Fig16a3). As reported by Li et *al*, (Li et al., 2005) at their final stage of development *ena* mutant Class IV clones show defects in dendrite branch number only. The striking similarity of dendrite phenotypes between *ena* and *robo* mutants and the well proven, biochemical and genetic interaction between the two proteins suggests that Ena may be acting downstream of Robo during dendrite field development.

We also addressed the role of the Dock protein during Class IV dendrite field formation. A previous study has shown high expression level of the protein in md-da neurons, making it a good candidate acting downstream of Robo during dendrite field formation of Class IV neurons (Desai et al., 1999). To test this, we performed loss-of-function and MARCM analyses.

dock^{P13421,} *80G2* mutant embryos did not show any defects in their dendrite architecture (data not shown). In these mutants however, only zygotic Dock protein is absent, the high amount of maternally supplied *dock* mRNA might be sufficient to define the basic architecture of md-da dendrite trees during embryogenesis. We also performed MARCM analyses for *dock*^{P13421}. Presumably, due to the maternal supplement of Dock during embryogenesis, subtle defects in arbor complexity at final stages of ddaC development would reflect a possible, late requirement for the protein in dendrite patterning. We obtained *dock* mutant clones for Class I and Class IV neurons. Class I neurons mutant for *dock* did develop normal dendrite tree similar to those of the control (data not shown). Unlike Class I, Class IV *dock* mutant clones formed more high order dendrite branches with some self-recognition and tiling defects (Fig.22). Such phenotype in *dock* mutant clones, although interesting could not provide further insights about a possible downstream interaction between Robo and Dock during dendrite field formation of Class IV neurons.

In summary, the highly similar loss-of-function phenotypes in *robo*, *slit* and *ena* suggest a model for the Slit/Robo/Ena signaling system acting to regulate dendrite branch elongation. Furthermore, these observations propose that in both the growth cone of an axon and the tip of a dendrite branch Robo activation via Slit recruits Ena.
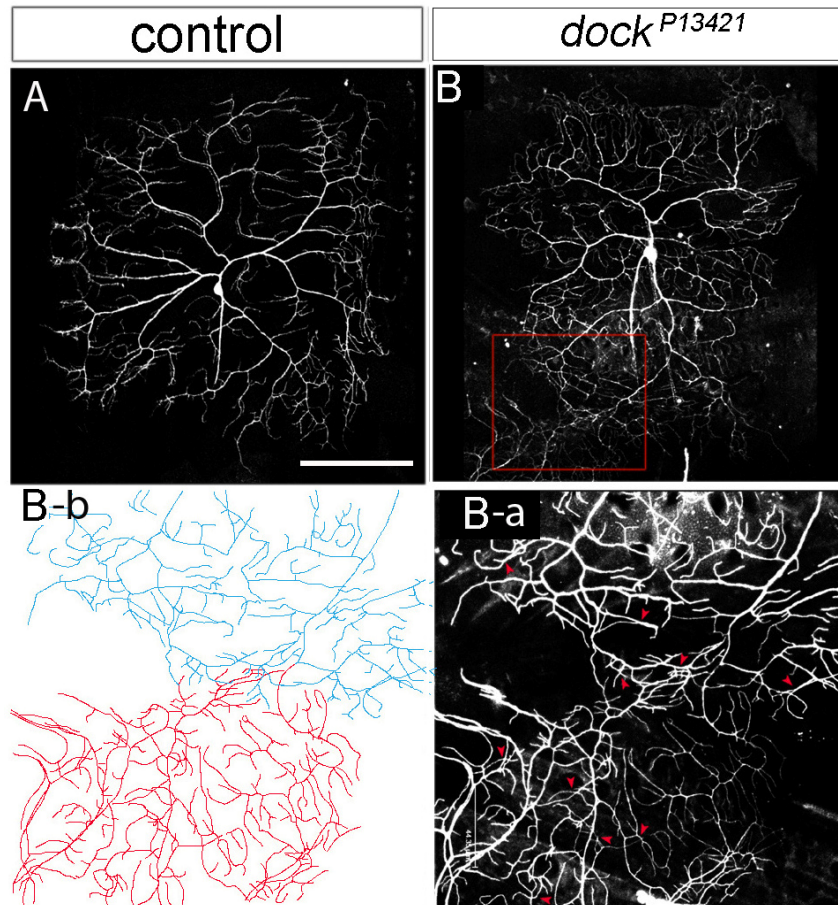
FIGURE *22. dock* Class IV neurons show more high order branches and subtle defects tiling and self –self recognition defects.
A) control Class IV clone
B) *dock* Class IV clone. Scale bar 150μm.
B-a) magnification of the region squared with red line in B), red arrowheads point to branches that cross each other.
B-b) Colored tracing of the B-a) image. In blue are traced all dendritic processes coming from a dorsally positioned Class IV neuron and in red are traced the dendritic processes coming from a ventrally positioned Class IV neuron. Processes show an overlap a phenomenon that is not observed in the control situation.

2.13. Robo2 functions during axon guidance of md-da neurons to specifically down regulate Slit-Robo activation.

The presence of an axon guidance phenotype in *robo2* but not in *robo*, *slit* or *robo,robo2* double mutants of the dorsal da cluster neurons has been reported previously by Parson L. *et al* (Parsons et al., 2003). Their results have suggested a novel, non-cell-autonomous mechanism for Robo2 during axon guidance of dorsal sensory neurons. Moreover, they proposed that Robo2, expressed in the trachea acts as an attractant for these neurons. These conclusions were in partial contradiction with our results, because mosaic analyses of *robo2^8* mutant clones, at least for Class IV neurons suggest a cell-autonomous role for Robo2 in the axons. Furthermore, overexpression of Robo in dorsal Class IV (and Class III) neurons result in similar axon patterning defects to those observed in *robo2* mutant clones (Fig.21).Taken together all these data suggest that Robo2 function may be required to downregulate Slit/Robo activation during the directed axonal growth of dorsal multidendritic neurons.

To test whether Robo2 could have a regulatory role during Slit-mediated Robo activation we reduced *slit* gene dosage in *robo2* homozygous mutants. Similarly, axons of md-da neurons misprojected as *robo2^8* single null mutants, however the frequency of these path finding errors was reduced almost by half (5.29% dorsally misguided and 3.17% ventrally misprojecting axons, n=189 segments scored) (Fig.23F and 23I).

A control; B robo^(GA285); C slit^(2); D robo2^8,robo^(GA285); E robo2^(8); F slit^(2)+/-;robo2^(8)-/-; G robo2^(8) 9-10h; H robo2^(8) 18-20hAEL

I	dorsally misguided	segments scored	%	ventrally misguided	segments scored	%	totally misguided	segments scored	%
control(80G2)	0	140	0.0	0	140	0.0	0	140	0.0
robo2^(8)	12	140	8.6	18	140	12.9	30	140	21.4
robo^(GA285)	0	119	0.0	3	119	2.5	3	119	2.5
slit^(2)	0	147	0.0	6	147	4.1	6	147	4.1
robo2^(8),robo^(GA285)	0	140	0.0	5	140	3.6	5	140	3.6
robo2^(8),slit^(2)	1	140	0.7	2	140	1.4	5	140	3.6
robo2^(8)+/-,slit^(2)-/+	10	189	5.3	6	189	3.2	16	189	8.5

J ventrally misguided / dorsally misguided — dorso-laterally; anteriorly or posteriorly

87

FIGURE 23. **robo2 mutants show severe axon guidance defects.**
A) 80G2 control dorsal cluster of neurons.
B, C and **D)** *robo*, or *slit* single mutants and *robo, robo2* double mutants show normal axon projections. Only a few axons are shortly misguided, however these patterning defects appear to later be corrected.
E and **F**) in *robo2* homozygous mutants or *robo2$^{-/-}$,slit$^{-/+}$* double mutants, axons are misprojected. However the expressivity of the phenotype in *robo2$^{-/-}$,slit$^{-/+}$* mutants is lower.
G) at the time point of dendritogenesis axons misprojected in a straight line dorsally, towards the dendrite field.
H) axon guidance defects often intermingle with the dendrite field projections.
I) quantification of the expressivity of axon guidance phenotype of all analyzed genotypes.
J) Schematic view representing the types of axonal misprojections. For simplicity the phenotypes are grouped into two groups ventrally misprojecting and dorsally misprojecting axons.

robo2[8] null mutants axons are misprojected in a variety of directions in some but not all abdominal segments of an embryo: quite often dorsally, towards the dorsal midline, but also anteriorly and/or posteriorly towards the segmental borders (Fig.22J). Thus, we classified the phenotype in *robo2[8]* null mutants and *robo2^{-/-},slit^{-/+}* mutants into two groups – *dorsally misguided axons,* which include all axons misprojecting over the level of the cell bodies and *ventrally misprojecting axons*, including those which showed abnormal projection under the level of the dorsal cluster of cell bodies (Fig.23J). For both phenotypic classes we observed a similar frequency of errors (8.57% dorsally misguided and 12.86% ventrally misprojecting axons, n=140 segments scored) (Fig.23I). We observed only subtle axon guidance errors in *slit[2]* (n=6 out of 147 segments scored) or *robo[GA285],robo2[8]* (n=5 out of 140 segment scored) double mutants as shown in (Fig.23C and 23D**)** which seemed to be corrected over a short distance.

We also looked at when the axon guidance defects appear and observed that this happens at the time point of axon outgrowth initiation. In the representative example, axons, in 9h-10h AEL old *robo2* mutants (the time point of axon outgrowth) instead of growing ventrally, grew directly dorsally (Fig.23G).

Together, the expression pattern of Robo2 (Fig.14) and MARCM analysis of *robo2* clones and *robo*-overexpressing clones (Fig.19 and Fig 21) strongly suggest that Robo2 exerts both cell- and non-cell-autonomous function during axon guidance of dorsal cluster da neurons to down regulate activation of Robo via Slit. Without Robo2, dendrite field development is often disorganized, as a result of dorsally disoriented axons, which tend to innervate the dendrite field (Fig.23H and see Results 2.1).

The lack of axon guidance errors in either *robo[GA285]* or *slit[2]* mutants suggests that the Robo/Slit system does not work as a guidance system for the axons of dorsal md neurons but is most probably required for targeting.

This is the first functional data providing a model in which Robo2 works to down regulate Robo activation via Slit. Such a role for Robo2 has been speculated but not yet demonstrated

3. Discussion

In this study we investigated the physiological function of Roundabout receptor during dendrite field development of *Drosophila* sensory neurons. Gain-of-function and loss-of-function analyses of *robo* strongly suggest a ***role for Robo working as a sensor*** and allowing a neuron to efficiently innervate a receptive area with dendrites. Robo is required for proper dendrite field formation of Class IV neurons ***during late embryogenesis and beyond***. The developmental analyses of dendrite tree formation suggest that removing completely or adding too much of such sensor Robo, affects the homeostatic regulation of dendrite branch extension and new branch formation at earlier stages so that at a neuron's final developmental stage the dendritic architecture emerges as ***highly simplified***. Thus, we postulate a ***permissive, repulsive role for Robo*** in limiting branching elongation of fine, high order processes without affecting the basic dendritic skeleton of a neuron. The function for the Robo receptor during dendrite development demonstrated here solves some outstanding questions as to how a ***combination of cell-intrinsic and –extrinsic factors regulates dendrite field complexity*** and provides neurons with the ability to innervate territories to form functional maps.

Finally, these data provide a model in which ***Slit responsiveness*** of md-da ***axons via Robo*** might be ***down regulated by Robo2***. That the data demonstrated different rather than redundant functions for Robo and Robo2 suggests that ***Robo2***, similarly as Robo3 (Rig-1) in vertebrates has a regulatory role for Robo responsiveness to Slit (Marillat et al., 2004). The data provide also some new hypotheses of how a neuron can actively use the same cell-surface ligand-receptor pairs during axonal and dendrite development.

Summary of the results

gene name	neuronal compartm.	developmental stage	method	all six md-da neurons	Class I	Class IV
robo	dendrite	~16h -20h AEL	LOF	no dendrite phenotype	n.a.	
		~22h AEL late embryonic	LOF	**dendrite phenotype** longer dendritic processes	no dendrite phenotype	**dendrite phenotype** longer but fewer filopodia-like dendrite branches
		~70h AEL third instar larvae	LOF (MARCM)		no dendrite phenotype	**dendrite phenotype** simplified dendrite field less high order branched
		~16-20h AEL	GOF	no dendrite phenotype	n.a.	
		~22h AEL late embryonic	GOF	**dendrite phenotype** ectopic filopodia-like processes formed at the tip of dendritic branch	no dendrite phenotype	**dendrite phenotype** ectopic filopodia-like processes formed at the tip of dendritic branch
		~48h AEL second instar larvae	GOF	n.a.	n.a.	**dendrite phenotype** simplified dendrite field membrane ruffle formation
		~70h AEL third instar larvae	GOF (MARCM)			**dendrite phenotype** simplified dendrite field site-directional growth of the dendrite field
	axons	~9-10h AEL early embryonic	LOF	no axon guidance phenotype	n.a.	no axon guidance phenotype
		~22h AEL late embryonic	LOF	no axon guidance phenotype	no axon guidance phenotype	no axon guidance phenotype
		~70h AEL third instar larvae	LOF (MARCM)	no axon guidance phenotype		no axon guidance phenotype
		~70h AEL third instar larvae	GOF (MARCM)			**axon guidance phenotype**
slit	dendrite	~16h -20h AEL	LOF	no dendrite phenotype	n.a.	
		~22h AEL late embryonic	LOF	**dendrite phenotype** longer dendritic processes		**dendrite phenotype** longer but fewer filopodia-like dendrite branches
		~70h AEL third instar larvae	LOF (MARCM)		no dendrite phenotype	no dendrite phenotype
	axons	~9-10h AEL early embryonic	LOF	no axon guidance phenotype	n.a.	no axon guidance phenotype
		~22h AEL late embryonic			no axon guidance phenotype	no axon guidance phenotype
		~70h AEL third instar larvae	LOF (MARCM)	no axon guidance phenotype		no axon guidance phenotype
robo, robo2		~16h -20h AEL	LOF	no dendrite phenotype	n.a.	n.a.
		~22h AEL late embryonic	LOF	**dendrite phenotype** longer dendritic processes	n.a.	n.a.
		~9-10h AEL early embryonic	LOF	no axon guidance phenotype	n.a.	n.a.
		~22h AEL late embryonic	LOF	no axon guidance phenotype	n.a.	n.a.

gene name	neuronal compartm.	developmental stage	method	all six md-da neurons	Class I	Class IV
robo2	dendrite	~16h -20h AEL	LOF	no dendrite phenotype	n.a.	
		~22h AEL late embryonic	LOF	no dendrite phenotype	no dendrite phenotype	no dendrite phenotype
		~70h AEL third instar larvae	LOF (MARCM)		no dendrite phenotype	no dendrite phenotype
	axons	~9-10h AEL early embryonic	LOF	axon guidance phenotype		
		~22h AEL late embryonic	LOF	axon guidance phenotype	axon guidance phenotype	
		~70h AEL third instar larvae	LOF (MARCM)			axon guidance phenotype
ena	dendrite	~16h -20h AEL	LOF	dendrite phenotype Gao et al,1999	n.a.	
		~22h AEL late embryonic	LOF	n.a.	n.a.	dendrite phenotype fewer but longer filopodia
		~70h AEL third instar larvae	LOF (MARCM)		dendrite phenotype Li et al, 2005	dendrite phenotype Li et al, 2005
	axons	~9-10h AEL early embryonic	LOF	n.a.	n.a.	n.a.
		~22h AEL late embryonic	LOF	n.a.	no axon guidance phenotype	no axon guidance phenotype
		~70h AEL third instar larvae	LOF (MARCM)			no axon guidance phenotype
dock	dendrite	~16h -20h AEL	LOF	no dendrite phenotype	n.a.	
		~22h AEL late embryonic	LOF		n.a.	n.a.
		~70h AEL third instar larvae	LOF (MARCM)		no dendrite phenotype	dendrite phenotype increased number of high order dendrite branches, tiling defects
	axons	~9-10h AEL early embryonic	LOF	no axon guidance phenotype	n.a.	n.a.
		~22h AEL late embryonic	LOF	no axon guidance phenotype	n.a.	n.a.
		~70h AEL third instar larvae	LOF (MARCM)		no axon guidance phenotype	no axon guidance phenotype
robo2, slit	axons	~9-10h AEL early embryonic	LOF	no axon guidance phenotype		
robo2, slit(-/+)	axons	~9-10h AEL early embryonic	LOF	axon guidance phenotype		

n.a…not analysed, **LOF**…loss-of-function, **GOF**…gain-of-function,

LOF (MARCM)…clonal loss-of-function, **GOF (MARCM)…** clonal gain of-function

Dendrite field development proceeds in a stereotyped manner also during larval stages.

The descriptive and quantitative analyses of dorsal da dendrite field development demonstrate that this is a stereotyped but not a temporally distinct process during larval stages. The stereotyped nature of dendrite field formation suggests that growth, organization, body wall innervations and termination are all regulated processes. We could not ascertain the presence of temporally distinct growth phases of development as it has been previously hypothesized by others (Gao et al., 1999Gao et al., 2000; Sugimura et al., 2003). This conclusion is based on the quantitative observation of the growth curve of dorsal dendrite extension during the different time points we analyzed (Fig.12). However, dendrite field development might involve functionally different growth phases due to the developmental differences that distinct classes of md-da neurons have. This has indeed been demonstrated in the example of Class I and Class IV neuron development. While the first acquires its overall morphology by the end of embryogenesis the second, Class IV, does so by the beginning of the second instar larvae stage (Sugimura et al., 2003) (Fig.20). The assumption that differences in morphology reflects possibly distinct biological functions of these neurons raising the question of the reason for such a delay of dendrite maturation of one neuron over the other (Grueber et al., 2002; Grueber et al., 2007). Several studies have shown that temporal sequence of axon development plays an important role during visual and olfactory nervous system development (Clandinin and Zipursky, 2000; Lin et al., 1995; Sweeney et al., 2007). For example, in *Drosophila* olfactory antennal receptor neuron (ORN), axons reach first their targets and act as a pioneer to guide maxillary pulp axons by using the Sema 1a/Plexin ligand/receptor system. In this temporal target restriction model, antennal ORNs, although expressing both Sema1a and PlexinA, do not necessarily use these proteins during their own path finding but rather to instruct the maxillary pulp ORN axonal pathway. Comparing these findings with the observations made in the current study, we envision a similar temporal model for dendrite field development of md-da neurons. At the time point in which Class IV neurons have just initiated their primary dendritic branch growth, Class I neurons have already acquired their overall complexity (Sugimura

et al., 2003). Interestingly, secondary and tertiary dendritic branches of Class IV neurons converge with second order dendritic branches of Class I neurons (my observation). Additionally, selective overexpression of Robo protein in Class IV neurons resulted in a side-directional dendritic arbor growth, a phenotype inconsistent with when Robo was simultaneously overexpressed in all six md-da neurons (compare Fig.15 and Fig.21). Finally, both Slit and Robo are expressed in all six md-da neurons (Fig.14). However as similarly described for ORN neurons, their function seems to be cell-autonomously required in Class IV but not in Class I neurons (Fig.19). These observations provide few indications that temporal control of dendrite field development could similarly, as for axon, play an important role during nervous system development. Exploring such hierarchical interactions could prove to be an important and critical step of dendrite field development.

Several hours after hatching, although possessing innate behavioral properties, such as crawling towards a food source, possessing rhythmic movements and breathing, the *Drosophila* larval body wall is not yet fully covered with dendrites (Fig.12 and Fig.20) (Song et al., 2007; Suster et al., 2004). In fact, the epidermal body wall of *Drosophila* larvae is fully covered with dendrites only by the beginning of the second instar larval stage and this is mediated via the morphologically most complex, field filling neuron, Class IV (Fig.20). Few studies have shown that multidendritic arborization neurons are a part of the sensory system which provides the animal with information about temperature, odors, touch, sounds, light, or electrical field and thus can be of significant importance for survival (Lee et al., 2005; Liu et al., 2003; Tracey et al., 2003). Peripheral sensory input is required during the *Drosophila* larvae locomotion and lack of sensory inputs, including those of md-da neurons leads to a cessation of larval crawling (Song et al., 2007). Why such an important system shows such a delay in its development remains an unanswered question.

We observed a highly stereotyped pattern of development for Class IV neuron, the observation is supported by quantitative analyses on the morphology of Class IV dendrite trees at different time points analyzed (Fig.20). Importantly, fractions of dendrite

branches within a length category are kept constant during a neuron's development. Although new branch formation is gradually increasing, consistent with the idea for the presence of a well coordinated mechanism of dendrite field establishment that involves the balance of new branch formation, their precise elongation/retraction and stabilization.

Robo acts cell-class specifically and cell-autonomously to establish the dendrite arbor complexity of Class IV but not Class I neurons.

We observed that Robo protein is required to shape the dendritic arbor of the field-filling Class IV neurons and does not play a role in the establishment of Class I dendritic architecture; by using cell-class specific genetic markers we could ascertain that both Robo and Slit act during dendrite field formation of Class IV but not Class I neurons. Consistent with this idea are the mosaic analyses of *robo* Class I and Class IV neurons - while the first type of neurons were able to develop a normal dendrite tree despite the lack of functional Robo, in the second, Class IV neurons, the dendritic architecture appeared highly simplified, with significantly reduced high order dendritic branches (Fig.19).

Given the temporally distinct modes and strategies of development these two types of md-da neurons have, this provides a plausible explanation for the preferential requirement of Robo and its ligand Slit during late embryonic/early larval stage to promote dendrite arborization of the much later developing Class IV neurons (Fig.12 and Fig.16) (Grueber et al., 2003b; Sugimura et al., 2003). While Class I neurons, the morphologically simplest, have established their overall complexity by late embryogenesis (20h-22h AEL), by this stage, Class IV neuron has developed only low order branches and possess a visibly simple dendritic arbor (Sugimura et al., 2003). Both loss-of-function and gain-of-function analyses at two different time points of Class IV dendrite field development revealed two different phenotypes which share certain similarities, including reduced number of high order branches and simplified dendrite morphology. While at earlier stages of Class IV dendrite field development the removal or addition of Robo resulted in defects of dendrite branch length and number, at later

stages such alteration of Robo function only affected branch number. Hence, it is possible that Robo protein can act at during different time points of dendrite field development to control diverse steps of the dendrite architecture via separate pathways. Alternatively, the defects observed at the final stage of development of Class IV dendrite arbor may be a consequence of the early embryonic defects caused by removal or addition of too much of the protein.

Recent *in vivo* time lapse analysis with cell-specific Gal4 lines has provided information about the development of Class IV neurons for only 3 time points, namely ~24h, ~40h and ~65h AEL; and leaves the question as to how this neuron accomplish its arbor complexity still unanswered (Grueber et al., 2003b; Sugimura et al., 2003). It could first send several dendrite processes which increase in length and thus occupy certain territories, which are later filled with branches. Alternatively, the neuron may gradually increase in arbor complexity by iterative branch addition, stabilization and elongation. We performed detail developmental analyses of the Class IV neuron in order to provide some further insights into the function of Robo. Static time-point analysis on Class IV neuron for 10 different time points supports the hypothesis that the dendrite complexity of those neurons is achieved gradually, through well regulated steps of new branch formation and dendrite branch elongation (Fig.20). Such mechanisms of development led us to suggest that alterations in Robo function at early stages of dendrite field development would reflect defects in dendritogenes also at later stages.

Furthermore, we observed that the Robo/Slit signaling system is not necessary for the establishment of the basic architecture of Class IV neurons but is required to regulate dendrite branch elongation and formation of high order processes (Fig.19). In addition, detailed phenotype analysis, beginning from the time point when dendritogenesis is initiated, suggests that Slit and Robo are not required during dendrite growth initiation (Fig.13 and Fig.23). Such a function has been observed for the *Drosophila* protocadherin Flamigo (*Fmi)* and the transcription factor *sequoia* (Brenman et al., 2001; Gao et al., 2000).

Several lines of evidence strongly suggest that dendrite innervation defects in *robo* mutants (Fig.16 and Fig.19) are a primary cause of loss of Robo function and are not due

to some other developmental defects such as cell clustering, cell migration or mild muscle patterning defects resulting upon *robo* loss-of-function (Kramer et al., 2001). If muscle patterning defects are the primary cause, such a dendrite phenotype would appear earlier during embryogenesis and would not be restricted to only a specific class of neurons (Gao et al., 1999). Furthermore, *robo2* mutants, similar to *robo* mutants, show similar cell-clustering and cell-migration defects; however in these mutants dendrite field development is not affected.

Certainly, a primary function of Robo in regulating fine branch formation during dendrite field development of Class IV neurons is firmly established by three key findings; MARCM and rescue experiment together with the expression of Robo in md-da neurons provide strong support that dendrite field developmental defects caused by *robo* are upon its direct and specific role in regulating high order branch elongation and their formation. In addition, transgenic expression of Robo in md-da neurons only partially restored the normal projection of dendrite fields; however one caution is needed in interpreting these results. Transgenic rescue experiments, by their nature do not necessarily tell us how the endogenous Robo protein operates and often have some crucial caveats. For example, the level and timing of transgenic Robo protein could conceivably be influenced by the Gal4 amplification system.

Robo is required for the filling in response during dendrite development of the neuron

We propose a model for which the function of the Robo/Slit signaling system is a part of the molecular mechanism required to promote a stop or inhibitory signal in high order dendrite branch elongation. While at later stages of dendrite field development, dendro-dendritic contact-mediated inhibitory mechanisms (such as tiling and self-self recognition mechanisms) may act to limit the size and the shape of the dendrite field of Class IV neurons (Grueber et al., 2002; Grueber et al., 2003b), it is highly anticipated that during early larval stages such control is molecularly mediated (Emoto et al., 2006; Gao et al., 2000).

We suggest a molecularly mediated homeostatic regulation of dendrite branch number and length of a dendrite field during early stages. In support of this is the observation that a loss-of-function mutation in *robo*, *slit* or *ena* genes did not alter the total dendrite length of Class IV neurons at ~ 22h AEL (Fig.16). Presumably, loss-of-function of any of these proteins, including Slit, Robo and Ena does not affect the ability of a neuron to compete for a territorial space. We speculate that an inhibitory signal for high order dendrite branch elongation during dendrite development is what ensures the uniform and efficient innervation with fine dendrite processes of an area of the *Drosophila* epidermal body wall and that regulatory mechanisms, such as the filling-in response and competition are linked together, however are molecularly separable. Lack of Robo or Slit function did not change the ability of homologous dendritic branches to recognize each other and tile properly. Defects in territory size due to lack of dendritic avoidance have been reported for other molecules such as Flamingo, Furry (Fry) and Tricornered (Trc) (Emoto et al., 2004; Gao et al., 2000). Interestingly, alterations of the function of any of these proteins, as similarly observed for Robo or Slit proteins, do not affect the dendritic branching pattern in a global way; instead Flamingo is required to limit the extension of dorsally extending dendrite processes and thus regulates tiling, while Fry and Trc mediate tiling by controlling terminal branch numbers. These studies together with the data obtained in our analyses suggest that the onset of competition, dendrite territory size specification, filling-in responses, tiling and cell-cell avoidance mechanisms can be differentially modulated due to distinct molecular systems used by the neuron to control this processes.

In our current model, we propose a function for Robo in mediating the filling-in response of Class IV neurons. There are a few reasons why we think this might be the case- the overall dendrite architecture of *robo* mutant Class IV neurons is not affected and primary and secondary branches show the same number and length supporting the observation that Robo has no effect on establishing the overall dendrite architecture. Furthermore, the regulation of dendrite outgrowth, involving the formation of low (primary, secondary, tertiary) branch order seems to be under a molecular control distinct to that of the Robo/Slit receptor–ligand system (Fig.12 and Fig.23)

An indirect but supportive observation is the lack of a role for Robo in dendrite field development of Class I neurons, although this neuron expresses the protein (Fig.14). Until now, all of the effort aimed to identifying factors that regulate dendrite patterning of Class I neurons have found molecules involved in cytoskeleton regulation or transcription factors (Grueber and Jan, 2004; Li et al., 2004; Parrish et al., 2006; Sugimura et al., 2003). This, the relatively simple dendrite morphology of Class I neurons, and the fact that they are able to cover only a small fragment of the dorsal abdominal segment favors the idea that removing a sensor for filling-in response such as Robo would not change the dendrite architecture of Class I neurons.

It appears that at late embryonic stages of Class IV dendrite field development, removing Robo function results in a disturbance of the balance between branch elongation and new branch formation. At this point it is difficult to determine whether restricting branch elongation is instructive for new branch formation, but it is an attractive speculation. Further support for this idea comes from the time-lapse imaging gain-of-function analyses (Fig.17 and Fig.18). It is the repulsive activity of Robo which seems to affect dendrite branch elongation and block new branch formation, resulting in more simplified dendrite morphology. In support of this is also our observation that at ~22h AEL, overexpression of Robo results in ectopically formed filopodia-like structures at the tip of a dendrite shaft, also later, at ~48h AEL, we observed formation of membrane ruffle-like structures, which have been proposed to be the precursor of a filopodia (Fig.16). Thus, Class IV neurons overexpressing Robo have not lost their capacity to form branches.

An anticipated model is that Robo, in its classical function as a transducer of repulsion, limits the elongation of high order dendritic branches and thus enables the formation of new ones. Once the receptive field area is covered with dendrites and each cell has invaded and specified its territories, in addition to the molecular mechanisms that restrict the growth and determine the field size, cellular mechanism also come into play (Grueber et al., 2003b).

Robo plays a permissive role in dendrite branch formation and elongation.

Neurons need to be able to determine when and where to make branches. A single extrinsic factor can help sculpt different branch morphologies via distinct actions. For example, in an instructive model, Robo may mediate signals that directly target new branch formation; in a permissive model, Robo activation would result in activation of other signals that allow the dendrite tree to shape its architecture. The gain-of-function analyses support a model in which Robo plays a permissive role during dendrite field development. Elevated levels of Robo did not result in increased dendrite branch formation, reflecting a scenario in which Robo protein levels are a crucial factor for activating signaling events directly involved in dendrite growth and branching (Fig.15, Fig.16 and Fig.21). Importantly, a recent study from the laboratory of J. Brenman with the example of CaMKII and its role in dendrite plasticity provides convincing data elucidating the distinction between cytoskeleton regulation and morphological regulation (Andersen et al., 2005). Their work suggests that morphological stability and cytoskeletal stability are differentially regulated processes and explains how a neuron can adapt its function to environmental changes. Such mechanisms that distinctly regulate morphological plasticity and cytoskeletal dynamics can be crucially important during synapse formation and neurite outgrowth. What is the biological significance of Robo during dendrite field development? It is attractive to think that Robo may play a role in regulating morphological plasticity but not cytoskeletal stability during dendrite field development to affect synapse formation. Previous studies have shown that the processes of arborization and synaptogenesis are ultimately connected (Niell et al., 2004; Sanchez et al., 2006). And a recent *in vivo* time lapse imaging study on zebrafish RGC arbor formation provides compelling evidence that the Slit-Robo ligand–receptor system can, in contrast to its positive role on DRGs axon arborization, inhibit axon arborization and regulate synaptogenesis (Campbell et al., 2007). The lack of presynaptic partners for dorsal da neurons is a drawback of the system, but does not exclusively preclude similar requirements for Robo. Changing the anatomy of the neuron by affecting its fine branch formation could in principle reflect an indirect but important role for Robo in synaptogenesis. Thus, the cell-class specific effect of Robo on fine dendrite branch formation indirectly, but importantly, affects the functional specificity of this neuron.

Robo acts in its classical role as a receptor for the repulsive cue Slit to limit dendrite branch elongation

New branch formation, stabilization, elongation and/or retraction are all processes involving the activation of regulators of actin and microtubule dynamics. Dendrite shafts are composed of microtubules, while dendrite fine processes are built of extremely dynamic actin networks. During dendrite outgrowth and arborization the actin and microtubule composed cytoskeleton must be continuously regulated. Fine dendritic branches arise as filopodia like structures which subsequently have to extend and/or retract, and/or stabilize. Loss-of-function analyses of *robo* or *slit* mutant Class IV neurons revealed that these proteins affect the elongation of fine processes. Given the classical, most well understood function for Slit in mediating axon repulsion at the midline of invertebrates and vertebrates, it is likely that such dendrite elongation defects are due to the lack of a repulsive function for Slit mediated via its receptor Robo. Similarly*, in vivo* time-lapse imaging of *robo* mutant *Drosophila* motor neuronal growth cones form longer filopodia due to the lack of a repulsive mechanism mediated via Robo (Murray and Whitington, 1999).

Genetic analyses of factors involved in axon guidance identified Ena and Abl as key signaling components of Robo mediated repulsion in the CNS of *Drosophila* (Bashaw et al., 2000). Abl can interact with Ena, the cyclase-associated protein (Capulet), and the microtubule plus-end tracking protein Orbit/MAST/CLASP und thus induce some effects on actin and microtubule assembly thought to lead in both cases to repulsion at the growth cone of an axon (Bashaw et al., 2000; Wills et al., 2002Lee et al., 2004). Genetic loss-of-function and gain-of-function experiments for Robo result in a similar effect on the dendrite field architecture of Class IV neurons, causing a highly simplified dendritic arbor of the neuron (Fig.16, Fig.21**).** Such an unexpected, corresponding outcome of increasing or decreasing Robo function suggests that activation of downstream signaling

pathways leads to similar rather than opposite cytoskeleton rearrangements. Indeed, as we observed in this study for Robo, it has previously been shown that increasing or decreasing Abl function during axon guidance at the *Drosophila* midline leads to the same phenotypic defects (Bashaw et al., 2000).

Interestingly, both Ena and Abl have been analyzed and the loss-of-function of any of these proteins affects md-da dendrite field development (Gao et al., 1999; Li et al., 2005). *ena* mutant Class IV neurons show a strikingly similar phenotype to those of *robo* at both embryonic and final stages of dendrite arborization (Fig.16) (Li et al., 2005). However, unlike Robo, Ena is required in all four types of md-da neurons. Such a general requirement for a protein known to act downstream of many other receptor proteins and induce remodeling of the actin cytoskeleton is not surprising (Dwivedy et al., 2007; Gitai et al., 2003). Ena/VASP proteins are a conserved family of actin regulatory proteins known to localize at the distal tip of a growth cone filopodia and have been implicated in regulating actin dynamics (Korey and Van Vactor, 2000; Rottner et al., 1999). Known to act as a factor promoting filopdia formation, the reduced branch number in both *ena* and *robo* mutants favors a model in which the ability of neurons to form new filopodia is indeed partially intact. Filopodia are considered to serve as sensory or exploratory structures dictating the response of a growth cone to its environment (Faix and Rottner, 2006). Given the postulated role for Robo as a sensor that enables the ddaC neurons with the ability to fill-in a receptive field area with dendrites, it is a tempting scenario that filopodia-like structures, formed as precursors for dendrite branches, are able to code a signal mediated through Robo and thus decide whether or not to extend and/or stabilize. Similarly, overexpression of Robo might strongly impair the Ena mediated effect because bound to Robo, Ena cannot mediate its proposed function on filopodia growth and elongation (Bashaw et al., 2000). Consistent with this idea are also previous observations made in studies using growth cones with impaired Ena/VASP protein function. These failed to form filopodia but frequently developed large lamellipodia like structures, thought to be the precursors for filopodia (Faix and Rottner, 2006; Lebrand et al., 2004). Although it is not yet clear whether lamellipodia-like membrane ruffles are the structures from which filopodia arise or if they form independently, it is an appealing hypothesis that membrane ruffle formation, induced upon *robo* overexpression might be the outcome

of an impairment of filopodia formation due to reduced activity of Ena when bound to Robo.

In addition, a study by Fan *et al* has shown that Dock the *Drosophila* homologue of Nck, together with Pak and Rac are essential components of Robo-mediated signaling pathways (Fan et al., 2003). Whether this protein complex acts downstream of Robo during dendrite maturation remains an open question and requires further investigations. Few lines of evidence suggest that in dendrites, the Slit-Robo-Dock-Pak protein complex may be another active but limiting pathway for dendrite branch formation. Overexpression of Robo in Class IV neurons results in lamellipodia-like structures, known to be a hallmark of Rac activation. A study by Yong and Bashaw has recently reported the formation of membrane ruffles-like structures in cells transfected with human Robo receptor and stimulated with Slit (Yang and Bashaw, 2006). Thus, the high expression pattern of Dock protein in md-da neurons and the cell-autonomous and cell-class specific but opposite effect to *robo* of *dock* loss-of-function on high order dendrite branch formation of Class IV neurons (Fig.22) suggest a model in which the activation of this molecular pathway, namely Sli-Robo-Dock and the resulting cytoskeleton rearrangement events might be acting as a limiting process during new dendrite branch formation. In support of this hypothesis comes the recent report by Hughes *et al*. showing that the dominant active form of Pak in Class I neurons is strongly increased in tertiary branches (Hughes et al., 2007).

How the specific activation of Robo via Slit might regulate dendrite field development.

Loss-of-function analyses of *slit* and *robo* single and *robo, robo2* double mutant embryos in two different genetic backgrounds (80G2 and ppk-eGFP; Fig.12 and Fig.16) suggest

that Robo activation is mediated via Slit. In addition to this, MARCM of *robo2* mutant clones preclude a possible function for Robo2 receptor in dendritogenesis.

The expression pattern analyses, ectopic expression analyses, as well as MARCM analyses for *slit* did not provide any conclusive indications about the specific activation of Robo via Slit during dendrite field development.

Interestingly Slit protein is localized, as with Robo receptor, to the neurons themselves. In addition to this during larval stages, Slit appears to be localized to all muscles, suggesting that dendrite growth proceeds on a Slit positive terrain (Fig.14).

The lack of any effect on dendrite field formation upon ectopic overexpression of *slit* could alternatively be explained by the fact that the UAS-*slit* construct lacks regulatory sequences, such as 3' and 5' ends which seem to be crucial for mRNA stability, and/or translational efficacy (Mendell and Dietz, 2001). Finally, little is known about Slit protein regulation. Increasing gene dosage is the easiest but not always most promising way to generate a gain-of–function scenario for the protein. Thus, introducing another copy of the *slit* gene did not allow us to conclude how Slit may mediate its specific activation during dendrite field development of Class IV neurons.

Biochemical experiments have shown that Slit exists in a least three isoforms; a full length, a N-terminal and a C-terminal fragments produced by proteolytic cleavage of the full length version (Brose et al., 1999). Vertebrate Slit proteins were shown to be capable of repelling axonal explants (Brose et al., 1999). This function is mediated via the C-terminal portion of the protein. Interestingly, Wang *et al.* demonstrated, using cultures of DRG neurons, that the N-terminal portion of the protein can have an opposite effect and promote branching (Wang et al., 1999). Such an effect of Slit is antagonistically silenced by the full length Slit protein. Thus, it is thought that the processing of Slit into C- and N-terminal fragments is what accounts for its diverse biological function. In fact, similar observations have been made in the Eph/ephrin receptor–ligand system. Their bifunctionality in mediating both positive (i.e. attractive) or negative (i.e. repulsive) effects on cell-cell interactions can be mediated by receptor mediated endocytosis and or a cleavage (reviewed in Egea and Klein, 2007). Whether Slit undergoes cleavage and thus exerts its specific effect on dendrite branch length and number via Robo, remains an open but quite interesting matter for investigation. Cleavage mediated activation of Slit

provides an acceptable explanation why the ectopic expression of an additional *slit* gene copy does not exert any effect on dendrite branch morphology. Overexpressing a UAS-*slit* construct might require the co-overexpression of its protease in order to generate a real gain-of-function scenario.

One interesting, and at present speculative, possibility is that the regulation of Robo protein levels is a crucial factor for specificity during dendrite field development. Although one of the most extensively studied systems during nervous system development, little is known about Robo protein level regulation (Dickson and Gilestro, 2006). In the *Drosophila* CNS, the Commissureless (Comm) protein appears to specifically downregulate Robo during midline crossing of commisureless axons. However, there is no functional data demonstrating a similar role for Comm protein in the PNS of *Drosophila*, and it seems that the protein is even not express in this area (Keleman et al., 2005; Tear et al., 1996). Thus, Robo protein level regulation and specific activation during dendrite field development favors a model in which Slit itself might provide some regulatory role for Robo levels. Surprisingly, this model seems to gain on preference also during commissural axon pathfinding (Dickson and Gilestro, 2006). How can such model provide an explanation for the observed effect of Robo on dendrite field development? A plausible explanation is that the differential sensitivity of dendrite elongation and/or retraction, new branch formation, and stabilization of high order branches would require different Robo protein levels. One possible scenario is that newly formed branches have low levels of Robo or none at all and thus can grow on a Slit positive terrain. An increase in Robo protein levels would result in an increased sensitivity, slow down the growth and thus promote stabilization of the dendrite branch. Such a scenario is supported by the gain-of-function experiment and the time-lapse analyses (Fig.15 and Fig.17 and Fig.18). The increased sensitivity of a dendrite branch having high levels of Robo, fails to extend or even form. Thus the highly repulsive environment generated by introducing additional *robo* copies works as an obstruction for elongation and new branch formation and assists the hypothesis that Robo protein levels might be the key to Slit mediated specific regulation during dendrite field formation.

A final possibility is based on the speculation that Robo and Slit, may similarly, as recently shown for Eph A3 and ephrin A5, undergo possible interactions in *cis* and *in trans* to respectively inactivate or activate each other during dendrite field formation (Carvalho et al., 2006; Egea and Klein, 2007).

Robo and Robo2 function differently in axons and dendrites

A crucial question that arises from our analyses is how a protein, which plays a fundamental role during axon guidance and patterning, could distinguish its function on dendrite growth and branching. The answer to this question may come from our phenotype analyses on axon projection of dorsal da neurons.

robo2 mutants, but not *robo*, *slit* or *robo,robo2* double mutants show severe axon pathfinding defects, suggesting a role for Robo2 in negatively regulating Slit-Robo activation during axon guidance (Fig.12 and Fig.23). Axons expressing Robo can, in the absence of Robo2 but presence of Slit, change their growth directions dramatically and even often intermingle with the future dendrite field (Fig.23). To ascertain the regulatory role for Robo2 during axon guidance we generated and tested double mutants homozygous for *robo2* and heterozygous for *slit*. As expected, removing Robo2 completely and reducing Slit levels generated a condition in which Robo activation is still possible, supporting the idea that Robo2 acts to downregulate Slit mediated activation of Robo and allows axons to reach their targets (Fig.23). In addition, overexpression of Robo with a pan neuronal marker, such as *elav*–Gal4, results in axon guidance patterning defects. In such a scenario, increased levels of Robo protein generated conditions, similar to those when Slit protein, was reduced on a *robo2* null background. Taken together, expression pattern and phenotype analyses suggest a requirement for Robo2 during axogenesis but not dendritogenesis. These observations provide us with an indirect but helpful explanation of how a neuron uses one and the same protein to regulate the development of its functionally and morphologically distinct processes - axons and dendrites. Furthermore, it suggests that although axons and dendrites develop in a different chronological order, a molecular control is required to keep these processes

growing away from each other. Otherwise, axons would show a high tendency of growing within their own dendrite field or a neighboring one. In this scenario the establishment of a neuronal network within an organism is highly disrupted. It would be interesting to follow how such a disrupted pattern of connectivity affects the behavioral response of the *Drosophila* larvae. Since in *robo2* mutants often only some md-da neurons from only a few abdominal segments show severe axon guidance defects of md-da neurons, these mutants offer a great model to explore and address questions about the circuits that underlie such control.

The lack of an axon guidance phenotype in *robo* mutants, suggests that in dorsal da neurons this protein is required for targeting only (Parsons et al., 2003; Zlatic et al., 2003). Interestingly, analyses on bipolar neurons, a type of dorsal da neuron, in *slit* mutants have shown that axons of this neuron fail to branch and continue to grow across the midline. These observations suggest that Robo protein involved in neuronal branching appears to function similarly in axons and dendrites of dorsal da neurons. Thus, the requirement of Robo(s) proteins in both dendrites and axons might be an economical strategy of the neuron to keep available a protein whenever and wherever it is needed.

Our results are consistent with a model for Robo/Slit signaling in which these proteins are a part of the molecular mechanism involved in keeping the balance between new dendrite branch formation, elongation, and stabilization; thus sculpting the dendritic architecture of Class IV neurons (Fig.24).
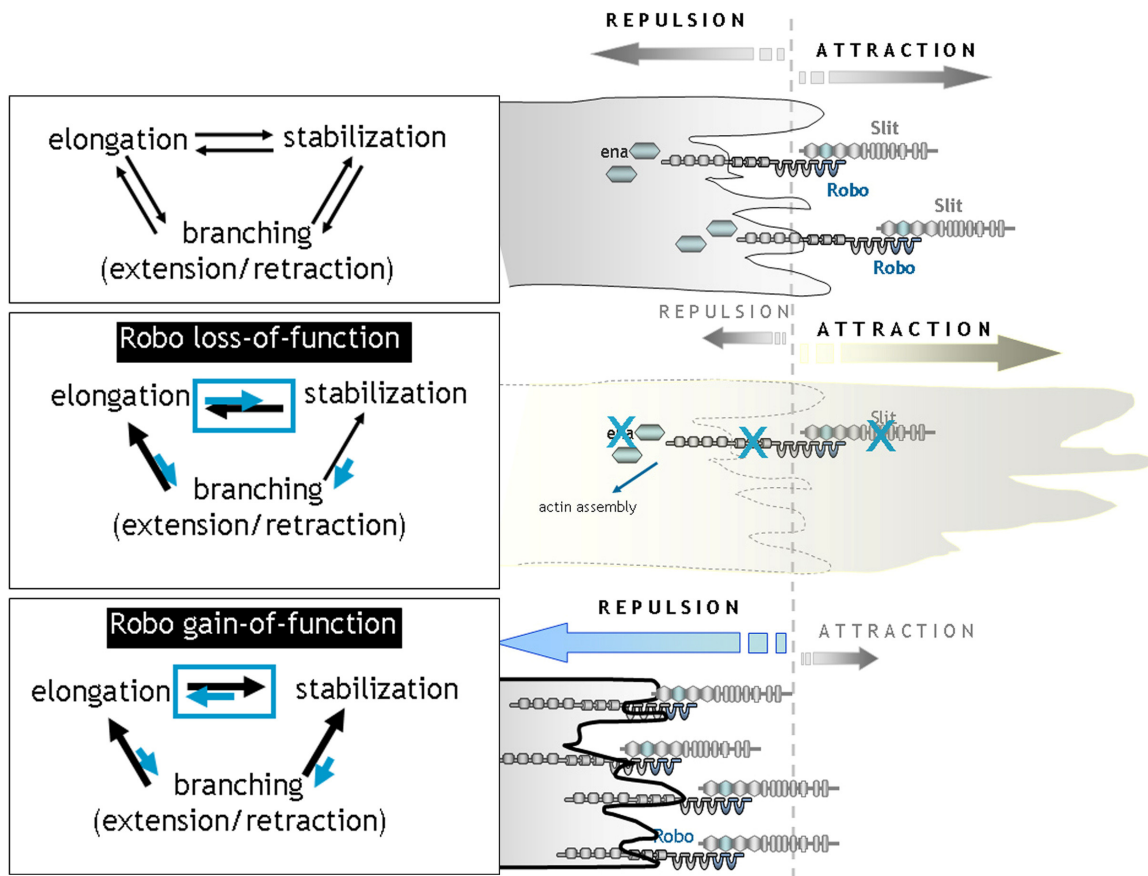
FIGURE 24 A model for dendrite branch formation with a possible requirement for the Robo/Slit/Ena signaling system

Formation of branches involves the well coordinated balance between new branch formation in the form of filopodia that either elongate or retract. Growing filopodia need to stabilize and become a substrate for new branch formation. Lack or overexpression of Robo disturbs the balanced mechanisms of branch elongation, new branch formation and stabilization. A complete Robo loss-of-function results in the formation of longer and fewer high order branches, due to the lack of an inhibitory signal that mediates the levels of extension, while adding too much of the receptor induces more repulsion. The model suggests that the precise balance between dendrite branch elongation, stabilization and new branch formation is under a complex molecular control a part of which is the Robo/Slit receptor- ligand system.

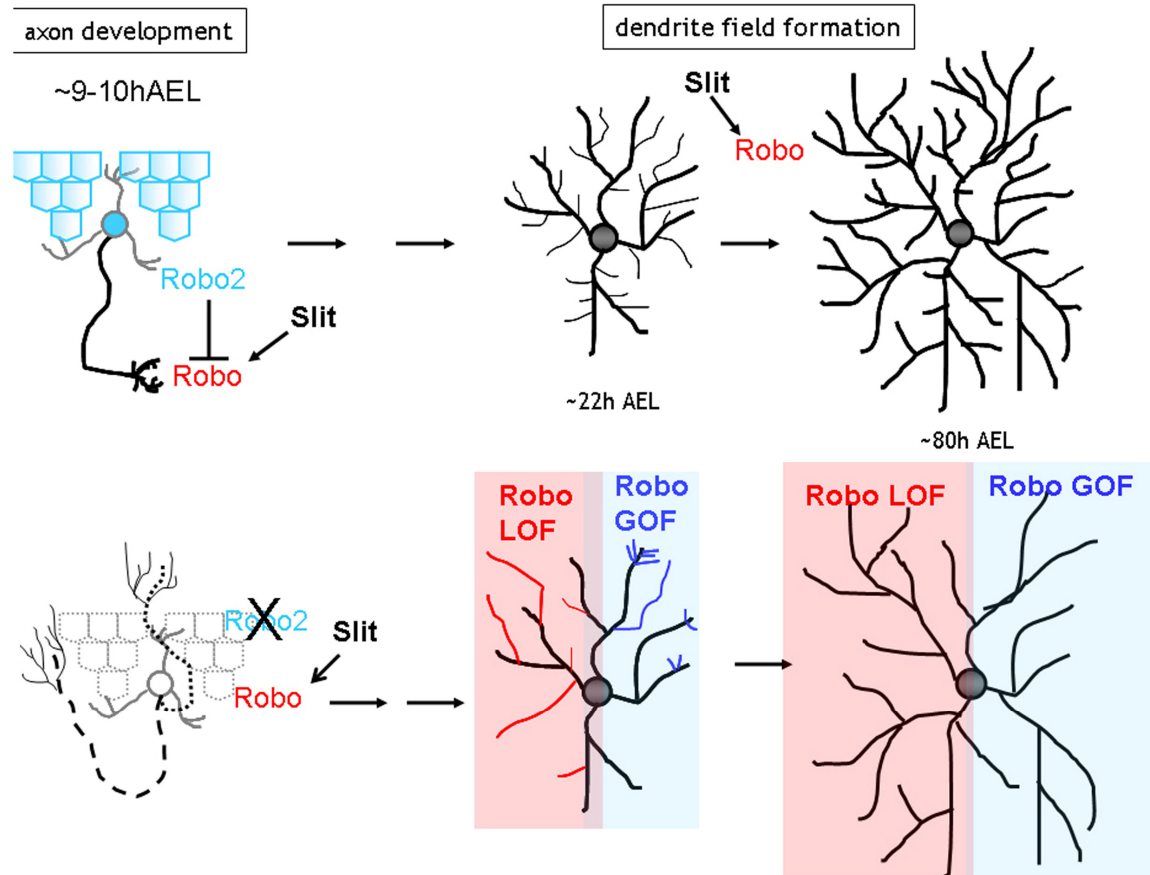**FIGURE 25. <u>Schematic representation of the Robo2-Robo-Slit functions during axon and dendrite field development</u>**

Robo2-expressed in sensory neurons and in a layer of epithelial cells (depicted as blue pentamers), at the time of axogenesis, is probably required to downregulate the activation of Robo via Slit. Loss-of Robo2 function results in severe guidance defects.

During late embryonic/early larval stages Class IV neurons gain in complexity by highly stereotyped mechanisms that promote the regulation of high order dendrite branch number and their level of elongation. This homeostatic regulation of branch length and new branch formation seems to require the activation of Robo via Slit. Robo is not required during the establishment of the basic dendrite architecture of Class IV neuron, but mediates the formation of high order branches by acting as a growth inhibitory signal for the fine dendritic processes and enabling the neuron to fully cover its receptive field with branches. Removing Robo function (LOF) or adding too much of the protein (GOF) disturbs the pattern of dendritic branch elongation and new branch formation at late embryonic/early larval stages (~22h AEL). At the final stage (~80h AEL) of dendritic arborization, the ddaC neuron looks highly simplified in its dendritic architecture.

Concluding remarks

The Robo family is a highly conserved group of proteins across species and is essential and required during nervous system development. However its specific function during dendritogenesis is poorly understood, but as it is obvious from our analyses, is important for establishing a functional nervous system because of its role during axon path finding. Of significant importance for our understanding as to how dendrite architecture is finely shaped, would be to find out how Slit and Robo interact in space and time to orchestrate such a dynamic process as dendrite field development. Recent advances in dendrite development have revealed that Golgi outposts possess crucial role for dendritic arbor patterning (Ye et al., 2006). Robo is postranslationally regulated, and surface labeling experiments have shown that in commissural axons, Comm brings Robo to endosomes directly from the Golgi (Keleman et al., 2005). The lack of Comm in PNS neurons needs to be further investigated and leaves the question about Robo protein regulation unanswered. Given the cell-class specific effect of Robo on dendrite field development of Class IV neurons, it would be interesting to investigate whether these mutants show some behavioral defect, such as alteration in touch and/or temperature sensation.

4. Materials and methods

4.1 Fly Stocks

NAME / GENOTYPE	SOURCE / DONOR
Deficiency Kit for the second left Chromosome	Bloomington Stock Center http://flystocks.bio.indiana.edu/Browse/df-dp/dfkit.htm
$y^1, w^{67c23}, dock^{P13421}$ / CyO	Bloomington Stock Center
cn^1, sli^2, bw^1, sp^1 / CyO	Bloomington Stock Center (BL#3266)
y^1, w^1;FRT^{40A}	Bloomington Stock Center
w^1,elav-Gal4,hs-FLP, UAS-mCD8-GFP; FRT^{40A}, tubGal80 / CyO	Yuh Nung Jan – UCSF - USA
y^1, w^1;P(GaWB)109(2)80, P(UAS-GFP)–**80G2**	Yuh Nung Jan – UCSF - USA
y^1, w^1;P(GaWB)109(2)80, P(UAS-GFP), girandola / CKG	Yuh Nung Jan – UCSF - USA
y^1, w^1;P(ppk-eGFP)	Yuh Nung Jan – UCSF - USA
y^1, w^1;P(UAS-robo^{T187}) / TM3,Sb,Ubx,lacZ	Barry Dickson – IMP Vienna -Austria
y^1, w^1;robo2^8 / CyO,wg-lacZ)	Barry Dickson – IMP Vienna -Austria
y^1, w^1;robo2^9 / CyO,wg-lacZ)	Barry Dickson – IMP Vienna -Austria
y^1, w^1;P(UAS-robo^{T186}) / TM3,y^+	Barry Dickson – IMP Vienna -Austria
w^1,elav-Gal4,hs-FLP, UAS-mCD8-GFP; FRT^{42D},tubGal80 / CyO	Takashi Suzuki- MPI Munich -Germany
y^1, w^1;FRT^{42D}	Takashi Suzuki- MPI Munich -Germany
y^1;FRT^{42D}, ena^{46} / CyO	Fen-Biao Gao-UCSF - USA
robo^{GA285} / CyO	Guy Tear–UC- London- UK

Fly Stocks generated during the work
y^1,w^1;*robo2^8*,80G2 / CKG
y^1,w^1;*robo2^8*,80G2, *robo^{GA285}* / CKG
y^1,w^1;*robo2^8*80G2,*slit^2*, / CKG
y^1,w^1,80G2, *robo^{GA285}* / CKG
80G2,*slit^2*, / CKG
y^1,w^1;Gal4(109(2)80);ppk-eGFP,P(UAS-robo^{T186}) / TKG
y^1,w^1;80G2;P(UAS-*robo*^{T186}) / TKG
y^1,w^1;FRT^{42D}, *dock^{P13421}* / CyO
y^1,w^1;FRT^{40A} *robo2^8* / CyO
y^1,w^1;FRT^{42D}, *robo^{GA285}* / CyO

4.2 Immunohistochemistry

4.2.1 General Antibody Staining for *Drosophila* mounts

Fixation

Embryos were collected for 1h in population cages with yeast-apple agar plates, and allowed to develop at 25°C until they reached the time point of interest (either 9h -10h AEL or ~20h - 21h AEL) These were then decorinated in 50% bleach (NaCLO) for 3 minutes and rinsed well with PBT (0.1%Triton in 1%PBS). The decorinated embryos were then fixed. By placing them into a scintillation vial containing heptane:PBS-FA (4% formaldehyde in PBS) in a 1:1 ration (vol:vol) and shacked gently for 20 to 45 minutes. The lower, aqueous layer was then removed and replaced with methanol (CH$_3$OH). In this solution, fixed embryos were stored at -20°C

113

Staining

For staining embryos were washed for~1h-2h in PBT and incubated for 60 min in blocking solution containing 5% normal goat serum or fetal goat serum and 0.1% Triton or Tween in PBS. Monoclonal antibody raised against MAP1b-Futsch (Hummel et al., 2000) was diluted (1:100) in Phosphate-buffered saline (PBS) containing 0.1% Triton (PBT). Slit (6D.4 from DSHB), Robo (13c9) monoclonal antibody (DSHB) and Robo2 (kindly provided by B.J.Dickson) were diluted (1:50) in PBS containing 0.1% Tween-20 (Sigma). Embryos were then incubated with a fluorescent secondary antibody, diluted 1:100 (Alexa 488, Jacksons Laboratories). Whole embryos were mounted in 90% glycerol and visualized by confocal microscopy (Leica TCS SP2).

Embryo Filet

Fixed and stained embryos were placed onto a glass slide in order to make the embryo stick to the cover glass and not move for reorientation. A tungsten needle was used for dissections. First, a piece of the anterior and posterior part of the body was cut. By rubbing the needle up and down along the ventral or dorsal midline a thin cut onto the epidermal body wall was made. Once a cut is made the epidermal body wall of the embryo is gently pressed down onto the glass. Next, the gut was to be removed, leaving only a filet of an epidermis and muscle tissue mounted on the glass ready for imaging.

General Antibody staining on third Instar Larvae Filet

3rd instar larvae were immersed in PBS and opened along the ventral midline. Filleted and pinned larvae were fixed with 4% formaldehyde for 30min at room temperature, rinsed several times in PBS with 0.5% Tween-20 (Sigma) and blocked in 5% normal goat serum (NGS; Jackson Laboratories). Primary antibodies were used at a concentration of 1:10 for mouse anti-Robo or mouse anti-Slit (Hybridoma Bank) and incubated overnight at 4°C. Secondary antibodies used were Rhodamine-Rx-conjugated donkey anti-mouse (diluted 1:50; Jackson Laboratories) and CyTM2-Conjugated AffiniPure Goat Anti-

Rabbit (diluted1:50 Jackson Immuno Research). After overnight incubation in secondary antibodies, the tissue was washed for several hours in PBS-Tween, mounted in 90% glycerol and immediately imaged.

Antibody-Name	Source/Donor
mouse anti Slit (C555.6D)	Hybridoma Bank USA
mouse anti Robo((13C9)	Hybridoma Bank USA
mouse anti Futsch/22C10	Hybridoma Bank USA
mouse anti-Fasciclin II(1D4)	Hybridoma Bank USA
rabbit anti Robo2	Barry Dickson-IMP Vienna
Alexa Fluor 488 goat anti mouse IgG	Molecular probes - Germany
Cy^{TM}2-conjugated AffiniPure Goat Anti-Rabbit IgG	Jackson ImmunoResearch- USA
Rhodamine RedTM-X-conjugated AffiniPure Fragment Donkey Anti-Mouse	Jackson ImmunoResearch- USA

4.3 Instruments

Leica SP2 Confocal Microscope, Leica GmbH Heidelberg Germany
Leica MZ16 Fluorescent Dissect scope Leica GmbH, Heidelberg Germany
DNA engine, (Thermocycler), BIORAD, Munich, Germany

4.4 Consumables

Fly food vials, Greiner Bioone, Germany

Fly food plugs, Kunststoffteile Klühspies, Germany

Microscope slides 76mm x 26mm, Menzel Gläser, Germany

Microscope cover glasses 24mm x 40mm, Menzel Gläser, Germany

Small petri dishes, Mat Tek Corporation, USA

Staining Cups, Lymphbecken, Germany

Reaction Strip 0.2ml, Biozym, Germany

Immersion Oil Leica GmbH, Heidelberg (Germany)

Halocarbon Oil-S3, Germany

Granulated Yeast, Fermipan, Holland

Dissection Sessiors F.S.T, Heidelberg, Germany

4.5 Solutions and Media

Phosphate Buffer Saline (1x), MPI for Neurobiology, Martinsreid, Germany

PBT (1x) 0.01% Triton X-100 in 1x PBS

Triton, Carl Roth , Karlsruhe, Germany

PFA (4%), 4% Paraformaldehyde in 1x PBS, pH 7.4

Glycerol, MERCK, Darmstadt, Germany

Methanol, MERCK, Darmstadt, Germany

Sodium Hypochlorite Solution, MERCK, Darmstadt, Germany

Tween 20, Sigma, Germany

Ethanol, MERCK, Darmstadt, Germany

Glacial Acetic Acid, MERCK, Darmstadt, Germany

Tris (2-Amino, 2-(hydroxymethyl), 1.3- Propanediol) Hydrochloride (0.1M), Sigma Germany

EDTA (Ethylene diamine tetracetic acid) (0,1M), Sigma, Germany

SDS Sodium Dodacyl Sulfate (1.1%vol), Sigma, Germany

DEPC (1%) Diethyl Pyrocabornate, Sigma, Germany

KAc (Potassium Acetate) 8M, MERCK, Darmstadt, Germany

4.6 Fly maintenance

Drosophila melanogaster flies were kept on a standard fly media at 25° C and ~80% relative humidity (RH)

Fly food

(1L) Yeast 15.0g

Agar 11.7g

Molasses 80.0g

Corn flour 60.0g

Methylparaben 2.4g

Propionic Acid 6.3ml

Yeast paste (yeast granules and fly water) was added to the bottles in order to enhance egg lying.

Fly water 0.8% $CH_3 COOH$ in dd H_2O

Apple agar for Embryo Collection

500 ml 100%Apple juice

480ml ddH^2O)

40mg Agar

10.5 ml 95% Ethanol

10ml Glacial Acetic Acid

4.7 Molecular biology

DNA Isolation

20-30 Flies were smashed in Solution containing 0.1M Tris HCL, 0.1M EDTA, 1.1 % vol SDS and 1% DEPC. The smashed flies were incubated for 30 min at 90°C and then for 30 min on ice. 14µl per 100 µl 8M KAc was add to the solution in order to precipitate all tissue compartments and cellular proteins. After 15min centrifugation the supernatant was extracted in Chlorophorm/Benzol (1:1) elute. The dissolved DNA was precipitated with isopropanol, the pellet washed in 70% ethanol, aired dried and resuspended in 100µl water.

Polymerase Chain Reaction

PCR amplification with genomic DNA **,**

Primers (0.4µm)

$MgCl_2$ (1.5 mM)

dNTPs (0.2mM)

TaqPolymerase (5000U/ml)

Cycle conditions were as follows: Denaturation at 94°C for 5min, followed by 36cycles at 94°C for 30sec, annealing at 59° C for 30sec and elongation at 72° C for 90sec and final extension at 72° C for 10 min. We carried out PCR in a Thermocycler BIORAD, Germany. The PCR products were loaded on a 0,8% Agarose Gel and analyzed using a UV Transilluminator Herolab, Germany. Amplification reactions which resulted in a single band were further treated with ExoSAP-IT (US Biochemicals) to remove primers and excess nucleotides. For sequence analyses, two separate reactions were prepared, each using one of the PCR primers as a sequencing primer.

Mutation identification

We searched for sequence polymorphism in an aligned DNA fragment from 80G2 versus *80G2,girnadola* homozygous DNA; Pair-wise computational alignment of the corresponding DNA fragments using a SeqMan Programm(DNA STAR) were prepared.

Primer Sequences

Robo2

GT78 LEFT PRIMER Tm 57.3°C, GC 50.0%   GCGCGTATCGAGAAATGAGT
GT79 RIGHT PRIMER Tm 58.8°C, GC 57.9%   AGTGCAGCGACATGAGGAG
PRODUCT SIZE **508**bp

GT80 LEFT PRIMER Tm 57.3°C, GC 50.0%   ACATCCAACACGCACTCAAG
GT81 RIGHT PRIMER Tm 59.4°C, GC 55.0%   GTCGTCTAACCCCAACGAGA
PRODUCT SIZE **617**bp

GT82 LEFT PRIMER Tm 55.9°C, GC 42.9%   GCTCGTGTGTCTAATAATCTC
GT83 RIGHT PRIMER Tm 55.3°C, CG 45.0%   AGTCGCATTTGTGTCGCTTT
PRODUCT SIZE **372**bp

GT84 LEFT PRIMER Tm 60.5°C, GC 55.0%   AAGCCGTAAACCCTGAGTCC
GT85 RIGHT PRIMER Tm60.2°C, GC 55.0%   CCCCAGTAAGAGAGCCAACA
PRODUCT SIZE **940**bp

GT86 LEFT PRIMER Tm 57.3°C, GC 50.0%   CCATTCCACACATCCTCACA
GT87 RIGHT PRIMER Tm 59.4°C, GC 55.0%   ACATCTCCGGACAGCAGACT
PRODUCT SIZE **1438**bp

GT88 LEFT PRIMER Tm 55.3°C, GC 45.0%   CAACGGAAAATCCTCTTGGA
GT89 RIGHT PRIMER Tm 56.7°C GC 55.0%   CTTCAATCGTCATCCACCG
PRODUCT SIZE **1188**bp

GT90 LEFT PRIMER Tm 60.2°C, GC 55.0%   TCCTCAATCTCAGCCGTACC
GT91 RIGHT PRIMER Tm 60.2°C, CG 40.0%   AAAGCGATTTTGGCAACAAG
PRODUCT SIZE **843**bp

GT92 LEFT PRIMER Tm 59.2°C, CG 45.0%   GGCGGCTCTTTTGTATGTTT
GT93 RIGHT PRIMER Tm58.1°C, GC 38.1%   TTTTATTGTCGTCGCTTTGAG
PRODUCT SIZE **778**bp

GT94 LEFT PRIMER Tm 60.0°C, CG 50,0%   GCCAGTGGGTCAGAGGAATA
GT95 RIGHT PRIMER Tm 59.9°C GC 55.0%   TGCAGATCACTCTGGGACTG
PRODUCT SIZE **1192**bp

4.8 MARCM Analyses

For MARCM experiments, *robo2^8* was recombined with FRT^{40A} (obtained from Bloomington Stock center) and *robo^{GA285}* or *slit^2* with FRT^{42D} kindly provided by T. Suzuki (MPI of Neurobiology, Germany). MARCM analyses were performed as described previously with some modifications (Grueber et al., 2002). In brief, to generate mosaic mutant clones *robo2^8, FRT^{40A}/ CyO*, or *w; FRT^{40A}*, or *FRT^{42D}, robo^{GA285}/ CyO* or *w; FRT^{42D}* flies were mated with *w; elav-Gal4, hsFLP; FRT^{40A}, tub-Gal80/ CyO or w; elav-Gal4, hsFLP; FRT^{42D}, tub-Gal80/ CyO,* respectively. Embryos were collected for 2h and allowed to develop for 3h–5h at 25°C before being heat-shocked at 37°C for 45 min, followed by room temperature recovery for 30 min, and an additional exposure to 37°C for 30 min. The eggs were kept at 25°C and third instar larvae were directly examined for mutant clones. Fluorescence images were obtained by confocal microscopy (Leica TCS SP2).

<u>MARCM method;</u>

MARCM (mosaic analyses with a repressible cell marker) is a widely used technique in *Drosophila* which enables the establishment of a labeled (mostly with GFP) homozygous mosaic clone in otherwise unlabeled heterozygous animal.
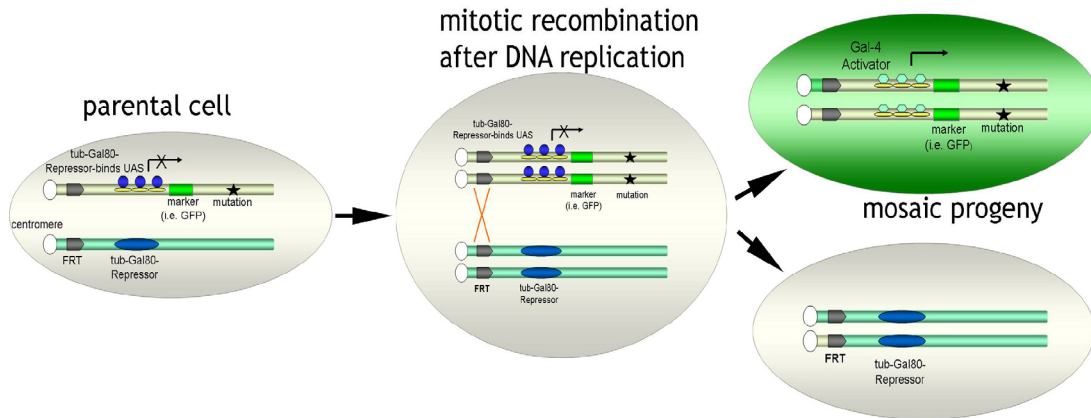
FIGURE 26.**The MARCM strategy.** A transgene encoding the repressor (tubGAL80, depicted in blue) of a marker gene expression (in this case UAS-GFP, UAS represented as yellow ellipsoids and gfp as a green bar) is placed distal to the FRT (gray bars) site of a homologous chromosome arm from the mutant gene (depicted as a black star). Upon heat shock induced mitotic recombination (activation of a Flipase enzyme introduced on any other chromosome can induce a FRT side-directed mitotic recombination). Only the homozygous mutant cell can express the marker gene (in the example gfp) because of the lost of the repressor protein expression (loss of tubGal80). Thus, the green daughter cell is labeled and homozygous mutant.
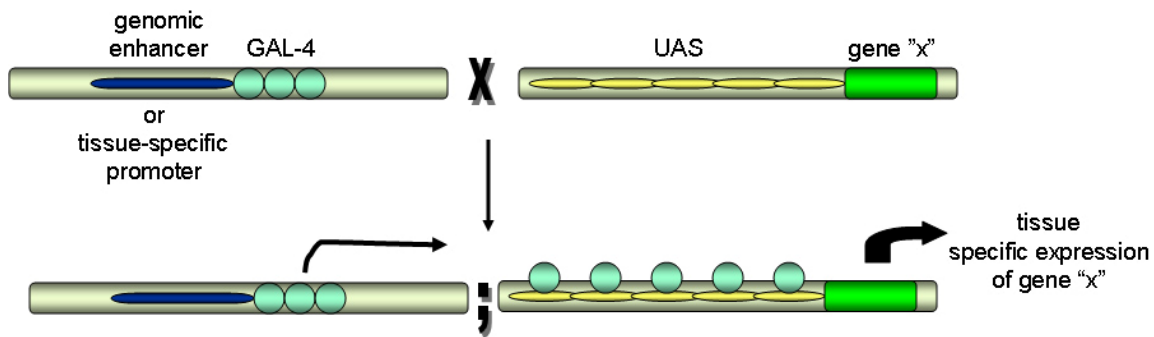
4.9 The GAL4-UAS System

FIGURE 26.**The GAL4-UAS genetic system.**
This system was introduced to fly genetics by Brand and Perrimon (Brand and Perrimon, 1993). Flies transgenic for a Gal4 transgene (blue circles) inserted into a tissue specific genomic enhancer or downstream of a tissue specific promoter (dark blue bar) are crossed to transgenic flies carrying a gene of interest (i.e. a GFP sequence-green box)

fused downstream of a UAS element (yellow ellipsoids). In the progeny, of this cross Gal4 can bind to the UAS and thus induce a tissue specific expression of the gene"x".

4.10 Imaging and image processing

Staged embryos were collected on apple- agar plates, dechorionated in 50% bleach and mounted in 90% Glycerol (MERK). The dendritic morphology of GFP-labeled dorsal md-da neurons was imaged by confocal microscopy (Leica TCS SP2). Images were further processed with Photoshop to remove tracheal branches visualized due to their auto fluorescence. Some images were further processed to reduce the background noise and enhance the signal- to noise ratios or to optimize color intensity.

4.11 Time-lapse analyses

For time lapse imaging second instar larvae (~48h AEL) of control and Gal4109(2)80;UAS-*robo*,ppk were mounted in a halocarbon oil (S3) and fixed with a specially designed cover sieve (designed by a PhD student in our laboratory, Madhuri Shivalkar and generated by the Workshop of MPI of Neurobiology). Pressing between the cover sieve and a microscopic slide prevents the larvae from any movements allowing the imaging of a dendrite segment for up to 60minutes.

4.12 Quantitative analysis of md-da neuron dendrites

The dendrite length and branching number was quantified manually by using **Image J** (National Institutes of Health, Bethesda, Maryland, USA, http://rsb.info.nih.gov/ij/, 1997-2006.) Quantitative analyses of all neurons have been performed by using similar criteria as described in (Grueber et al., 2002). At least 4-5 MARCM Class- specific clones per

genotype were used for quantification. All statistical analyses were done with Student's t

tests. We used the "reverse" Strahler method; dendrites growing from the cell bodies

were signet as first order. Interstitially growing branches from the primary order of

branch were assigned as second order. Where two second order branches met an order of

third is created and so on. Terminal branches were assigned as with the highest order of

branches.

Dendrite length in *109(2)80,UAS-GFP* line (n=10 animals per time point) was measured

from the most dorsally positioned neuronal cell body to the tip of the longest dendrite

within an abdominal cluster of neurons, this length is denoted as L_b. In the same

abdominal cluster we measured also the distance between the most dorsally positioned

cell bodies of the contra lateral cluster of neurons and this was and denoted as L_a.

Each single time-lapse image was separately analyzed. We measured the dendrite length

of a basal dendrite branch (corresponding to a third or second order of branch) within the

imaged segment. To determine the newly formed, elongated and fully retracted branches

we compared the image at time point "start" to the image at time point 'end". The

number of branches assigned as newly formed, elongated and fully retracted was then

normalized to 10μm basal dendrite length and a minute. The number of transient

branches was determined per 10μm basal dendrite length and minute by comparing single

images and counting the branches which have formed and disappeared within the whole

period of imaging.

5. Bibliography

Adams, M. D. and Sekelsky, J. J. (2002). From sequence to phenotype: reverse genetics in Drosophila melanogaster. *Nat Rev Genet* **3**, 189-98.

Aizawa, H., Hu, S. C., Bobb, K., Balakrishnan, K., Ince, G., Gurevich, I., Cowan, M. and Ghosh, A. (2004). Dendrite development regulated by CREST, a calcium-regulated transcriptional activator. *Science* **303**, 197-202.

Akum, B. F., Chen, M., Gunderson, S. I., Riefler, G. M., Scerri-Hansen, M. M. and Firestein, B. L. (2004). Cypin regulates dendrite patterning in hippocampal neurons by promoting microtubule assembly. *Nat Neurosci* **7**, 145-52.

Amthor, F. R. and Oyster, C. W. (1995). Spatial organization of retinal information about the direction of image motion. *Proc Natl Acad Sci U S A* **92**, 4002-5.

Andersen, R., Li, Y., Resseguie, M. and Brenman, J. E. (2005). Calcium/calmodulin-dependent protein kinase II alters structural plasticity and cytoskeletal dynamics in Drosophila. *J Neurosci* **25**, 8878-88.

Bagri, A., Cheng, H. J., Yaron, A., Pleasure, S. J. and Tessier-Lavigne, M. (2003). Stereotyped pruning of long hippocampal axon branches triggered by retraction inducers of the semaphorin family. *Cell* **113**, 285-99.

Bashaw, G. J. and Goodman, C. S. (1999). Chimeric axon guidance receptors: the cytoplasmic domains of slit and netrin receptors specify attraction versus repulsion. *Cell* **97**, 917-26.

Bashaw, G. J., Kidd, T., Murray, D., Pawson, T. and Goodman, C. S. (2000). Repulsive axon guidance: Abelson and Enabled play opposing roles downstream of the roundabout receptor. *Cell* **101**, 703-15.

Berger, J., Suzuki, T., Senti, K. A., Stubbs, J., Schaffner, G. and Dickson, B. J. (2001). Genetic mapping with SNP markers in Drosophila. *Nat Genet* **29**, 475-81.

Bodmer, R., Carretto, R. and Jan, Y. N. (1989). Neurogenesis of the peripheral nervous system in Drosophila embryos: DNA replication patterns and cell lineages. *Neuron* **3**, 21-32.

Brand, A. H. and Perrimon, N. (1993). Targeted gene expression as a means of altering cell fates and generating dominant phenotypes. *Development* **118**, 401-15.

Brenman, J. E., Gao, F. B., Jan, L. Y. and Jan, Y. N. (2001). Sequoia, a tramtrack-related zinc finger protein, functions as a pan-neural regulator for dendrite and axon morphogenesis in Drosophila. *Dev Cell* **1**, 667-77.

Brose, K., Bland, K. S., Wang, K. H., Arnott, D., Henzel, W., Goodman, C. S., Tessier-Lavigne, M. and Kidd, T. (1999). Slit proteins bind Robo receptors and have an evolutionarily conserved role in repulsive axon guidance. *Cell* **96**, 795-806.

Campbell, D. S., Stringham, S. A., Timm, A., Xiao, T., Law, M. Y., Baier, H., Nonet, M. L. and Chien, C. B. (2007). Slit1a Inhibits Retinal Ganglion Cell Arborization and Synaptogenesis via Robo2-Dependent and -Independent Pathways. *Neuron* **55**, 231-245.

Carmeliet, P. and Tessier-Lavigne, M. (2005). Common mechanisms of nerve and blood vessel wiring. *Nature* **436**, 193-200.

Carvalho, R. F., Beutler, M., Marler, K. J., Knoll, B., Becker-Barroso, E., Heintzmann, R., Ng, T. and Drescher, U. (2006). Silencing of EphA3 through a cis interaction with ephrinA5. *Nat Neurosci* **9**, 322-30.

Challa, A. K., Beattie, C. E. and Seeger, M. A. (2001). Identification and characterization of roundabout orthologs in zebrafish. *Mech Dev* **101**, 249-53.

Chen, M., Lucas, K. G., Akum, B. F., Balasingam, G., Stawicki, T. M., Provost, J. M., Riefler, G. M., Jornsten, R. J. and Firestein, B. L. (2005a). A novel role for snapin in dendrite patterning: interaction with cypin. *Mol Biol Cell* **16**, 5103-14.

Chen, Y., Wang, P. Y. and Ghosh, A. (2005b). Regulation of cortical dendrite development by Rap1 signaling. *Mol Cell Neurosci* **28**, 215-28.

Clandinin, T. R. and Zipursky, S. L. (2000). Afferent growth cone interactions control synaptic specificity in the Drosophila visual system. *Neuron* **28**, 427-36.

Cline, H. T. (2001). Dendritic arbor development and synaptogenesis. *Curr Opin Neurobiol* **11**, 118-26.

Dent, E. W., Barnes, A. M., Tang, F. and Kalil, K. (2004). Netrin-1 and semaphorin 3A promote or inhibit cortical axon branching, respectively, by reorganization of the cytoskeleton. *J Neurosci* **24**, 3002-12.

Desai, C. J., Garrity, P. A., Keshishian, H., Zipursky, S. L. and Zinn, K. (1999). The Drosophila SH2-SH3 adapter protein Dock is expressed in embryonic axons and facilitates synapse formation by the RP3 motoneuron. *Development* **126**, 1527-35.

Dickson, B. J. (2001). Rho GTPases in growth cone guidance. *Curr Opin Neurobiol* **11**, 103-10.

Dickson, B. J. (2002). Molecular mechanisms of axon guidance. *Science* **298**, 1959-64.

Dickson, B. J. and Gilestro, G. F. (2006). Regulation of commissural axon pathfinding by slit and its robo receptors. *Annu Rev Cell Dev Biol* **22**, 651-75.

Dwivedy, A., Gertler, F. B., Miller, J., Holt, C. E. and Lebrand, C. (2007). Ena/VASP function in retinal axons is required for terminal arborization but not pathway navigation. *Development* **134**, 2137-46.

Egea, J. and Klein, R. (2007). Bidirectional Eph-ephrin signaling during axon guidance. *Trends Cell Biol* **17**, 230-8.

Emoto, K., He, Y., Ye, B., Grueber, W. B., Adler, P. N., Jan, L. Y. and Jan, Y. N. (2004). Control of dendritic branching and tiling by the Tricornered-kinase/Furry signaling pathway in Drosophila sensory neurons. *Cell* **119**, 245-56.

Emoto, K., Parrish, J. Z., Jan, L. Y. and Jan, Y. N. (2006). The tumour suppressor Hippo acts with the NDR kinases in dendritic tiling and maintenance. *Nature* **443**, 210-3.

Englund, C., Steneberg, P., Falileeva, L., Xylourgidis, N. and Samakovlis, C. (2002). Attractive and repulsive functions of Slit are mediated by different receptors in the Drosophila trachea. *Development* **129**, 4941-51.

Erskine, L., Williams, S. E., Brose, K., Kidd, T., Rachel, R. A., Goodman, C. S., Tessier-Lavigne, M. and Mason, C. A. (2000). Retinal ganglion cell axon guidance in the mouse optic chiasm: expression and function of robos and slits. *J Neurosci* **20**, 4975-82.

Faix, J. and Rottner, K. (2006). The making of filopodia. *Curr Opin Cell Biol* **18**, 18-25.

Fan, X., Labrador, J. P., Hing, H. and Bashaw, G. J. (2003). Slit stimulation recruits Dock and Pak to the roundabout receptor and increases Rac activity to regulate axon repulsion at the CNS midline. *Neuron* **40**, 113-27.

Furrer, M. P., Kim, S., Wolf, B. and Chiba, A. (2003). Robo and Frazzled/DCC mediate dendritic guidance at the CNS midline. *Nat Neurosci* **6**, 223-30.

Gallegos, M. E. and Bargmann, C. I. (2004). Mechanosensory neurite termination and tiling depend on SAX-2 and the SAX-1 kinase. *Neuron* **44**, 239-49.

Gao, F. B., Brenman, J. E., Jan, L. Y. and Jan, Y. N. (1999). Genes regulating dendritic outgrowth, branching, and routing in Drosophila. *Genes Dev* **13**, 2549-61.

Gao, F. B., Kohwi, M., Brenman, J. E., Jan, L. Y. and Jan, Y. N. (2000). Control of dendritic field formation in Drosophila: the roles of flamingo and competition between homologous neurons. *Neuron* **28**, 91-101.

Garbe, D. S. and Bashaw, G. J. (2007). Independent functions of Slit-Robo repulsion and Netrin-Frazzled attraction regulate axon crossing at the midline in Drosophila. *J Neurosci* **27**, 3584-92.

Gaudilliere, B., Konishi, Y., de la Iglesia, N., Yao, G. and Bonni, A. (2004). A CaMKII-NeuroD signaling pathway specifies dendritic morphogenesis. *Neuron* **41**, 229-41.

Gitai, Z., Yu, T. W., Lundquist, E. A., Tessier-Lavigne, M. and Bargmann, C. I. (2003). The netrin receptor UNC-40/DCC stimulates axon attraction and outgrowth through enabled and, in parallel, Rac and UNC-115/AbLIM. *Neuron* **37**, 53-65.

Godenschwege, T. A., Simpson, J. H., Shan, X., Bashaw, G. J., Goodman, C. S. and Murphey, R. K. (2002). Ectopic expression in the giant fiber system of Drosophila reveals distinct roles for roundabout (Robo), Robo2, and Robo3 in dendritic guidance and synaptic connectivity. *J Neurosci* **22**, 3117-29.

Gorski, J. A., Zeiler, S. R., Tamowski, S. and Jones, K. R. (2003). Brain-derived neurotrophic factor is required for the maintenance of cortical dendrites. *J Neurosci* **23**, 6856-65.

Greig, S. and Akam, M. (1993). Homeotic genes autonomously specify one aspect of pattern in the Drosophila mesoderm. *Nature* **362**, 630-2.

Grueber, W. B., Graubard, K. and Truman, J. W. (2001). Tiling of the body wall by multidendritic sensory neurons in Manduca sexta. *J Comp Neurol* **440**, 271-83.

Grueber, W. B., Jan, L. Y. and Jan, Y. N. (2002). Tiling of the Drosophila epidermis by multidendritic sensory neurons. *Development* **129**, 2867-78.

Grueber, W. B., Jan, L. Y. and Jan, Y. N. (2003a). Different levels of the homeodomain protein cut regulate distinct dendrite branching patterns of Drosophila multidendritic neurons. *Cell* **112**, 805-18.

Grueber, W. B. and Jan, Y. N. (2004). Dendritic development: lessons from Drosophila and related branches. *Curr Opin Neurobiol* **14**, 74-82.

Grueber, W. B., Ye, B., Moore, A. W., Jan, L. Y. and Jan, Y. N. (2003b). Dendrites of distinct classes of Drosophila sensory neurons show different capacities for homotypic repulsion. *Curr Biol* **13**, 618-26.

Grueber, W. B., Ye, B., Yang, C. H., Younger, S., Borden, K., Jan, L. Y. and Jan, Y. N. (2007). Projections of Drosophila multidendritic neurons in the central nervous system: links with peripheral dendrite morphology. *Development* **134**, 55-64.

Hao, J. C., Yu, T. W., Fujisawa, K., Culotti, J. G., Gengyo-Ando, K., Mitani, S., Moulder, G., Barstead, R., Tessier-Lavigne, M. and Bargmann, C. I. (2001). C. elegans slit acts in midline, dorsal-ventral, and anterior-posterior guidance via the SAX-3/Robo receptor. *Neuron* **32**, 25-38.

Horton, A. C., Racz, B., Monson, E. E., Lin, A. L., Weinberg, R. J. and Ehlers, M. D. (2005). Polarized secretory trafficking directs cargo for asymmetric dendrite growth and morphogenesis. *Neuron* **48**, 757-71.

Howitt, J. A., Clout, N. J. and Hohenester, E. (2004). Binding site for Robo receptors revealed by dissection of the leucine-rich repeat region of Slit. *Embo J* **23**, 4406-12.

Hua, J. Y., Smear, M. C., Baier, H. and Smith, S. J. (2005). Regulation of axon growth in vivo by activity-based competition. *Nature* **434**, 1022-6.

Hughes, M. E., Bortnick, R., Tsubouchi, A., Baumer, P., Kondo, M., Uemura, T. and Schmucker, D. (2007). Homophilic Dscam interactions control complex dendrite morphogenesis. *Neuron* **54**, 417-27.

Huminiecki, L., Gorn, M., Suchting, S., Poulsom, R. and Bicknell, R. (2002). Magic roundabout is a new member of the roundabout receptor family that is endothelial specific and expressed at sites of active angiogenesis. *Genomics* **79**, 547-52.

Hummel, T., Krukkert, K., Roos, J., Davis, G. and Klambt, C. (2000). Drosophila Futsch/22C10 is a MAP1B-like protein required for dendritic and axonal development. *Neuron* **26**, 357-70.

Hummel, T., Schimmelpfeng, K. and Klambt, C. (1999). Commissure formation in the embryonic CNS of Drosophila. *Development* **126**, 771-9.

Hutson, L. D., Jurynec, M. J., Yeo, S. Y., Okamoto, H. and Chien, C. B. (2003). Two divergent slit1 genes in zebrafish. *Dev Dyn* **228**, 358-69.

Jan, Y. N. and Jan, L. Y. (2001). Dendrites. *Genes Dev* **15**, 2627-41.

Jan, Y. N. and Jan, L. Y. (2003). The control of dendrite development. *Neuron* **40**, 229-42.

Kage, E., Hayashi, Y., Takeuchi, H., Hirotsu, T., Kunitomo, H., Inoue, T., Arai, H., Iino, Y. and Kubo, T. (2005). MBR-1, a novel helix-turn-helix transcription factor, is required for pruning excessive neurites in Caenorhabditis elegans. *Curr Biol* **15**, 1554-9.

Kantor, D. B. and Kolodkin, A. L. (2003). Curbing the excesses of youth: molecular insights into axonal pruning. *Neuron* **38**, 849-52.

Keleman, K., Ribeiro, C. and Dickson, B. J. (2005). Comm function in commissural axon guidance: cell-autonomous sorting of Robo in vivo. *Nat Neurosci* **8**, 156-63.

Kidd, T., Bland, K. S. and Goodman, C. S. (1999). Slit is the midline repellent for the robo receptor in Drosophila. *Cell* **96**, 785-94.

Kidd, T., Brose, K., Mitchell, K. J., Fetter, R. D., Tessier-Lavigne, M., Goodman, C. S. and Tear, G. (1998). Roundabout controls axon crossing of the CNS midline and defines a novel subfamily of evolutionarily conserved guidance receptors. *Cell* **92**, 205-15.

Kim, S. and Chiba, A. (2004). Dendritic guidance. *Trends Neurosci* **27**, 194-202.

Komiyama, T., Sweeney, L. B., Schuldiner, O., Garcia, K. C. and Luo, L. (2007). Graded expression of semaphorin-1a cell-autonomously directs dendritic targeting of olfactory projection neurons. *Cell* **128**, 399-410.

Korey, C. A. and Van Vactor, D. (2000). From the growth cone surface to the cytoskeleton: one journey, many paths. *J Neurobiol* **44**, 184-93.

Kornack, D. R. and Giger, R. J. (2005). Probing microtubule +TIPs: regulation of axon branching. *Curr Opin Neurobiol* **15**, 58-66.

Kramer, S. G., Kidd, T., Simpson, J. H. and Goodman, C. S. (2001). Switching repulsion to attraction: changing responses to slit during transition in mesoderm migration. *Science* **292**, 737-40.

Kraut, R. and Zinn, K. (2004). Roundabout 2 regulates migration of sensory neurons by signaling in trans. *Curr Biol* **14**, 1319-29.

Kuo, C. T., Zhu, S., Younger, S., Jan, L. Y. and Jan, Y. N. (2006). Identification of E2/E3 ubiquitinating enzymes and caspase activity regulating Drosophila sensory neuron dendrite pruning. *Neuron* **51**, 283-90.

Lebrand, C., Dent, E. W., Strasser, G. A., Lanier, L. M., Krause, M., Svitkina, T. M., Borisy, G. G. and Gertler, F. B. (2004). Critical role of Ena/VASP proteins for filopodia formation in neurons and in function downstream of netrin-1. *Neuron* **42**, 37-49.

Lee, H., Engel, U., Rusch, J., Scherrer, S., Sheard, K. and Van Vactor, D. (2004). The microtubule plus end tracking protein Orbit/MAST/CLASP acts downstream of the tyrosine kinase Abl in mediating axon guidance. *Neuron* **42**, 913-26.

Lee, T. and Luo, L. (2001). Mosaic analysis with a repressible cell marker (MARCM) for Drosophila neural development. *Trends Neurosci* **24**, 251-4.

Lee, T., Marticke, S., Sung, C., Robinow, S. and Luo, L. (2000). Cell-autonomous requirement of the USP/EcR-B ecdysone receptor for mushroom body neuronal remodeling in Drosophila. *Neuron* **28**, 807-18.

Lee, Y., Lee, J., Bang, S., Hyun, S., Kang, J., Hong, S. T., Bae, E., Kaang, B. K. and Kim, J. (2005). Pyrexia is a new thermal transient receptor potential channel endowing tolerance to high temperatures in Drosophila melanogaster. *Nat Genet* **37**, 305-10.

Li, H. S., Chen, J. H., Wu, W., Fagaly, T., Zhou, L., Yuan, W., Dupuis, S., Jiang, Z. H., Nash, W., Gick, C. et al. (1999). Vertebrate slit, a secreted ligand for the transmembrane protein roundabout, is a repellent for olfactory bulb axons. *Cell* **96**, 807-18.

Li, W., Li, Y. and Gao, F. B. (2005). Abelson, enabled, and p120 catenin exert distinct effects on dendritic morphogenesis in Drosophila. *Dev Dyn* **234**, 512-22.

Li, W., Wang, F., Menut, L. and Gao, F. B. (2004). BTB/POZ-zinc finger protein abrupt suppresses dendritic branching in a neuronal subtype-specific and dosage-dependent manner. *Neuron* **43**, 823-34.

Li, Z., Van Aelst, L. and Cline, H. T. (2000). Rho GTPases regulate distinct aspects of dendritic arbor growth in Xenopus central neurons in vivo. *Nat Neurosci* **3**, 217-25.

Lin, B., Wang, S. W. and Masland, R. H. (2004). Retinal ganglion cell type, size, and spacing can be specified independent of homotypic dendritic contacts. *Neuron* **43**, 475-85.

Lin, D. M., Auld, V. J. and Goodman, C. S. (1995). Targeted neuronal cell ablation in the Drosophila embryo: pathfinding by follower growth cones in the absence of pioneers. *Neuron* **14**, 707-15.

Lin, D. M., Fetter, R. D., Kopczynski, C., Grenningloh, G. and Goodman, C. S. (1994). Genetic analysis of Fasciclin II in Drosophila: defasciculation, refasciculation, and altered fasciculation. *Neuron* **13**, 1055-69.

Liu, L., Yermolaieva, O., Johnson, W. A., Abboud, F. M. and Welsh, M. J. (2003). Identification and function of thermosensory neurons in Drosophila larvae. *Nat Neurosci* **6**, 267-73.

Liu, Z., Patel, K., Schmidt, H., Andrews, W., Pini, A. and Sundaresan, V. (2004). Extracellular Ig domains 1 and 2 of Robo are important for ligand (Slit) binding. *Mol Cell Neurosci* **26**, 232-40.

Lohmann, C. and Wong, R. O. (2005). Regulation of dendritic growth and plasticity by local and global calcium dynamics. *Cell Calcium* **37**, 403-9.

Long, H., Sabatier, C., Ma, L., Plump, A., Yuan, W., Ornitz, D. M., Tamada, A., Murakami, F., Goodman, C. S. and Tessier-Lavigne, M. (2004). Conserved roles for Slit and Robo proteins in midline commissural axon guidance. *Neuron* **42**, 213-23.

Luo, L. (2000). Rho GTPases in neuronal morphogenesis. *Nat Rev Neurosci* **1**, 173-80.

Luo, L., Hensch, T. K., Ackerman, L., Barbel, S., Jan, L. Y. and Jan, Y. N. (1996). Differential effects of the Rac GTPase on Purkinje cell axons and dendritic trunks and spines. *Nature* **379**, 837-40.

Ma, L. and Tessier-Lavigne, M. (2007). Dual branch-promoting and branch-repelling actions of Slit/Robo signaling on peripheral and central branches of developing sensory axons. *J Neurosci* **27**, 6843-51.

Marillat, V., Sabatier, C., Failli, V., Matsunaga, E., Sotelo, C., Tessier-Lavigne, M. and Chedotal, A. (2004). The slit receptor Rig-1/Robo3 controls midline crossing by hindbrain precerebellar neurons and axons. *Neuron* **43**, 69-79.

Marin, E. C., Watts, R. J., Tanaka, N. K., Ito, K. and Luo, L. (2005). Developmentally programmed remodeling of the Drosophila olfactory circuit. *Development* **132**, 725-37.

Marrs, G. S., Honda, T., Fuller, L., Thangavel, R., Balsamo, J., Lilien, J., Dailey, M. E. and Arregui, C. (2006). Dendritic arbors of developing retinal ganglion cells are stabilized by beta 1-integrins. *Mol Cell Neurosci* **32**, 230-41.

Masland, R. H. (2005). The many roles of starburst amacrine cells. *Trends Neurosci* **28**, 395-6.

Matthews, B. J., Kim, M. E., Flanagan, J. J., Hattori, D., Clemens, J. C., Zipursky, S. L. and Grueber, W. B. (2007). Dendrite self-avoidance is controlled by Dscam. *Cell* **129**, 593-604.

McAllister, A. K. (2000). Cellular and molecular mechanisms of dendrite growth. *Cereb Cortex* **10**, 963-73.

Medina, C. R., Indes, J. and Smith, C. (2006). Endovascular treatment of an abdominal aortic pseudoaneurysm as a late complication of inferior vena cava filter placement. *J Vasc Surg* **43**, 1278-82.

Mendell, J. T. and Dietz, H. C. (2001). When the message goes awry: disease-producing mutations that influence mRNA content and performance. *Cell* **107**, 411-4.

Miller, F. D. and Kaplan, D. R. (2003). Signaling mechanisms underlying dendrite formation. *Curr Opin Neurobiol* **13**, 391-8.

Murray, M. J. and Whitington, P. M. (1999). Effects of roundabout on growth cone dynamics, filopodial length, and growth cone morphology at the midline and throughout the neuropile. *J Neurosci* **19**, 7901-12.

Myers, E. W., Sutton, G. G., Delcher, A. L., Dew, I. M., Fasulo, D. P., Flanigan, M. J., Kravitz, S. A., Mobarry, C. M., Reinert, K. H., Remington, K. A. et al. (2000). A whole-genome assembly of Drosophila. *Science* **287**, 2196-204.

Newey, S. E., Velamoor, V., Govek, E. E. and Van Aelst, L. (2005). Rho GTPases, dendritic structure, and mental retardation. *J Neurobiol* **64**, 58-74.

Niell, C. M., Meyer, M. P. and Smith, S. J. (2004). In vivo imaging of synapse formation on a growing dendritic arbor. *Nat Neurosci* **7**, 254-60.

Nusslein-Volhard C, W. E., Kluding H. (1984). Mutations affecting the pattern of the larval cuticle in Drosophila melanogaster. *Roux Arch. Dev. Biol.* **193:**, 267–82.

Parks, A. L., Cook, K. R., Belvin, M., Dompe, N. A., Fawcett, R., Huppert, K., Tan, L. R., Winter, C. G., Bogart, K. P., Deal, J. E. et al. (2004). Systematic generation of high-resolution deletion coverage of the Drosophila melanogaster genome. *Nat Genet* **36**, 288-92.

Parrish, J. Z., Emoto, K., Jan, L. Y. and Jan, Y. N. (2007a). Polycomb genes interact with the tumor suppressor genes hippo and warts in the maintenance of Drosophila sensory neuron dendrites. *Genes Dev* **21**, 956-72.

Parrish, J. Z., Emoto, K., Kim, M. D. and Jan, Y. N. (2007b). Mechanisms That Regulate Establishment, Maintenance, and Remodeling of Dendritic Fields. *Annu Rev Neurosci*.

Parrish, J. Z., Kim, M. D., Jan, L. Y. and Jan, Y. N. (2006). Genome-wide analyses identify transcription factors required for proper morphogenesis of Drosophila sensory neuron dendrites. *Genes Dev* **20**, 820-35.

Parsons, L., Harris, K. L., Turner, K. and Whitington, P. M. (2003). Roundabout gene family functions during sensory axon guidance in the drosophila embryo are mediated by both Slit-dependent and Slit-independent mechanisms. *Dev Biol* **264**, 363-75.

Piper, M., Georgas, K., Yamada, T. and Little, M. (2000). Expression of the vertebrate Slit gene family and their putative receptors, the Robo genes, in the developing murine kidney. *Mech Dev* **94**, 213-7.

Polleux, F., Morrow, T. and Ghosh, A. (2000). Semaphorin 3A is a chemoattractant for cortical apical dendrites. *Nature* **404**, 567-73.

Qian, L., Liu, J. and Bodmer, R. (2005). Slit and Robo control cardiac cell polarity and morphogenesis. *Curr Biol* **15**, 2271-8.

Rajagopalan, S., Nicolas, E., Vivancos, V., Berger, J. and Dickson, B. J. (2000a). Crossing the midline: roles and regulation of Robo receptors. *Neuron* **28**, 767-77.

Rajagopalan, S., Vivancos, V., Nicolas, E. and Dickson, B. J. (2000b). Selecting a longitudinal pathway: Robo receptors specify the lateral position of axons in the Drosophila CNS. *Cell* **103**, 1033-45.

Redmond, L. and Ghosh, A. (2005). Regulation of dendritic development by calcium signaling. *Cell Calcium* **37**, 411-6.

Rothberg, J. M., Jacobs, J. R., Goodman, C. S. and Artavanis-Tsakonas, S. (1990). slit: an extracellular protein necessary for development of midline glia and commissural axon pathways contains both EGF and LRR domains. *Genes Dev* **4**, 2169-87.

Rottner, K., Behrendt, B., Small, J. V. and Wehland, J. (1999). VASP dynamics during lamellipodia protrusion. *Nat Cell Biol* **1**, 321-2.

Ruthazer, E. S., Akerman, C. J. and Cline, H. T. (2003). Control of axon branch dynamics by correlated activity in vivo. *Science* **301**, 66-70.

Sanchez, A. L., Matthews, B. J., Meynard, M. M., Hu, B., Javed, S. and Cohen Cory, S. (2006). BDNF increases synapse density in dendrites of developing tectal neurons in vivo. *Development* **133**, 2477-86.

Seeger, M., Tear, G., Ferres-Marco, D. and Goodman, C. S. (1993). Mutations affecting growth cone guidance in Drosophila: genes necessary for guidance toward or away from the midline. *Neuron* **10**, 409-26.

Shang, Y., Claridge-Chang, A., Sjulson, L., Pypaert, M. and Miesenbock, G. (2007). Excitatory local circuits and their implications for olfactory processing in the fly antennal lobe. *Cell* **128**, 601-12.

Shima, Y., Kengaku, M., Hirano, T., Takeichi, M. and Uemura, T. (2004). Regulation of dendritic maintenance and growth by a mammalian 7-pass transmembrane cadherin. *Dev Cell* **7**, 205-16.

Simpson, J. H., Bland, K. S., Fetter, R. D. and Goodman, C. S. (2000a). Short-range and long-range guidance by Slit and its Robo receptors: a combinatorial code of Robo receptors controls lateral position. *Cell* **103**, 1019-32.

Simpson, J. H., Kidd, T., Bland, K. S. and Goodman, C. S. (2000b). Short-range and long-range guidance by slit and its Robo receptors. Robo and Robo2 play distinct roles in midline guidance. *Neuron* **28**, 753-66.

Smith, C. D., Shu, S., Mungall, C. J. and Karpen, G. H. (2007). The Release 5.1 annotation of Drosophila melanogaster heterochromatin. *Science* **316**, 1586-91.

Soba, P., Zhu, S., Emoto, K., Younger, S., Yang, S. J., Yu, H. H., Lee, T., Jan, L. Y. and Jan, Y. N. (2007). Drosophila sensory neurons require Dscam for dendritic self-avoidance and proper dendritic field organization. *Neuron* **54**, 403-16.

Song, H., Ming, G., He, Z., Lehmann, M., McKerracher, L., Tessier-Lavigne, M. and Poo, M. (1998). Conversion of neuronal growth cone responses from repulsion to attraction by cyclic nucleotides. *Science* **281**, 1515-8.

Song, W., Onishi, M., Jan, L. Y. and Jan, Y. N. (2007). Peripheral multidendritic sensory neurons are necessary for rhythmic locomotion behavior in Drosophila larvae. *Proc Natl Acad Sci U S A* **104**, 5199-204.

St Johnston, D. (2002). The art and design of genetic screens: Drosophila melanogaster. *Nat Rev Genet* **3**, 176-88.

Sugimura, K., Satoh, D., Estes, P., Crews, S. and Uemura, T. (2004). Development of morphological diversity of dendrites in Drosophila by the BTB-zinc finger protein abrupt. *Neuron* **43**, 809-22.

Sugimura, K., Yamamoto, M., Niwa, R., Satoh, D., Goto, S., Taniguchi, M., Hayashi, S. and Uemura, T. (2003). Distinct developmental modes and lesion-induced reactions of dendrites of two classes of Drosophila sensory neurons. *J Neurosci* **23**, 3752-60.

Suster, M. L., Seugnet, L., Bate, M. and Sokolowski, M. B. (2004). Refining GAL4-driven transgene expression in Drosophila with a GAL80 enhancer-trap. *Genesis* **39**, 240-5.

Sweeney, L. B., Couto, A., Chou, Y. H., Berdnik, D., Dickson, B. J., Luo, L. and Komiyama, T. (2007). Temporal target restriction of olfactory receptor neurons by Semaphorin-1a/PlexinA-mediated axon-axon interactions. *Neuron* **53**, 185-200.

Tear, G., Harris, R., Sutaria, S., Kilomanski, K., Goodman, C. S. and Seeger, M. A. (1996). commissureless controls growth cone guidance across the CNS midline in Drosophila and encodes a novel membrane protein. *Neuron* **16**, 501-14.

Tessier-Lavigne, M. and Goodman, C. S. (1996). The molecular biology of axon guidance. *Science* **274**, 1123-33.

Tracey, W. D., Jr., Wilson, R. I., Laurent, G. and Benzer, S. (2003). painless, a Drosophila gene essential for nociception. *Cell* **113**, 261-73.

Truman, J. W. and Reiss, S. E. (1995). Neuromuscular metamorphosis in the moth Manduca sexta: hormonal regulation of synapses loss and remodeling. *J Neurosci* **15**, 4815-26.

Van Aelst, L. and Cline, H. T. (2004). Rho GTPases and activity-dependent dendrite development. *Curr Opin Neurobiol* **14**, 297-304.

Van Vactor, D., Wall, D. P. and Johnson, K. G. (2006). Heparan sulfate proteoglycans and the emergence of neuronal connectivity. *Curr Opin Neurobiol* **16**, 40-51.

Wang, K. H., Brose, K., Arnott, D., Kidd, T., Goodman, C. S., Henzel, W. and Tessier-Lavigne, M. (1999). Biochemical purification of a mammalian slit protein as a positive regulator of sensory axon elongation and branching. *Cell* **96**, 771-84.

Watts, R. J., Hoopfer, E. D. and Luo, L. (2003). Axon pruning during Drosophila metamorphosis: evidence for local degeneration and requirement of the ubiquitin-proteasome system. *Neuron* **38**, 871-85.

Wayman, G. A., Impey, S., Marks, D., Saneyoshi, T., Grant, W. F., Derkach, V. and Soderling, T. R. (2006). Activity-dependent dendritic arborization mediated by CaM-kinase I activation and enhanced CREB-dependent transcription of Wnt-2. *Neuron* **50**, 897-909.

Wen, Z. and Zheng, J. Q. (2006). Directional guidance of nerve growth cones. *Curr Opin Neurobiol* **16**, 52-8.

Whitford, K. L., Marillat, V., Stein, E., Goodman, C. S., Tessier-Lavigne, M., Chedotal, A. and Ghosh, A. (2002). Regulation of cortical dendrite development by Slit-Robo interactions. *Neuron* **33**, 47-61.

Williams, D. W., Kondo, S., Krzyzanowska, A., Hiromi, Y. and Truman, J. W. (2006). Local caspase activity directs engulfment of dendrites during pruning. *Nat Neurosci* **9**, 1234-6.

Williams, D. W. and Truman, J. W. (2005). Cellular mechanisms of dendrite pruning in Drosophila: insights from in vivo time-lapse of remodeling dendritic arborizing sensory neurons. *Development* **132**, 3631-42.

Wills, Z., Bateman, J., Korey, C. A., Comer, A. and Van Vactor, D. (1999). The tyrosine kinase Abl and its substrate enabled collaborate with the receptor phosphatase Dlar to control motor axon guidance. *Neuron* **22**, 301-12.

Wills, Z., Emerson, M., Rusch, J., Bikoff, J., Baum, B., Perrimon, N. and Van Vactor, D. (2002). A Drosophila homolog of cyclase-associated proteins collaborates with the Abl tyrosine kinase to control midline axon pathfinding. *Neuron* **36**, 611-22.

Wu, G. Y. and Cline, H. T. (2003). Time-lapse in vivo imaging of the morphological development of Xenopus optic tectal interneurons. *J Comp Neurol* **459**, 392-406.

Wu, G. Y., Zou, D. J., Rajan, I. and Cline, H. (1999). Dendritic dynamics in vivo change during neuronal maturation. *J Neurosci* **19**, 4472-83.

Wu, J. S. and Luo, L. (2006). A protocol for dissecting Drosophila melanogaster brains for live imaging or immunostaining. *Nat Protoc* **1**, 2110-5.

Yang, L. and Bashaw, G. J. (2006). Son of sevenless directly links the Robo receptor to rac activation to control axon repulsion at the midline. *Neuron* **52**, 595-607.

Ye, B., Petritsch, C., Clark, I. E., Gavis, E. R., Jan, L. Y. and Jan, Y. N. (2004). Nanos and Pumilio are essential for dendrite morphogenesis in Drosophila peripheral neurons. *Curr Biol* **14**, 314-21.

Ye, B., Zhang, Y. W., Jan, L. Y. and Jan, Y. N. (2006). The secretory pathway and neuron polarization. *J Neurosci* **26**, 10631-2.

Zlatic, M., Landgraf, M. and Bate, M. (2003). Genetic specification of axonal arbors: atonal regulates robo3 to position terminal branches in the Drosophila nervous system. *Neuron* **37**, 41-51.

Zou, Y. and Lyuksyutova, A. I. (2007). Morphogens as conserved axon guidance cues. *Curr Opin Neurobiol* **17**, 22-8.

7. Acknowledgments

Curriculum Vitae

S V E T L A   D I M I T R O V A

Personal Details:

Address:	Leonrodstrasse 31
	80636 Munich - Germany
e-mail:	svetka@hotmail.com
Place of birth:	Sofia, Bulgaria
Date of birth:	05.12.1973
Nationality:	Austrian

Education

Nov. 2003- present	**Max Planck Institute of Neurobiology** **PhD thesis** in the group of Dr. G. Tavosanis, in the Department of Prof.Ruediger Klein
Oct.2001 - Aug. 2002	**Research Institute of Molecular Pathology** **Diploma thesis** in the Lab of Dr. Barry Dickson (IMP) Vienna, Austria
Oct.1993 - Nov. 2002	**TU WIEN**, **Master Degree** in Chemical Engineering Vienna University of Technology –
Sept.1991 – Oct.1992	**Sofia University of Technology** Undergraduate studies in Materials Chemistry